Evaluating the Impact Reduced *FBXO30* Expression has on Chromosome Instability in Colonic Epithelial Cell Lines

by

Nicole Gerber

A Thesis submitted to the Faculty of Graduate and Postdoctoral Studies of
the University of Manitoba
in partial fulfillment of the requirements of the degree

MASTER OF SCIENCE

Department of Biochemistry and Medical Genetics
University of Manitoba
Winnipeg

ABSTRACT

Colorectal cancer (CRC) is the fourth most commonly diagnosed and second most lethal cancer in Canada. While there are effective screening programs and therapeutic options, individuals are often diagnosed with CRC at late disease stages. Despite the high morbidity and mortality rates facing Canadians, the underlying mechanisms driving CRC pathogenesis remain poorly understood. Chromosome instability (CIN), is an ongoing phenomenon defined by the increased changes in chromosome complements and occurs in ~85 % of all CRC cases. Recent evidence from the McManus laboratory demonstrates that decreased expression of core SKP1-CUL1-F-box (SCF) E3 ubiquitin ligase complex members induce CIN and promote early CRC development. However, the role of the variable 69 F-box protein subunits in driving CIN remains largely unknown. Therefore, this thesis examines the impact of reduced *FBXO30* expression on CIN in early CRC development. Quantitative imaging microscopy techniques coupled with siRNA-based silencing were used to assess CIN-associated phenotypes, including changes in nuclear areas, micronucleus formation, and chromosome numbers in karyotypically stable non-malignant and malignant colonic epithelial cell lines. As a result, reduced *FBXO30* expression induced significant changes (increases and/or decreases) in nuclear areas, micronucleus formation, and chromosome numbers in non-malignant, non-transformed 1CT and A1309 cell lines. Additionally, in the malignant context, *FBXO30* silencing induced significant increases in nuclear areas and aberrant chromosome numbers in HCT116 cells. Collectively, these data identify *FBXO30* as a novel CIN gene and may provide novel insights into the etiological events promoting CRC pathogenesis.

Acknowledgements

First, I would to thank my supervisor Dr. Kirk McManus for their support, guidance, and patience throughout this work. Since starting in the lab, I could never have predicted the personal and professional growth that I would undergo over these past two years and the valuable lessons that have made me a better scientist. Thank you for letting me be a member of the McManus lab team.

Thank you to my committee members, Dr. Jeffrey Wigle and Sabine Hombach-Klonisch, for their feedback, constructive criticism, and encouragement at every stage of this thesis project. Their questions and suggestions pushed me to think more critically about my research.

This research would not have been possible without the financial support from the *Cancer Research Society*, *CancerCare Manitoba Foudation*, *Research Manitoba*, the *Department of Biochemistry and Medical Genetics* and the *University of Manitoba*. Thank you to these generous organizations for their support in advancing scientific research.

To all the McManus laboratory members, thank you for fostering a supportive and collaborative environment. I am thankful for the technical help, training, troubleshooting sessions, and the many scientific discussions that contributed to the completion of this project. The welcoming environment of the lab has made the move to the University easier, while also providing the encouragement and patience in training to work independently in the lab. I am grateful to have known each of you

Finally, I would like to dedicate this thesis to my amazing parents Laurie and Manfred Gerber. Your unconditional love, support, and belief in me have carried me through every obstacle throughout this journey. Thank you for always encouraging me to follow my goals and never doubting my ability to pursue a Masters degree in a new city. Your unwavering support has

allowed me to overcome many challenges throughout these few years and contributed to my completion of this Master's program.

DEDICATION

To my wonderful parents,

Thank you for your unwavering love and support in the pursuit of my academic goals. Thank you for encouraging me to always be my best self.

With all my love,

Nicole

TABLE OF CONTENTS

LIST OF TABLES

LIST OF FIGURES

ABBREVIATIONS

~	Approximately
°C	Degrees Celsius
>	Greater than
≥	Greater than or equal to
<	Less than
%	Percent
µg	Microgram(s)
µL	Microliter(s)
µm	Micrometer(s)
µM	Micromolar
2D	Two-dimension
3D	Three-dimension
5-FU	5-Fluorouracil
aa	Amino Acid(s)
AJCC	American Joint Committee on Cancer
ATP	Adenosine triphosphate
APC	Adenomatous Polyposis Coli
ATCC	American Type Culture Collection
BCA	Bicinchoninic Acid
BioID	Biotin Identification
BirA	Biotin Protein Ligase
bp	Base Pair(s)
BRAF	B-Raf Proto-Oncogene, Serine/Threonine Kinase
BSA	Bovine Serum Albumin
CCNE1	Cyclin E1
ccRCC	Clear Cell Renal Cell Carcinoma
CCS	Cosmic Cal Serum
CIMP	CpG Island Methylator Phenotype
CIN	Chromosome Instability
cm	Centimeter(s)
CNV	Copy Number Variations
CO_2	Carbon Dioxide
CPTS	Copper phthalocyanine 3, 4', 4", 4'''-tetrasulfonic acid tetrasodium salt
CRC	Colorectal Cancer
CT	Computed tomography
CUL1	Cullin 1
DAPI	4', 6-Diamidino-2-Phenylindole
DMEM	Dulbecco's Modified Eagle Medium
DSB	Double-strand Break
EDTA	Ethylenediaminetetraacetic Acid
EGFR	Epidermal Growth Factor Receptor
FAP	Familial Adenomatous Polyposis
FBS	Fetal Bovine Serum
FISH	Fluorescence in situ Hybridization

FIT	Fecal immunochemical test
FOLFIRI	Folinic acid, 5-fluorouracil, irinotecan
FOLFOX	Folinic acid, 5-fluorouracil, oxaliplatin
g	gravitational force
GTP	Guanosine 5'-triphosphate
h	Hour(s)
HRP	Horseradish Peroxidase
HNPCC	Hereditary Non-polyposis Colorectal Cancer
IVIS	In Vivo Imaging System
KCl	Potassium Chloride
KIF11	Kinesin Family Member 11
KM	Kaplan-Meier
KS`	Kolmogorov-Smirnov
KRAS	Kirsten Rat Sarcoma Virus Oncogene
MAP	MUTYH Polyposis
MAPK	Mitogen-activated Protein Kinase
Min	Minute(s)
mL	Milliliter(s)
mM	Millimolar
MMR	Mismatch Repair
MN	Micronuclei
MSI	Microsatellite Instability
MSS	Microsatellite Stable
MW	Mann-Whitney
N_2	Nitrogen
ng	Nanogram(s)
NK	Natural Killer
nm	Nanometer(s)
NSG	NOD scid gamma
O_2	Oxygen
PBS	Phosphate Buffered Saline
PCM	Pericentriolar Material
PFA	Paraformaldehyde
PGCC	Polyploid Giant Cancer Cell
PI3K	Phosphoinositide 3-Kinase
rpm	Revolutions per minute
RT	Room Temperature
RIPA	Radioimmunoprecipitation Assay
s	Second(s)
SCF	SKIP1-CUL1-F-box
SDS	Sodium Dodecyl Sulfate
SLBP	Stem-loop Binding Protein
scQUANTIM	Single-cell Quantitative Imaging Microscopy
scWGS	Single-cell Whole-genome Sequencing
SKY	Spectral Karyotyping
SV	Structural Variant

TCGA	The Cancer Genome Atlas
TBS	Tris-buffered Saline
TBS-T	Tris-buffered Saline with Tween-20
TP53	Tumor Protein p53
VEGF	Vascular Endothelial Growth Factor
V	Volt(s)
vs	Versus
WNT	Wingless-related Integration Site

USED WITH PERMISSION

PREFACE

This thesis contains materials, images and/or ideas from one article published in the peer-reviewed journal *Cells*. This journal applies the open-access Creative Commons Attribution (CC BY) license, in which no permission is required to reuse any published material if the original article is properly cited.

CHAPTER 1: INTRODUCTION

1.1. COLORECTAL CANCER OVERVIEW

Colorectal cancer (CRC) is a multi-factorial disease that impacts millions of individuals worldwide. CRC is the third most commonly diagnosed and second most lethal cancer, accounting for ~10 % of all cancer cases globally[1]. The name is derived from its tissues of origin, the colon and rectum, and develops through the accumulation of genetic and epigenetic mutations and other contributing factors, such as lifestyle choices, high-risk behaviors, and environmental exposures. Despite the improvement to screening methods and current therapeutic approaches that have ultimately improved CRC patient outcomes, it still remains a major global health concern.

1.1.1. Incidence and Survival

The global pattern of CRC incidence reflects a complex mosaic of diverse risk factors influenced by a transition to the Western lifestyle in countries undergoing significant economic growth[2]. According to the World Health Organization, in 2020 alone, approximately (~) 1.9 million individuals were diagnosed and ~930,000 succumbed to the disease[3]. By 2024, it is estimated by the International Agency for Research on Cancer that the CRC burden on the global population will markedly rise by 63 percent (%) to 3.2 million diagnoses and by 73 % to 1.6 million deaths[3]. Although the risk of CRC increases with age (> 50 years), there is a concerning increase in individuals under 50 years of age being diagnosed with CRC and the etiological events driving early-onset CRC remain unknown[4]. Incidence and mortality of CRC varies by geographical distribution (*i.e.*, continent) but also between ethnic groups within the same country, suggesting a close relation to risks factors associated with CRC. For example, Europe has the highest incidence (30.4%) of CRC succeeded by Oceania (29.8%) and North America (26.2%), whereas incidence rates are lower in Asia (17.6%), Latin America/Caribbean (16.6%) and Africa (8.4%)[1]. In regards

to geographical distribution of CRC mortality rates, Europe is leading at 12.3%, followed by Oceania (9.3%) with lower mortality rates in Asia (8.6%), Latin America/Caribbean (8.2%), North America (8.2%), and Africa (5.6%)[1]. Geographical location is a determinant of CRC incidence and mortality rates and must be taken into consideration for research studies.

In Canada, CRC is the fourth most diagnosed and second most lethal cancer that poses a significant burden to the healthcare system, in which approximately 25,200 individuals were diagnosed and 9,400 people died in 2024[5]. Men are also at a greater risk of being diagnosed with CRC with 1.3 times greater incidence and mortality compared to women[5]. Additionally, CRC in Canada presents notable disparities in disease burden stemming from numerous factors, including socioeconomic status, racial and ethnic backgrounds, healthcare accessibility, and geographical location in the provinces or territories[6,7]. Individuals that live in rural areas and/or socially economically disadvantaged groups face challenges in accessing healthcare, such as CRC screening methods that delay diagnoses and lead to poorer patient outcomes[7]. Notably, African-Americans, Hispanics, and Indigenous populations experience higher CRC incidence and mortality rates compared to Caucasians (*i.e.*, individuals of European descent)[7]. Thus, there is a dire need to address these disparities in the Canadian healthcare system amongst the highly diverse population to improve CRC patient outcomes for the general public. Despite effective screening methods for early detection, approximately half of all Canadians determined to have CRC will be diagnosed at late disease stages (stage III or IV), when treatment options are limited. Therefore, gaining a better understanding of molecular mechanisms driving CRC development are essential to develop novel screening methods and therapeutic strategies aimed at improving overall patient outcomes.

1.1.2. Initiation and Progression of Colorectal Cancer

The anatomical landscape of the large intestine (*i.e.*, colon) is vital to understanding the origins and physiological implications of CRC. The colon is subdivided into several distinct regions known as the cecum, ascending colon, transverse colon, descending colon, sigmoid colon, and rectum (Fig. 1-1). However, the heterogenous nature of CRC tumors is influenced by etiological factors (see Section 1.1.3.) and mechanisms underlying CRC development. As shown in Figure 1-1, the colon is subdivided into two distinct regions, the proximal (cecum, ascending colon, and 2/3 transverse colon) and distal (1/3 transverse colon, descending colon, and sigmoid colon) colon to differentiate the molecular heterogeneity underlying CRC development within the tissue of origin. CRC development is a multi-step process defined by four stages: initiation, promotion, progression, and metastasis[2,8] (Fig. 1-2). The initiation stage takes place over decades and consist of the acquisition of irreversible genetic mutations in genes governing cellular proliferation, such as tumor suppressor genes and oncogenes[2]. During the promotion stage, the cells will undergo successive divisions forming small benign neoplasms (*i.e.*, adenomas) with the potential to progress into malignancies[2]. Following promotion, the adenomas will continue to grow and proliferate into larger adenomas gaining additional genetic and epigenetic alterations to promote malignancy[2]. During progression, once the adenoma has invaded the basement membrane, it is considered malignant and will continue to grow and proliferate acquiring invasive and metastatic capabilities[2]. In the final metastatic stage, cancer cells will disseminate from the primary tumor (adenoma carcinoma) to distant tissues through the circulatory or lymphatic systems[2]. As observed in patients, the temporal stratification of these stages can differ greatly, with the entire process occurring over the span of decades. Hereditary forms of CRC may accelerate through these stages more rapidly due to previously existing mutations within the cells that did not arise sporadically[2,8].

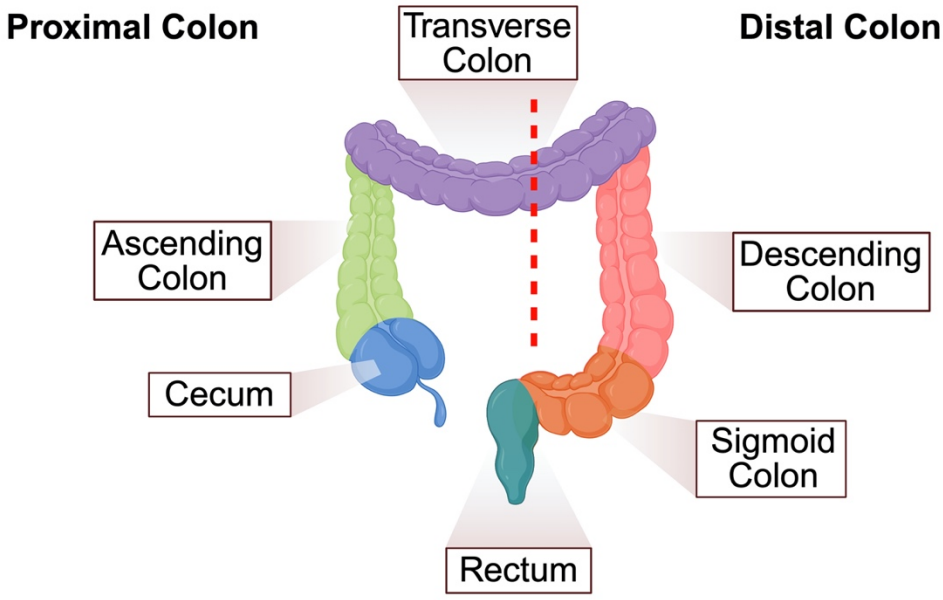

Figure 1-1. Anatomical Organization of the Colon and Rectum.
Schematic depicts the distinct regions of the colon, excluding the appendix. The proximal (right-sided) colon consists of the cecum (blue), ascending colon (light green), and 2/3 transverse colon (purple). The distal (left-sided) colon comprises of 1/3 transverse colon (purple), descending colon (pink), and sigmoid colon (green). Red dashed line highlights the division between proximal and distal colon. Figure was generated using BioRender.

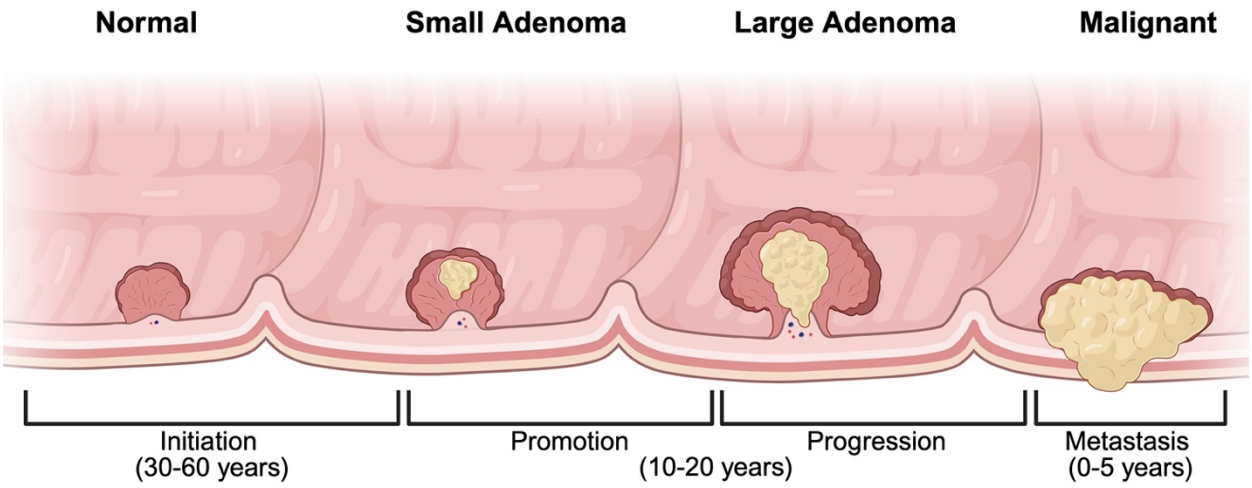

Figure 1-2. Initiation and Development of CRC.
Schematic depicting the initiation and development of CRC pathogenesis through four distinct stages: initiation, promotion, progression, and metastasis. Figure was generated using BioRender.

1.1.3. Genetic, Sex, Behavioral, and Environmental Risk Factors

CRC is a complex disease with several risk factors including inherited genetic predispositions to sex, age, behavioural, and environmental factors. While age and inherited predisposition set a baseline risk, sex, lifestyle, and exposures can substantially shift an individual's trajectory, both in terms of whether CRC develops and at what age it presents. Understanding these complexities is crucial for assessing risk stratification, prevention strategies, and explaining the geographic and temporal distribution in CRC incidences worldwide. Sex influences CRC incidence and mortality. Overall, men have a 1.5-fold higher incidence of CRC than women at most ages, and they more frequently develop distal and rectal tumors, whereas women typically present with proximal right-sided CRC tumors[3,8,9]. Endogenous estrogens and hormone replacement therapy appear to confer some protection by mechanisms not yet defined, which may account for the sex differences in CRC incidence and mortality between men and women, especially before advanced age[8,10,11]. Sex is also linked to other risk factors, such as obesity, diabetes, smoking and alcohol consumption, indicating that the same exposure can cause different outcomes in men and women[3,8,9].

Behavioral factors are among the most modifiable determinants of CRC risk. Diets high in red and processed meat, high in animal fat, and low in fiber, fruits, and vegetables are consistently associate with increased risk in CRC development, likely through carcinogenic nitroso compounds, heterocyclic aromatic amines and polycyclic aromatic hydrocarbons, secondary bile acids, and microbiome alterations[8,9,12,13]. Additionally, physical inactivity, sedentary lifestyle, and obesity further elevate risk of CRC by promoting insulin resistance and chronic low-grade inflammation, all of which can drive colorectal carcinogenesis[3,8,13]. Environmental and medical exposures can also contribute CRC risk factors. Long-standing inflammatory bowel disease (*e.g.*,

ulcerative colitis or Crohn's colitis) is a well-established risk factor, influenced by the duration of the chronic disease, the extent of colonic involvement, and the inflammatory burden [3,8]. Prior abdominopelvic radiation, especially at a young age, also increases the risk to develop CRC later on due to DNA damage induced by the radiation[3,9]. Newly emerging risk factors are intestinal microbiota and psychosocial stress, with accumulating evidence that chronic stress-related signaling can modulate inflammation burden, increase epithelial cell turnover, and increase rate of sporadic mutations in the colon[3,8,13]. Collectively, these sex-specific, behavioral, and environmental risk factors define a complex heterogenous network to improve early intervention and screening programs for CRC, especially in high-risk individuals.

1.1.4. Screening

In early stages of the disease, CRC patients often do not present with clinical manifestations of the disease or display non-specific signs causing difficulties in diagnosing and treatment. Screening methods for early CRC detection include the fecal immunochemical test (FIT) and colonoscopies. Screening is crucial in improving survival outcomes by identifying early asymptomatic CRC patients when therapeutic strategies are more aggressive (*i.e.*, surgery) and have greater success of eradicating the precancerous lesions (*i.e.*, polyps) or cancerous tumors[14]. Globally, it is proven that widespread screening programs have led to decreased CRC mortality rates[14].

In Canada, every province and territory are responsible for establishing colon screening programs that adhere to the Canadian Task Force on Preventative Health Care guidelines to screen individuals at average risk for CRC between the ages of 50 to 74 using stool-based assays as a first-line test[15] . Currently, all provinces and Yukon have established colon screening programs, while the Northwest Territories and Nunavut are undergoing planning and development to launch

their own screening programs[15]. As mentioned above, there exist several different stool-based tests for CRC screening; however, FIT has become the preferred test with high sensitivity and specificity that is not affected by diet[16]. FIT is a simple, at home cancer-screening test with high specificity for blood in the stool by using antibodies that target human hemoglobin to identify a common symptom of CRC[16]. As a tumor continues to grow and invade surrounding tissue, it leads to the rupturing blood vessels or eroding of the tissue resulting in blood entering the colon during the passage of stool[16].

The standard procedure in Canada following a positive identification of hemoglobin in the stool is performing a colonoscopy. Colonoscopies are the gold-standard for direct visualization of the colon to identify precancerous growths (*i.e.*, adenomas and sessile serrated lesions) for removal (*e.g.,* polypectomy) and prevention of CRC[16]. Thus, colonoscopy screening can reduce both CRC incidence and mortality yet remains highly invasive and burdensome to the patient[16]. Other visualization modalities that exist for CRC screening include sigmoidoscopy and computed tomography (CT) and may be used as alternatives to colonoscopies depending on medical contraindications or patient factors.

1.1.5. Diagnoses and Staging

CRC is typically asymptomatic in early development, reflected by ~ 50% of individuals diagnosed at advanced stages of the disease, stages III and IV[17], when symptoms present and therapeutic strategies are severely limited. Generally, an initial CRC diagnosis is determined using colonoscopy to extract tissue samples *(e.g*., biopsy) that undergo microscopy examination for histological confirmation of diagnosis. Biopsies are stained with hematoxylin and eosin and examined under a microscope to evaluate morphological features, such as presence and depth of tissue invasion, glandular architecture, disappearance of glands, cell polarity, and presence of

desmoplastic reacts to determine the deviation from normal tissue to a malignancy[18]. In the case of positive CRC identification, the tumor is further examined using CT of the chest, abdomen and pelvis for preoperative evaluation, staging, and therapeutic strategy[19]. Currently, CRC tumors are staged using the American Joint Commission on Cancer (AJCC) TNM system, which is the most commonly used tool globally to predict the survival of CRC patients[19,20]. The system incorporates the following factors, tumor depth of invasion (T), regional lymph node involvement (N), and distant metastasis (M) to determine tumor staging (0-IV) to predict a patient's prognosis[19,20]. Briefly, stage I describes the earliest stage of CRC progression, in which the tumor has only infiltrated the basement membrane[21]. Stage II exhibits larger tumors with no lymph node invasion or metastasis, while stage III defines CRC tumors that have infiltrated the proximal lymph nodes[21]. Lastly, stage IV describes tumors that have metastasized to distant tissues[21]. Approximately 20% of individuals diagnosed with CRC exhibit metastasis (*i.e.*, stage IV) and the most common sites of distant CRC metastasis are found in the liver, lung, and peritoneum[22]. Metastatic CRC remains a significant burden with a low ~14% 5-year survival rate, and limited treatment options that ultimately led to poor patient prognosis[23]. Therefore, establishing models for precise CRC staging enables the development of more accurate prognostic and therapeutic approaches.

1.1.6. Treatment Strategies

CRC treatment is highly dependent on the disease stage, molecular subtype of the tumor and localization of the tumor from time of diagnosis. For stage 0 and I CRC tumors, surgical excision of the malignant polyps (*i.e.,* polypectomy) or removal of the diseased section of the colon and a small portion of the surrounding healthy tissue (*i.e.,* partial colectomy) are standard procedures[9,24-26]. However, for all non-metastatic CRCs tumor depth invasion will highly influence the treatment modality and complete resection of the lesion including ~5 cm margin of adjacent

normal tissue remains the standard of care[24,25]. Following excision of the tumor and diseased tissue, healthy colon tissues can be reattached to maintain normal digestive functions, otherwise if not enough of the colon remains, a temporary or permanent colostomy with an external bag may be placed[24,25]. To reduce recurrence risk of CRC in stages II and sometimes stage III, surgeries are often coupled with adjuvant chemotherapies to ensure the removal of any residual cancer cells[24].[27] For higher stages of CRCs, regional lymph nodes may also be removed depending on the severity[25]. However, treatment efficacy becomes severely limited at stage IV and usually depends on chemotherapeutics to shrink the tumor bulk then attempt surgical removal[24,26]. First line chemotherapy treatment for CRC is comprised of a standard regimen of two 5-fluorouracil-based cytotoxic drugs, namely folinic acid, 5-fluorouracil (5-FU), along with oxaliplatin (FOLFOX) or irinotecan (topoisomerase I inhibitor; FOLFIRI)[24,26,28]. 5-FU is a fluoropyrimidine that inhibits thymidylate synthase, an enzyme required for nucleotide synthesis[27]. Folinic acid (leucovorin) stabilizes 5-FU to further enhance its effects while oxaliplatin inhibits DNA replication in cancer cells by inducing intra-strand crosslinks in DNA[24]. Lastly, FOLFIRI, utilizes irinotecan, a topoisomerase I inhibitor that prevents DNA re-ligation and interferes with the replication fork, resulting in the accumulation of double-stranded breaks to induce cell death[24]. While chemotherapeutic treatment strategies overall improve survival outcomes, these are often associated with severe side-effects, such as nausea, vomiting, diarrhea, neutropenia, and hepatotoxicity that can cause extreme discomfort to the patient and decline in the quality of life[24,26,28].

Targeted therapies take advantage of specific features of the cancer cells along with standard chemotherapies to mitigate chemoresistance while inhibiting the growth and progression of the cancer. The two most common molecular targets of CRC include vascular endothelial growth

factor (VEGF) and epidermal growth factor receptor (EGFR), which are often overexpressed in CRC [27]. Targeted therapies utilize inhibitors of VEGF and EGFR, such as cetuximab, panitumumab bevacizumab, to effectively treat patients with distal CRCs and with wild-type *Kirsten Rat Sarcoma Virus Oncogene* (*KRAS*)[24,27,29]. Immune checkpoint inhibitors, such as nivolumab, pembrolizumab and ipilimumab have exhibited to be effective against proximal colon tumors exhibiting DNA mismatch repair deficiencies[24,27,29-31]. Although these treatments are usually well tolerated, several patients have reported adverse immune responses in non-cancerous cells, causing autoimmune thyroiditis, hepatitis, pancreatitis, and acute kidney injuries[30,31]. Additionally, immune checkpoint inhibitors do not elicit a response in distal tumors or those with sufficient DNA mismatch repair mechanisms[24,27,29-31]. Hence, a greater understanding of the molecular mechanisms promoting the different CRC tumor subtypes is crucial to develop novel treatment strategies that improve the quality of life and outcomes of all patients.

1.2. MOLECULAR PATHOGENESIS OF CRC

CRC is a heterogenous tumor that can arise from underlying mechanisms associated with the type of precursor lesion, tumor location, and risk factors (see Section 1.1.3.). Inherited CRC syndromes are attributed to rare monogenic disorders, including Lynch syndrome (formerly known as hereditary non-polyposis colorectal cancer; HNPCC), familial adenomatous polyposis (FAP), and MUTYH polyposis (MAP) that account for ~5% of all CRC cases[32,33]. The other ~95% of cases are attributed to sporadic CRCS that development through a predicted sequence of genetic mutations known as the adenoma-carcinoma pathway[34]. It was determined that multiple genetic alterations are required for tumorigenesis and genome instability is a critical cellular mechanism that accompanies the acquisition of genetic mutations of the adenocarcinoma sequence[34].

Accordingly, genome instability in CRC has been classified into three distinct subtypes: chromosome instability (CIN), microsatellite instability (MSI), and CpG island methylator phenotype (CIMP), as described below.

1.2.1. Adenoma to Carcinoma Pathway

Under physiological conditions, the majority of sporadic CRC tumors arise from pre-cancerous polyps categorized as traditional tubular adenomas or serrated polyps[35]. The colon epithelial undergoes constant renewal from colon epithelium sloughing (*i.e.*, continued loss of epithelial cells from the intestinal mucosa) which increases the frequency for adenoma development from dysregulated DNA replication and repair mechanisms[35]. First proposed by Fearon and Vogelstein in 1990[36], the adenoma-carcinoma sequence is a multi-step genetic model of CRC pathogenesis. This model follows three key principles: 1) multiple genetic mutations are needed; 2) there are discrete intermediates in the progression of CRC; and 3) CRC development is dependent on the temporal acquisition of the genetic mutations[34]. The classical genes involved in the adenocarcinoma pathway model are *Adenomatous Polyposis Coli* (*APC), KRAS*, and *Tumor Protein p53* (*TP53*), in which mutations in these genes are required to produce a malignant tumor[34,35]. The inactivation of tumor suppressor gene *APC* or mutation *BRAF* oncogene, are the initiating event of the adenocarcinoma sequence that give rise to the development of traditional adenoma polyps or serrated polyps respectively[35]. Depending on the specific pathway engaged (*i.e.*, the initiating mutation), the subsequent mutations may vary depending on the molecular subtype of the tumor. Following *APC* inactivation, an activating mutation in the *KRAS* oncogene is usually next in the adenocarcinoma sequence to subsequently drive additional mutations in beta-catenin, PI3K, and finally *TP53* inactivation[34]. However, it is important to note that not all CRCs

follow this predicted pattern of genetic alterations or present with every mutation described in the adenocarcinoma pathway model.

1.2.1.a. *APC*

The majority of CRC tumors, ~80-90% contain inactivating mutations in *APC*, which normally functions as a tumor suppressor[37]. Individuals with specific germline mutations in *APC* develop early onset CRC known as inherited FAP, normally before the age of 35 and accounts for more than 600,000 deaths[37], rendering an interest in developing strategic therapeutics to exploit *APC* alterations. APC regulates critical cellular processes, including mitosis, migration, and maintenance of genome stability[37,38]. More specifically, APC is a member of a multi-protein complex that regulates wingless-related integration site (WNT) signalling pathway by promoting the localization and proteosome degradation of transcript factor beta-catenin[37,38]. *APC* mutations lead to nuclear accumulation of beta-catenin and increased transcription of oncogenes to promote CRC carcinogenesis[39,40]. As such *APC* truncations correlate with the constitutive activation of the canonical Wnt signaling pathway leading to widespread hyperproliferation and differentiation in the gastrointestinal tract and promoting early CRC development[38,40]. Although 100% of germline mutations in *APC* underlies FAP, somatic *APC* mutations are present in ~70% of all sporadic CRC cases[39]. Furthermore, *APC* dysfunction can severely impact mitosis through centrosome and spindle abnormalities that result in the propagation of chromosome segregation defects[41]. It has also been shown that in cultured colon cancer cells with *APC* mutations exhibit high levels of aneuploidy, indicating these cells in response to *APC* depletion do not undergo arrest but progress through mitosis with chromosome segregation defects[41]. Mutations in *APC* disrupts mitotic checkpoints and promotes CIN, thereby endowing cells with survival advantages required for CRC tumorigenesis[41].

1.2.1.b. *KRAS*

KRAS is oncogene of the RAS protein family that plays a critical role in regulating various cellular processes, including growth, differentiation, and survival[42]. It is a guanine nucleotide-binding protein that binds guanosine 5'-triphosphate (GTP) to transduce signals that regulates cell proliferation in both normal and malignant cell types[43]. Under normal physiological conditions KRAS switches between guanosine 5'-diphosphate and GTP-bounds states to activate downstream signalling pathways of proliferation and survival, such as mitogen-activated protein kinase (MAPK) and phosphoinositide 3-kinase (PI3K) pathways[43,44]. *KRAS* mutations occur at high frequency in ~40-50% of all CRCS and often indicates poor prognosis due to resistance to current therapeutic approaches[44,45]. In CRC, the most common point mutations occur in codons 12 and 13 that impact hydrolase activity and cause constitutive signalling activation, ultimately leading to the uncontrolled proliferation of the cancer cells[43-45]. Despite its prevalence across cancer types, *KRAS* mutations underly poor patient outcomes from lack of response to current therapeutic approaches targeting receptor tyrosine kinases or epidermal growth factor receptors[43,44]. Therefore, targeting *KRAS* has proven to be challenging and researchers aim to develop novel therapeutics targeting downstream signalling effectors to mitigate the aberrant effects of constitutive *KRAS* activation.

1.2.1.c. *TP53*

TP53 is a tumor suppressor gene referred to as "the Guardian of the Genome" as it monitors for stress signals to mediate different cellular responses, such as DNA repair, cell cycle arrest, or programmed cell death[46]. It is located on the short arm of chromosome 17 (17p13.1) and due to alternative promoters, splicing, and translation sites, p53 has at least twelve different isoforms expressed in a tissue-specific manner[46]. Hence, p53 serves as a multifaceted regulator of cellular

processes including DNA repair, cell cycle arrest, apoptosis, and metabolism to maintain cellular homeostasis and prevent tumorigenesis[47]. Therefore, in cases like cancer where *TP53* is inactive, these regulatory pathways would be ineffective and promote the uncontrolled growth, proliferation, and survival of cells with damaged DNA and propagation to successive daughter cells. *TP53* is the most commonly mutated gene in cancer and is found in ~43% of CRCs[46]. Although *TP53* mutations are primarily somatic and normally caused by environmental factors or sporadic replication errors, a heterozygous germline mutation in *TP53* can led to the rare hereditary disorder known as Li-Fraumeni syndrome, which is marked high risk for early onset of cancers[47]. Contrarily, the prevalence of sporadic p53 mutations varies depending on age of patient, tumor anatomical site, and tumor molecular subtype[46]. *TP53* mutations are more commonly found in younger patients (<40 years old) and in distal CRC tumors (~45%) compared to proximal tumors (34%)[46]. Targeting *TP53* alterations in tumors is a complex issue and proves challenging due to massive side effects from the function of p53 as an activator of apoptosis[46]. Therefore, more research is required to develop effective treatment strategies against *TP53* mutations in different tissues specific contexts to address the complexity of the p53 signalling network.

1.2.2. Molecular Subtypes of Colorectal Cancer

CRC pathogenesis occurs through three distinct mechanisms characterized by CIN, MSI, and CIMP. An important feature of CRC that develop from any of these mechanisms is the emergence of benign precursor lesions (*i.e.*, polyps) that begin as growths in the mucosa epithelium[2,35]. Over decades these lesions can continue to grow and acquire *de novo* mutations to transform into malignant adenomas[2,35]. The classification of the different subtypes reflects the different mechanisms of genome instability, signalling pathway activations, and tumor

microenvironment interactions[2,35]. Taken together, these molecular subtypes are utilized to determine CRC patient prognoses and influence treatment options.

1.2.2.a. Microsatellite Instability and CpG island Methylator Phenotype

MSI and the CpG island methylator phenotype (CIMP) describe two related but distinct molecular pathways of colorectal tumorigenesis. The MSI pathway is mutations in the DNA mismatch repair (MMR) genes (*e.g.*, *MLH1*, *MSH2*, *MSH6*, *PMS2*) that cause instability within the microsatellites regions in DNA[35]. DNA microsatellites are highly repetitive nucleotide sequences that can accumulate errors, as DNA polymerase struggles to function effectively on repeating genomic sequences[35,48]. Under normal conditions, MMR recognized the errors made by DNA polymerase and aims to perform a nucleotide excision prior to replication of the new strand[35]. However, failure of MMR genes, such as in MSI, results in the accumulation of these DNA errors and subsequent propagation into daughter cells for a hypermutation tumor phenotype[35,48]. MSI accounts for ~10-15% of all sporadic CRC tumors and almost all hereditary CRC tumors in Lynch Syndrome patients[35,49]. The most common cause of MSI is the epigenetic silencing of *MLH1* through promoter hypermethylation[35]. As previously mentioned, the initiating events of MSI pathway may vary yet in 35-50% of MSI tumors observe *APC* as the initiating event, which is a common feature of CIN tumors, while the other remaining tumors form via *BRAF* mutation[35]. Unlike CIN-based tumors that progress over decades, MSI-high tumors develop over shorter time periods, within 1-3 years, are typically located in the proximal colon, and more responsive to immune-based therapeutic approaches[35]. Therefore, the MSI subtype will influence the progression of CRC, the patient's prognosis, and the treatment options.

CIMP, also described as the serrated neoplasia pathway gives rise to serrated adenomatous polyps and accounts for 15-25% of CRCs[2,49]. It involves extensive epigenetic methylation of

promoter regions, CpG islands, of tumor suppressor genes, resulting in their transcriptional silencing[2,49]. CIMP tumors are strongly associated with *BRAF*^{V600E} mutations as the initiating event for the development of the precursor sessile serrated lesions[49]. The mechanisms underlying CIMP remain poorly understood due to lack of uniformity in the markers delineating the subtype[2]. Although CIMP and MSI are two distinct molecular subtypes, they frequently co-exist in CRC pathogenesis as CpG island hypermethylation can also inactivate MMR genes leading to MSI[2,49]. Most notably, CIMP corresponds with favorable responses to certain chemotherapeutic treatments highlighting the importance of investigating the role of epigenetic modification in therapeutic approaches[2,49].

1.2.2.b. Chromosome Instability

CIN is the major molecular subtype underlying CRC development and accounts for approximately 65-70% of all sporadic CRCS[34,35,49]. It is defined as the accelerated rate of gains or losses of whole or large segments of chromosomes that drives cell-to-cell heterogeneity[50-56]. Despite the majority of CRC cases exhibiting CIN, the underlying molecular mechanisms driving CIN remain largely unknown. CIN-based CRC tumors typically follow the classic adenocarcinoma sequence and are strongly linked to early disruption of the WNT pathway through bi-allelic *APC* inactivation, followed by stepwise accumulation of mutations in *KRAS*, *TP53*, and other gatekeeper and caretaker genes[34,35]. This cumulative copy-number and mutation burden generates extensive intertumoral heterogeneity, promoting cellular transformation, clonal evolution, multi-drug resistance, and metastasis[51,53,56]. Clinically, CIN tumors are usually microsatellite stable (MSS), often located in the distal colon, and correspond largely to molecular characterization, where chromosomal imbalance, rather than mismatch-repair defects, is the dominant driver of genomic instability[57]. Patients with CIN-high tumors often have poorer survival outcomes and

limited therapeutic strategies capable of effectively treating this tumor type[51,56,57]. Therefore, a better understanding of the drivers of CIN in CRC will ultimately led to the development of novel therapeutics to improve overall CRC patient survival.

1.3.CHROMOSOME INSTABILITY AND COLORECTAL CANCER

CIN is a phenomenon that occurs in the majority of sporadic of CRCs. It is defined as ongoing increases in gain or losses of whole chromosomes or large chromosomal fragments during cell division, resulting in aneuploidy and chromosomal rearrangements[50-56]. CIN arises from the dysregulation of several biological processes, including cell cycle checkpoint, DNA replication and repair, and sister chromatid cohesion[51,58]. In CRC, CIN drives the acquisition of copy-number mutations affecting key oncogenes and tumor suppressors, such as *APC*, *KRAS*, *TP53*[2,34,35,49]. CIN-positive tumors typically arise through the "classical" chromosomal instability pathway rather than the MSI pathway and are often associated with the distal colon, poor differentiation in advanced stages, and therapy resistance[51,57]. Due to the fact CIN drives intertumoral heterogeneity, it promotes tumor evolution and certain survival advantages while also being a major challenge for targeted therapeutics, making it a central focus of mechanistic and translational CRC research.

1.3.1. Structural and Numerical CIN

CIN can be broadly divided into two main forms: numerical and structural CIN, which often co-exist in CRC. Numerical CIN refers to an ongoing acquisition of gains or losses of whole chromosomes (*i.e.*, aneuploidy)[59-61]. It is often associated with chromosome segregation errors during mitosis leading to aberrant mitotic spindle assembly, sister chromatid cohesion defects, improper kinetochore–microtubule chromosome condensation defects or abnormal cytokinesis[59,61]. Contrarily, structural CIN refers to the structural changes in chromosomes, such

as gross chromosomal rearrangements comprising of amplifications, deletions, inversions, duplications, and translocations[59-61]. Structural CIN is commonly attributed with replication stress arising from stalled or collapsed replication forks, telomere defects or errors in DNA double-stranded break (DSB) repair[59-61]. Although homologous recombination is the most precise DNA DSB repair pathway, defects within the pathway can disrupt the repair mechanisms and cause an increased reliance on the error prone non-homologous end joining resulting in chromosomal amplifications, deletions, translocations, the formation of extrachromosomal structures, dicentric chromosomes, ring chromosomes, chromothripsis, and large-scale rearrangements[59]. These chromosomal alterations promote tumor heterogeneity, cancer progression, and tumor evolution[59]. Collectively, numerical and structural CIN define the classical CIN pathway, generating the complex heterogeneous karyotypes that characterize most sporadic CRCs.

1.3.2. Techniques to assess CIN

Several techniques are used to study CIN, spanning cytogenetic, molecular, imaging, and computational approaches that detect numerical CIN, structural CIN, or rates of change over cell successive cell generations. Generally, there are two main approaches used to evaluate CIN: first, tracking chromosome numbers within a single cell and progeny over time and secondly, quantitatively assess cellular heterogeneity within a population[54]. Over the past decade, the McManus laboratory has worked to establish single-cell quantitative imaging microscopy (scQuantIM) techniques to assess CIN[62] to address these approaches. However, there exist several other techniques available to evaluate changes in chromosome complements, including cytogenic, sequencing, and live-cell imaging approaches. Conventional karyotyping using G-banding or inverted-DAPI staining can be used to visualize the whole chromosomes in metaphase spreads, revealing aneuploidy, translocations, and heterogeneity when scoring multiple cells[54,63]. Spectral

karyotyping (SKY) and multiplex-banding provide assessment of the whole genome and intrachromosomal structural CIN event[54,63]. Finally, fluorescence *in situ* hybridization (FISH) enables the labelling of specific genes, regions or chromosomes for precise identification of structural abnormalities[54,63]. Single-cell whole-genome sequencing (scWGS) provides the gold standard for resolving cell-to-cell heterogeneity and identifying copy-number variations (CNVs)[54,63]. ScQuantIM enables the detection of CIN-associated phenotypes through DNA counterstaining while imaging flow cytometry is a high-throughput technique that can be paired with FISH to assess structural CIN[54]. Furthermore live-cell approaches can use fluorescently tagged chromatin-associated protein (*e.g.*, CENP-A for kinetochore proteins) to monitor chromosome dynamics and mitotic events or a fluorescent reporter system could be utilized to track specific chromosome gains or losses over successive cell generations[54]. Altogether, there are several methods to evaluate CIN and deciding which technique to use is dependent on what a researcher intends to investigate, the type of experiment, cost, availability of reagents, training and expertise and so much more.

1.3.3. CIN-associated phenotypes

CIN-associated phenotypes are involved in diverse cellular, morphological, and molecular aberrations stemming from ongoing chromosome missegregation events and structural rearrangements during mitosis[64,65]. These include aneuploidy (*i.e.*, change in chromosome numbers), polyploidy (*i.e.*, whole-genome duplication), micronucleus formation, nuclear envelope rupture, and chromatin bridge defects, centrosome amplification, multipolar spindles, and altered nuclear morphology (*e.g.*, enlarged or irregular nuclear areas)[64,65]. These phenotypes not only drive tumor evolution and chemotherapeutic resistance but also serve as quantifiable readouts for studying CIN mechanisms.

1.3.3.a. Polyploidy

Polyploidy refers to cells with more than two complete sets of chromosomes, such as tetraploid (4N) or higher ploidy states, and plays a significant role in CRC progression, therapy resistance, and tumor heterogeneity[66,67]. In CRC, polyploid cells often arise from mitotic errors like cytokinesis failure, endoreplication, or cell fusion, particularly under stress from oncogene activation, replication pressure, or exposure to genotoxic stress from chemotherapy and radiation[66,68]. Polyploid giant cancer cells (PGCCs) are not merely aberrant biproducts from mitotic failure but are a distinct subpopulation of tumor cells that exhibit malignant properties, including increased genomic instability and are capable of acting as stem cell-like characteristics generating viable progeny that drive cancer development and tumor evolution[66,68-70]. PGCCs are found in several cancer types, including breast, colorectal, glioblastoma, melanoma, lung, pancreatic, bladder kidney, and prostate cancer[68,70] and strongly associated with chemotherapeutic resistance, tumor recurrence and metastasis, ultimately leading to more aggressive tumors and poor patient outcomes[66,68-70]. In CRC, polyploidy can promote CIN, as tetraploidization can precede or amplify aneuploidy by doubling the genome before segregation errors[66,68]. Additionally, PGCCs exhibit characteristics, such as altered metabolism, enhanced survival signaling (*e.g.,* upregulated HIF1α), epithelial-mesenchymal transition, and stem-like traits, that enable dormancy, immune evasion, and metastasis[70,71]. Clinically, polyploidy correlates with poor prognosis in CRC, as these cells are resistant to common chemotherapeutic treatments, such as FOLFOX, which induce mitotic slippage leading to polyploid states rather than apoptosis and generate resistant progeny[66]. Studies using HCT116 cells have shown that polyploidy drives tumor reoccurrence, demonstrating their role in acquired resistance and highlighting the need to investigate polyploidy in CIN studies to better understand the mechanisms promoting CRC development and progression[72]. Therefore,

polyploidy is a mechanism that promotes CIN and exhibits key features of CRC development and progression.

1.3.3.b. Micronucleus Formation

Micronuclei (MN) form when whole chromosomes or acentric DNA fragments fail to incorporate into daughter nuclei during cell division, arising from lagging chromosomes or acentric fragment[73,74]. In mitosis, defective kinetochore attachments, spindle assembly defects, or cohesion defects may cause chromosomes to lag behind the properly segregating chromosomes, and cytokinesis may then encapsulate these lagging fragments and or chromosomes in a separate nuclear envelope, generating a micronucleus[73,74]. Alternatively, interphase processes like nuclear budding under replication stress can exclude chromatin from the nucleus[75,76]. MN are a marker of CIN and common in numerous cancer types, including CRC, where elevated MN frequency correlates with aneuploidy, oncogenesis, tumor grading, and poor patient prognoses[74,77,78]. In CRC, MN often arise from the classical CIN pathway from either numerical CIN (*e.g.*, aneuploidy) and structural CIN (*e.g.*, chromothripsis) or both. MN rupture is a seminal event and occurs in 40-50% of MN at any time as their nuclear envelope is fragile due to defective Lamin B1 assembly or persistent Aurora B signaling, exposing DNA within the MN to cytoplasmic nucleases and activating cGAS-STING inflammation[73,74,77]. In cancer progression, ruptured MN drive chromothripsis, a process described by localized shattering and rearranging of DNA to cause numerous mutations instantaneously[79]. Additionally, in the CRC context, MN are associated with heterogeneity, CRC pathogenesis and most recently linked to therapy resistance, as MN cells survive standard chemotherapeutics like FOLFOX by slippage into polyploidy, then spawn resistant aneuploid progeny[77,80]. MN can also trigger antitumor immunity and promote metastasis

through chronic NF-κB signaling and immune exhaustion[77,80]. As such MN assays serve as quantitative measures of CIN in CRC research and a biomarker of cancer in preclinical screening.

1.3.3.c. Aneuploidy

Aneuploidy defines a cell state that possess an abnormal number of chromosomes, deviating from the diploid (2N) karyotype by gains or losses of one or more whole chromosomes or chromosome arms[64,81-83]. It can arise from CIN, which drives chromosome missegregation events during mitosis through errors like defective kinetochore attachments, spindle multipolarity, or cell cycle checkpoint defects[64,82,83]. Although aneuploidy is rare in normal tissues as it triggers p53-mediated apoptosis or senescence, it is present in 70–90% of solid tumors[64,83]. In cancer, aneuploidy displays a dual role by promoting fitness from gene dosage imbalances that slow proliferation, and heighten sensitivity to stress, while simultaneously providing survival advantages by amplifying oncogenes or deleting tumor suppressor genes[83]. This phenomenon describes the "just-right" CIN model, in which intermediate aneuploidy optimize adaptability without lethality, to promote intratumor heterogeneity, metastasis, and drug resistance yet high levels of aneuploidy would be lethal to the cells[56,64,84]. HCT116 cells are an example of this phenomenon, in which their near-diploid karyotype demonstrate how aneuploidy sustains oncogenic signaling and optimize growth while tolerating perpetual genome flux[64]. In CRC, ~90% of tumors exhibit aneuploidy and often present with similar patterns of chromosome gains and losses[83]. Therefore, understanding the mechanisms of aneuploidy in cancer cell fitness and CRC pathogenesis will enable the development of better therapeutic treatments to ultimately improve patient outcomes.

1.4. THE SCF COMPLEX AND F-BOX PROTEINS

The Skp1-Cullin1-F-box (SCF) complex is an E3 ubiquitin ligase that plays a central role in targeting specific proteins for ubiquitin-mediated degradation by the 26S proteasome[85,86]. It consists of a conserved core made up of the scaffold protein CUL1, the adaptor SKP1, and the RING finger protein RBX1, which recruits the E2 ubiquitin-conjugating enzyme, plus a variable F-box protein that confers substrate specificity by binding phosphorylated targets[85-88]. By assembling hundreds of distinct E3 ubiquitin ligase complexes through different F-box proteins, SCF controls the timely turnover of key regulators of the cell cycle, transcription, and signaling pathways, thereby maintaining genome stability and ensuring orderly progression through the cell cycle.

1.4.1. Ubiquitination and The SCF Complex

Ubiquitination is a post-translational modification that regulates several key cellular processes, including proteolytic degradation, protein localization, DNA repair, chromatin remodeling, and cell cycle checkpoints[85,86,89]. The covalent attachment of ubiquitin to a protein substrate is achieved through three enzymatic actions: 1) E1, the ubiquitin-activating enzyme that activates available ubiquitin molecules and transfers them to E2; 2) E2, the ubiquitin-conjugating enzyme that brings the ubiquitin molecule to the SCF complex and in close spatial proximity to the substrate; and 3) E3, ubiquitin ligase enzyme that attaches the ubiquitin moieties to the target substrate. The ubiquitination of target substrates occurs through a two-step process[85-87]. First, E1 activates free ubiquitin molecules and transfers to E2 to bring the ubiquitin within close spatial proximity to the target substrate[85-87]. Next, the F-box protein will bind their associated target and recruit it to the complex to be polyubiquitinated[85-87]. The fate of the substate protein, such as degradation by the 26S proteosome is determined by the site of ubiquitin attachment (*i.e.*, lysine residues) and whether

the protein is mono- or poly-ubiquitinated[85]. For example, target proteins polyubiquitinated at lysine-48 are typically targeted for degradation by the 26S proteosome[85,90]. Whereas proteins polyubiquitinated at lysine-63 are known to regulate cells signaling in endocytosis, apoptosis, and kinase activity[85]. However, mono-ubiquitination is normally reserved for signaling pathways that promote DNA repair and chromatin remodeling[85]. As such, the F-box protein is crucial for conferring substate specificity and binding to the E3 ligase for subsequent proteolytic degradation to regulate important cell functions at the protein level[85-87,91]. Since the SCF complex regulates many critical biological processes, it is unsurprising that abnormal SCF complex functions can lead to pathogenetic events promoting cancer, including CRC development.

There exist over 600 E3 ubiquitin ligases predicted to be encoded by the genome, which are characterized into four major families: 1) RING-type, 2) HECT-type, 3) U-box type, and PHD-finger type[85,86,91]. The RING-finger type E3 ligases are further classified into subfamilies, with the largest subfamily comprising of Cullin-based, RING-finger type E3 enzyme[85,86,91]. The SCF complex is comprised of three invariable core subunits SKP1, CUL1, and RBX1 and one of 69 F-box proteins that confer substrate specificity, including FBXO30 (see Fig. 1-3) [85-88]. RBX1 recruits E2 conjugating enzyme to the complex to bring the ubiquitin in close spatial proximity, while CUL1 acts as the adaptor to physically link RBX1 to SKP1, and SKP1 binds the variable F-box protein subunit that recruits the target substrate to the complex[85-88]. Dysfunction of the SCF complex has been linked to the development of several cancers, thereby highlighting the importance of investigating the molecular mechanisms underlying the abnormal complex function to better understand the etiological events promoting CRC development.

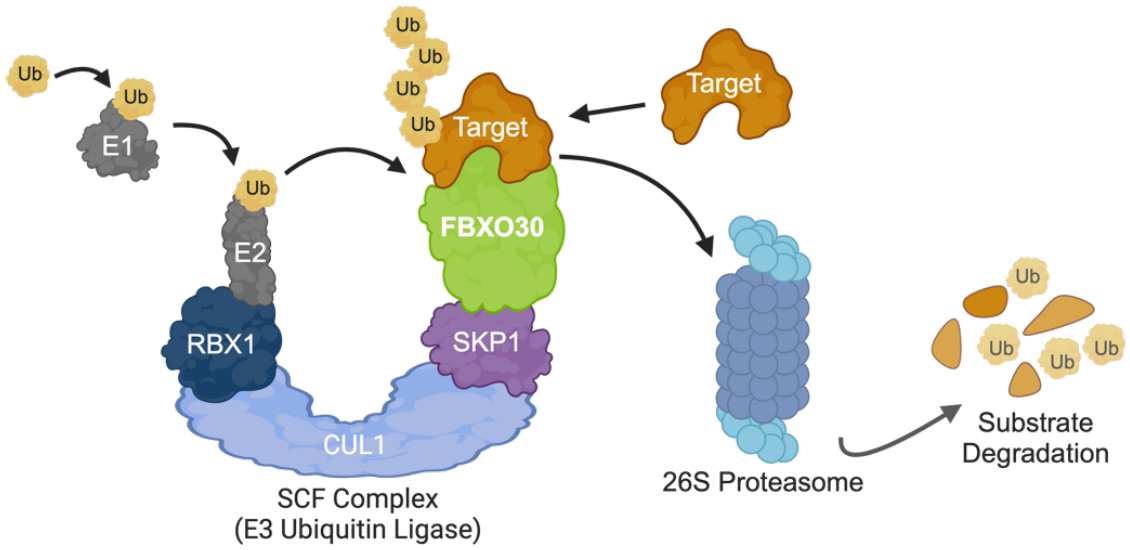

Figure 1-3. The SCF Complex with FBXO30 Subunit Targets Substrates for Proteolytic Degradation by the 26S Proteosome.
Schematic shows the four main components of the SCF complex, SKP1, CUL1, RBX1, and the variable F-box protein (*e.g.*, FBXO30). FBXO30 binds substrates for poly-ubiquitination by the SCF ubiquitin E3 ligase complex and subsequent degradation by the 26S proteasome. Figure was generated using BioRender.

1.4.2. The SCF complex Involvement in CRC Development

Recent data from the McManus laboratory has identified core members, *SKP1*, *CUL1*, and *RBX1*, of the SCF complex as novel CIN genes in the CRC cancer context[85,90,92]. In each case, reduced expression of each gene induced significant increases in CIN-associated phenotypes. Both transient siRNA-based silencing and CRISPR/Cas9 approaches were utilized to quantify the impact of gene copy number losses on different CIN phenotypes. The short- term siRNA-based assays demonstrated that reduced expression of all three core SCF complex members induced CIN, whereas, longer-term CRISPR/Cas9 studies revealed the dynamic and heterogynous nature of CIN phenotypes within heterozygous knockout clones compared to the control[85,90,92]. Semi-quantitative western blots also showed that reduced expression of each core SCF complex member resulted in the accumulation of Cyclin E1 (*CCNE1*), confirming *CCNE1* is an established target of the SCF

complex[92]. *CCNE1* is an oncogene implicated with cell cycle dysregulation, genome instability and cellular transformation[92]. Additionally, phenotypic rescue experiments co-silencing each of the core SCF complex members with Cyclin E1 revealed that reduced *SKP1*, *CUL1*, and *RBX1* expression adversely impacted the SCF complex leading to Cyclin E1 accumulation and ultimately CIN[85,92,93]. However, during these experiments only partial phenotypes were recovered suggesting there are other mechanisms (*i.e.*, other unknown substrates) contributing to CIN phenotypes. Recent studies from the McManus laboratory have not only identified core SCF complex members as CIN genes but have also identified the following F-box proteins, *FBXO7*, *FBXO5*, and *SKP2* as novel CIN genes using siRNA-based silencing and CRISPR/Cas9 approaches in which their reduced expression induced CIN and cellular transformation in colonic epithelial cell contexts[53,55,94]. Collectively, these findings suggest the role of SCF complex functions in cancer development yet the impact that the variable F-box proteins have on CIN, cellular transformation, and CRC development remains to be examined.

1.4.3. The F-box Proteins

The F-box proteins are a variable subunit of the SCF complex that confers substrate specificity. There exist 69 different F-box proteins in humans named after the conserved ~40 amino acid F-box motif that facilitates binding to the SCF complex through SKP1 (see Fig. 1-4)[85,86,88]. The F-box proteins are classified into three subfamilies based on their substrate binding domain. FBXW is the smallest subfamily consisting of only 10 proteins with WD (tryptophan-aspartic acid) amino acid repeats domain[88,91]. FBXL consists of 22 members with leucine-rich repeat domains[88,91]. Lastly, FBXO is the largest subfamily with 37 F-box proteins comprising of diverse unidentified domains[88,91]. Conceptually, since there exist 69 different F-box proteins there are essentially 69 unique SCF complexes with distinct protein substrates specificity exhibiting

functional redundancy in which multiple F-box proteins can share the same substrate. It is predicted that F-box proteins regulate up to thousands of proteins to regulate an array of cellular processes, such as cell cycle progression, mitosis, and DNA repair[85,86,89,90]. F-box proteins, such as *FBXO7*, *FBXO5*, and *SKP2*, have been identified as novel CIN genes through studies that examined their reduced expression in non-malignant and malignant colonic epithelial contexts induced CIN-associated phenotypes, including changes in nuclear areas, micronucleus formation, and changes in chromosome numbers[53,55,94].

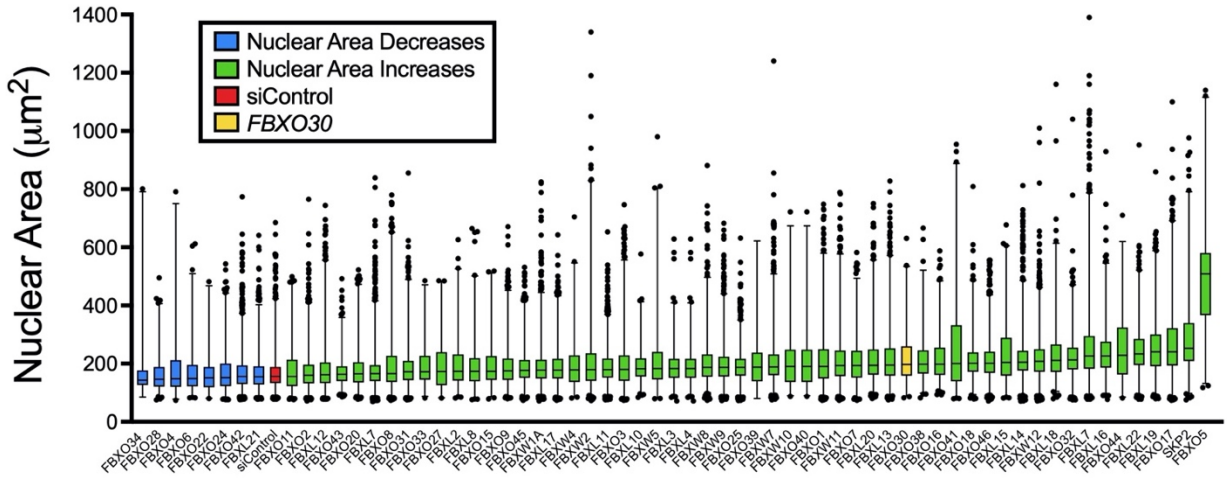

Figure 1-4. Comprehensive siRNA-Based Screen of 64 F-box Proteins.
Box-and-whisker plot presenting F-box genes that when silenced induced statistically significant changes in cumulative nuclear area distribution frequencies relative to the siControl. The putative CIN genes are arranged from decreasing to increasing median nuclear areas with boxes displaying the interquartile ranges (25th, 50th, 75th) and whiskers displaying the 1-99th percentiles. The screen identified *FBXO30* as a potential CIN gene. Screen was performed by Dr. Laura Thompson[55].

1.4.4. F-box only protein 30

FBXO30 is an F-box only (FBXO) protein that serves as the substrate-recognition subunit of the SCF E3 ubiquitin ligase complex, recruiting targets substrates for ubiquitination and timely proteasomal degradation by the 26S proteosome. *FBXO30* is encoded on chromosome 6 and comprises of an uncharacterized F-box domain for binding SKP1 and a zinc finger domain for

diverse substrate interactions[88,91,95]. It localizes primarily to the cytoplasm, with immunofluorescence showing nuclear enrichment in renal cells and oocytes, consistent with roles in chromosome dynamics and transcription factor regulation[96-98]. In physiological conditions where *FBXO30* expression is downregulated in cancers like clear cell renal cell carcinoma (ccRCC), reduced *FBXO30* expression corresponded with tumor progression and poor patient survival[98]. FBXO30 has also been linked to important cellular processes, most notably mitotic fidelity and genome stability. In mouse mammary epithelia cells, *FBXO30* depletion causes kinesin family member 11 (KIF11) accumulation, centrosome amplification, multipolar spindles, polyploidy, and G2/M arrest, ultimately promoting CIN[96]. Additionally, in oocyte meiosis, FBXO30 targeted stem-loop binding protein (SLBP) to prevent histone overload, chromosome overcondensation, and meiotic segregation errors[97]. Finally, *FBXO30* has also been shown to act as a tumor suppressor gene in which its expression in ccRCC inhibits proliferation, migration, invasion, and EMT via ubiquitination of hypoxia-inducible-factor-1-alpha[98]. Collectively, *FBXO30* has been associated with key cellular processes including proper chromosome segregation and genome stability, with the potential to be a novel therapeutic target for CIN-based CRCs.

1.4.5. FBXO30 Substrates and CIN

As mentioned above, FBXO30 is one of the remaining F-box proteins that has yet to be characterized. Therefore, our understanding of FBXO30 is limited and requires further study to evaluate the role of *FBXO30* expression in CIN and CRC pathogenesis. Current evidence reveals that FBXO30 regulates mitotic spindle functions and chromatin dynamics[96,97]. Through timely degradation of substrates like the KIF11 and SLBP, *FBXO30* expression inhibited mitotic and segregation errors that give rise to polyploidy, aneuploidy, and micronucleus formation[96,97]. Thus,

dysregulated *FBXO30* links ubiquitin-mediated proteolytic degradation of target substrates, such as KIF11 and SLBP, to CIN-associated phenotypes, indicating its potential to promote CRC development.

1.4.5.a. Kinesin Family Member 11 (KIF11)

KIF11, also known as Eg5, is a plus-end-directed kinesin motor protein essential for bipolar mitotic spindle assembly and chromosome segregation[99]. Its N-terminal motor domain hydrolyzes ATP to slide antiparallel microtubules apart, crosslinking and separating duplicated centrosomes during prophase and prometaphase to establish spindle bipolarity[99,100]. KIF11 localizes to interpolar microtubules and spindle poles, and its silencing collapses the spindle into monopolar structures, triggering mitotic arrest and apoptosis[99,100]. A study performed by Lui *et al.*, established that SCF^{FBXO30} specifically targeted KIF11 for proteasomal degradation, regulating its cell-cycle oscillation and preventing mitotic defects[96]. FBXO30 binds the C-terminus of KIF11, ubiquitinating an unidentified residue to regulate KIF11 degradation[99]. In *FBXO30*-depleted mammary epithelial cells, KIF11 protein levels rose prematurely *(i.e.*, peaking at S phase vs. M phase in normal cells) in the cell cycle, driving centrosome amplification, multipolar spindles, G2/M arrest, polyploidy, and proliferation defects[96]. Therefore, FBXO30 regulates KIF11 protein levels to ensure mitotic fidelity and genome stability.

1.4.5.b. Stem-Loop Binding Protein (SLBP)

SLBP is the key regulator of histone mRNA metabolism through binding the conserved stem-loop structure in the 3' untranslated region (UTR) of histone H1, H2A, H2B, and H3 mRNAs. SLBP is essential for 3' end processing of these non-polyadenylated pre-mRNAs[97,101]. Beyond processing, SLBP directs nuclear export and rapid degradation of histone mRNAs at S-phase exit, ensuring histone protein levels match DNA replication demands[101]. SLBP levels oscillate with the

cell cycle, peaking in S phase and degrading post-S phase through SCF complex ubiquitin-mediated activity[101]. A recent study showed that FBXO30 directly ubiquitinates SLBP through SCF functions, subsequently regulating SLBP levels to prevent histone mRNA overload during oocyte meiosis and most likely during mitosis[97]. Mass spectrometry and co-immunoprecipitation confirmed that FBXO30 binds SLBP, and *in vivo* Fbxo30 RNAi experiments in mouse oocytes resulted in SLBP accumulation, excess histone H3 loading on chromosomes, chromosome overcondensation, segregation defects, and meiotic arrest[97]. This suggests FBXO30 degrades excess SLBP to balance histone levels and maintain chromosome dynamics.

CHAPTER 2: RATIONALE, HYPOTHESIS, AND RESEARCH AIMS

2.1 RATIONALE

In 2024, CRC remains the fourth most diagnosed and second most lethal cancer in Canada[102]. Despite the availability and success of early screening methods, approximately 50% of patients are diagnosed at late disease stages (stages III and IV)[17], when treatment is limited and survival is severely impacted. Additionally, there is a notable rise in individuals under 50 years of age being diagnosed with CRC. To address these devasting statistics, we need to gain a greater understanding of the underlying mechanisms promoting CRC development. CIN, an enabling hallmark in many cancer types, occurs in ~85% of CRCs. However, the molecular determinants driving CIN and subsequent CRC development remain largely unknown. A comprehensive siRNA-based screen of suspected CIN genes (*i.e.*, F-box proteins), identified *FBXO30* as a potential candidate. Furthermore, of all the 69 F-box proteins evaluated in the siRNA-based screen, *FBXO30* is one of a few F-box genes with copy number losses observed at a high frequency in CRC (see Fig. 4-1), while also severely impacting patient survival (see Fig. 4-3)[103]. This suggests diminished *FBXO30* expression may be involved in the etiological events promoting early CRC development.

Currently, the impact of reduced *FBXO30* expression on CIN and CRC pathogenesis remains unknown. Hence, establishing the impact of reduced *FBXO30* expression in clinically relevant non-malignant and malignant colonic cellular contexts will provide novel insights into the underlying mechanisms driving CIN. Understanding the molecular mechanisms associated with CRC development is critical in developing new therapeutic strategies aimed at improving overall patient outcomes. In this regard, my research project seeks to gain novel insights into the molecular origins of CIN, an early event promoting early CRC development by assessing the effects of

reduced *FBXO30* expression on CIN in non-malignant and malignant colonic epithelial cell contexts.

2.2 HYPOTHESIS AND RESEARCH AIMS

Hypothesis: I hypothesize that reduced *FBXO30* expression induces CIN in colonic epithelial cell contexts. This hypothesis was addressed through two experimental research aims:

AIM 1: To determine the impact of reduced *FBXO30* expression on CIN in non-malignant colonic epithelial cell contexts.

AIM 2: To determine the impact of reduced *FBXO30* expression on CIN in a colorectal cancer cell line.

CHAPTER 3: MATERIALS AND METHODS

3.1. BIO-INFORMATICS APPROACHES

All relevant *FBXO30* copy number alterations, mRNA expression, genome instability markers, and patient survival data were acquired from The Cancer Genome Atlas (TCGA; Pan-Cancer Atlas dataset)[103], while data extraction and statistical analyses were performed using the open-access source, cBioPortal (www.cbioportal.org)[104,105]. No ethics approval was required to conduct these studies due to the use of the publicly available TCGA research network[103] and no other human specimens or clinical data were utilized in this research.

3.1.1. Genomic Alterations in Numerous Cancer Types

To determine the prevalence of *FBXO30* copy number losses in different cancer contexts, data from ten common solid cancer types (bladder, breast, colorectal, esophagus, glioblastoma, kidney, liver, prostate, testicular, and uterine) were extracted from TCGA Pan-Cancer Atlas database[103] and assessed for copy number alterations using the defined OncoQuery Language commands as follows: 1) HOMDEL, deep deletions (loss of both alleles); 2) HETLOSS, shallow deletion (loss of one allele); 3) GAIN (gain of one allele); and 4) AMP, large amplification (gain of two or more alleles). Following the generation of the OncoPrint segment in cBioPortal, *FBXO30* copy number variations (CNV) data were imported into Prism v10 (GraphPad), in which deep and shallow deletions were plotted for the ten cancer types (Fig. 4-1A).

3.1.2. mRNA Expression

To compare *FBXO30* shallow deletions and their associated mRNA expression, CRC patient sample data were extracted from the TCGA Pan-Cancer Atlas dataset[103] using cBioPortal[104,105]. Subsequently, *FBXO30* shallow deletions were compared to their corresponding mRNA expression z-score (z = expression in tumor sample – mean expression in reference

sample[diploid]/standard deviation of expression in reference sample [diploid]). *FBXO30* shallow deletions and their respective mRNA expression data were imported into Prism v10 (GraphPad), where normal (diploid) and shallow deletion samples were statistically compared using two-sample Mann-Whitney (MW) test (see *Section 3.6.1.*; Fig. 4-1B). Figure were assembled in Photoshop (Adobe).

3.1.3. Genome Instability Markers

To assess the impact of *FBXO30* shallow deletions on genome stability, different genome instability contexts, such as fraction genome altered, aneuploidy score and tumor break load were evaluated in CRC patient samples from the Pan-Cancer Atlas dataset[103] using cBioPortal[104,105]. Fraction genome altered compares the total percentage of the genome affected by copy number gains or losses between *FBXO30* shallow deletion and diploid CRC patient samples (Fig. 4-2). Aneuploidy score measures the total number of altered chromatid arms as a result of *FBXO30* shallow deletions relative to diploid (Fig. 4-2). Finally, tumor break load quantifies the sum of unbalanced structural variants (SV; *i.e.*, chromosome breaks), per tumor sample[106] with *FBXO30* shallow deletions compared to diploid CRC patient samples (Fig. 4-2). Data from fraction genome altered, aneuploidy score, and tumor break load and their respective *FBXO30* copy number loss information were imported into Prism v10 (GraphPad), in which diploid versus (vs) *FBXO30* shallow deletions in patient samples were statistically compared using MW tests (See *Section 3.6.1*). All figures were assembled in Photoshop (Adobe).

3.1.4. Patient Survival Analyses

Kaplan-Meier (KM) curves were generated using TCGA[103] patient data to compare significant differences in patient survival outcomes, including disease-free, disease-specific, progression free, and overall survival, between patients with *FBXO30* shallow deletions relative

to those with diploid *FBXO30* copy numbers (*i.e.*, diploid cases). The raw data were imported into Prism v10 (GraphPad) where KM curves were generated and statistically compared using log-rank tests with a p-value ≤ 0.05 considered statistically significant (See *Section 3.6.2.*; Fig. 4-3). All figures were assembled in Photoshop (Adobe).

3.2. REAGENTS

Appendix A contains a comprehensive list of all reagents and solutions employed in this study. In general, suppliers/manufacturers, include Abcam, Gibco (Life technologies), Molecular Devices, Sigma-Aldrich, and Thermo Scientific.

3.3. CELL CULTURE

The cell lines used in this research project are male karyotypically stable 1CT, A1309 and HCT116 colonic epithelial cells. 1CT are non-malignant, non-transformed colonic epithelial cell line, while A1309 cells are a derivative of 1CT cells line with a mutation in *KRAS* (G12V), 50% knockdown of *TP53*, and 70% knockdown of *APC* with expression of a truncated protein at codon 1309[107]. HCT116 cells are a malignant colorectal cancer cell line that exhibits MSI due to a mutation in *MLH1* that also harbor an additional mutation in *KRAS* (G13D), and are near diploid, with ~70% of cells exhibiting 45 chromosomes due to loss of the Y chromosome[52,94,108,109]. The growth conditions and maintenance for the non-malignant and malignant cell lines differ and are detailed below (see *Section 3.3.1.*).

3.3.1. Cell Lines and Growth Conditions

The distinct features of the three colonic epithelial cell lines utilized in this study are summarized in Table 3-1. Briefly, 1CT and its derivative cell line A1309, were generously

provided by Dr. Jerry Shay (University of Texas Southern Medical Center, USA), while HCT116 cells were purchased from American Type Culture Collection (Rockville, MD). 1CT and A1309 cells were cultured in X-medium (Dulbecco's Modified Eagle Medium [DMEM] with High Glucose/Medium 199; Hyclone) supplemented with 2% cosmic calf serum (CCS; Hyclone; Appendix A), while HCT116 cells were cultured in modified McCoy's 5A medium (Hyclone) supplemented with 10% fetal bovine serum (FBS; Sigma-Aldrich; Appendix A). 1CT and A1309 cells were cultured on Primaria (Corning) tissue culture plates with modified polystyrene surface containing oxygen and nitrogen functional groups supporting the growth of cells with poor attachment or differentiation (*e.g.*, endothelial, neuronal, primary, and tumor cells). 1CT and A1309 cells were grown in sealed, low oxygen (O_2) chambers containing 2% O_2, 7% carbon dioxide (CO_2), and 91% nitrogen (N_2) in 37 degrees Celsius (°C) incubator. HCT116 cells were cultured in standard 10 cm tissue culture plates (Sarstedt) and grown in 37 °C incubator with 5% CO_2. All cell lines used in this study were validated as karyotypically stable[52,94,107] with suitable FBXO30 protein abundance for future analyses. A metal tray containing Millipore-Q water and cupric sulfate pentahydrate (Appendix A) was placed in the bottom of the incubator to maintain humidity and prevent the growth of microorganisms that could contaminate the cells.

Table 3-1. Common Properties of the Human Colonic Epithelial Cell Lines Employed in The Research Study.

Cell Line	1CT	A1309	HCT116
Transformed or Immortalized	Immortalized (telomerase and *CDK4*[A])	Immortalized (telomerase and *CDK4*[A])	Transformed
Sex	Male	Male	Male
Culture Medium	X-media + 2% CCS	X-media + 2% CCS	McCoy's 5A + 10% FBS
Doubling Time	<22 hours	<22 hours	~22 hours
Karyotype	Diploid 46 XY, Stable	Diploid 46 XY, Stable	Near Diploid 45 X, Stable
Source	Dr. Jerry Shay (University of Texas)	Dr. Jerry Shay (University of Texas)	American Type Culture Collection (Rockville, MD)
Protein Expression Profile			
KRAS	Wild-type[B]	G12V[C]	G13D[C]
TP53	Wild-type[B]	Wild-type[B], ~50% knockdown[D]	Wild-type[B]
APC	Wild-type[B]	Expression of truncated protein[E], ~70% knockdown[D]	Wild-type[B]

[A]Cyclin Dependent Kinase 4, wild-type
[B]Refers to expression of wild-type protein
[C]Amino acid substitutions denoted by their single letter code
[D]Extent of knockdown relative to endogenous 1CT levels
[E]APC truncated at codon 1309

3.3.2. Cell Passaging

To maintain actively growing and sub-confluent cell cultures, cells were passaged in a biological safety cabinet every 2-4 days. Medium was aspirated from 10 cm tissue culture plates and adherent cells were washed with sterile phosphate buffered saline (1X PBS; Appendix A). To detach cells from their tissue culture plates, 1 milliliter (mL) of 0.05% trypsin containing chelating agent ethylenediaminetetraacetic acid (EDTA) (Gibco; Life Technologies) was added and incubated with cells at room temperature (RT) for 2 minutes (min; A1309) or 5 min (1CT and

HCT116). An inverted ID03 microscope (Zeiss) equipped with 10x objective lens was used to monitor cell detachment. Following detachment, trypsin was neutralized with 1 mL of trypsin neutralizer (Gibco; Life Technologies) and diluted with 3 mL of sterile 1X PBS (1CT and A1309) or diluted using 4 mL 1X PBS (HCT116). Tissue culture plates were washed with the 5 mL volume and cell suspension was transferred into a 15 mL conical tube (Sarstedt). Cell suspensions were centrifuged at 140 x gravitational force (g) for 5 min at 21 °C in a Legend XFR centrifuge (Thermo Scientific). The supernatant was aspirated from the conical tube and cell pellet was resuspending in 3 mL (1CT and A1309) or 8 mL (HCT116) of sterile 1X PBS. Approximately, 1 mL of cell suspension was added back to 10 cm plate that was washed with sterile 1X PBS and contains 10 mL of fresh complete medium. 1CT and A1309 cells were placed in a low O_2 chamber, filled with gas mixture previously described above (see *Section 3.1.1.*), and placed in a 37 °C incubator. HCT116 cells were directly placed into a 37 °C incubator containing 5% CO_2.

3.3.3. Cell Counting and Seeding

In preparation for seeding the CIN assays, cells were trypsinized, pelleted, and resuspended in 1X sterile PBS as detailed above. Additionally, highly aggregating cells, such as HCT116 cells, were passed through a 40 micrometer (μm) cell strainer (Falcon) into a 50 mL conical tube (Sarstedt). Straining 1CT and A1309 cells was unnecessary, as they form single cell suspensions. To determine cell counts for all cell lines, a 40 microliter (μL) aliquot of cell suspension was combined in a 1:1 ratio with 0.2% trypan blue dye (Gibco) in a 0.5 mL microcentrifuge tube. Afterwards, 20 μL of cell/trypan blue mixture was applied into a cell counter slide (Cedex Smart Slide, Roche) in duplicate (two wells). Cell counts (*i.e.*, the number of viable cells/mL in the cell suspension) were evaluated using Cedex XS cell counter and Cedex XS software (Cedex Smart Slide, Roche) to distinguish between live and dead cells based on trypan blue dye exclusion, as

trypan blue penetrates dead cells due to defective cell membranes. The viable cell concentration (cell/mL) was utilized to calculate the volume of cell suspension required for appropriate cell numbers in all subsequent experiments, summarized in Table 3-2.

Table 3-2. Cell Seeding Densities Required for the Respective CIN Assay.

CELL LINE	ASSAY[A]	PLATE TYPE	CELL COUNT	MEDIUM VOLUME/WELL (µL)
1CT	WB	6-well	30,000	2,000 µL
	NA/MNF	96-well	1,000	200 µL
	MCS	6-well	20,000	2,000 µL
A1309	WB	6-well	30,000	2,000 µL
	NA/MNF	96-well	1,000	200 µL
	MCS	6-well	20,000	2,000 µL
HCT116	WB	6-well	30,000	2,000 µL
	NA/MNF	96-well	800	200 µL
	MCS	6-well	15,000	2,000 µL

[A]WB, western blot; NA, nuclear area; MNF, micronucleus formation; MCS, mitotic chromosome spread

3.3.4. Short-Interfering RNA Transfection

A set of four individual ON-TARGETplus siRNA duplexes (siBFXO30-1, -2, -3, -4) targeting distinct exon regions within the *FBXO30* coding sequence and a non-targeting siRNA control (siControl) were purchased from Dharmacon (Fig. 3-1). Each individual siRNA duplex along with the siControl were resuspended in 1X siRNA buffer (Appendix A) to a stock concentration of 20 micromolar (µM) and working solution of 10 µM. A pooled (siFBXO30-P)

siRNA mixture comprised of the four individual siRNAs targeting *FBXO30* mentioned above, was formed by combining equimolar volumes of each 10 µM siRNA duplex (siBFXO30-1, -2, -3, -4). All siRNAs were aliquoted into smaller 10 µL volumes, stored at -80 °C and underwent a maximum of five freeze/thaw cycles to minimize RNA degradation.

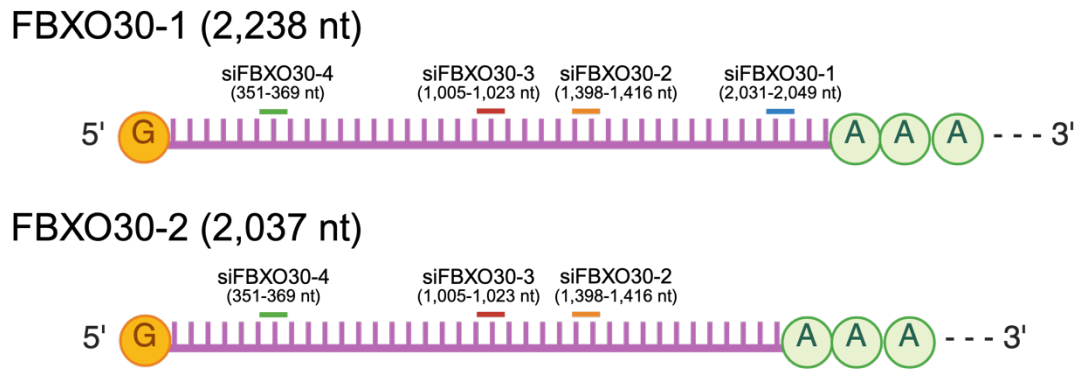

Figure 3-1. Specific Coding Regions of *FBXO30* Transcripts Targeted by the Individual siRNA Duplexes.
Schematic depicting the distinct target regions of the individual siRNAs within the *FBXO30* transcript. The top transcript is wild-type *FBXO30* and the bottom transcript is the alternative splice variant of *FBXO30*.

To perform siRNA-based silencing experiments, cells were seeded ~24 hours (h) prior to transfection at densities described in Table 3-2 and incubated at 37 °C to allow cells to adhere to the tissue culture plate. For transient lipid-based transfection, the volumes of complete medium, RNAiMAX (Invitrogen) transfection reagent, and siRNAs were scaled based on plate format (6-well vs. 96-well) and cell density, as summarized in Table 3-3. Each siRNA and RNAiMAX were diluted with appropriate volumes of complete medium in separate microcentrifuge tubes, indicated in Table 3-3. Each siRNA solution was gently inverted in a 1:1 ratio with the RNAiMAX solution and incubated for 20 min at RT. Following incubation, transfection mixtures were dispensed

dropwise into appropriate wells for each condition, rocked gently, and returned to the 37 °C incubator. Four days post-transfection, whole cell protein lysates are harvested or CIN assays (see *Section 3.5*) were performed.

Table 3-3. Transfection Protocols of *FBXO30* Silencing for the CIN Assays.

Cell Line	Assay[A]	Volume siRNA in Tube 1 (µL)	Volume RNAiMAX in Tube 1 (µL)	Volume Medium in Well (µL)	Total Volume (µL)
1CT	WB	1 µL in 250 µL medium	6 µL in 250 µL medium	2,000 µL	2,500 µL
	NA/MNF	0.1 µL in 10 µL medium	0.3 µL in 10 µL medium	200 µL	220 µL
	MCS	0.66 µL in 250 µL medium	6 µL in 250 µL medium	2,000 µL	2,500 µL
A1309	WB	1 µL in 250 µL medium	6 µL in 250 µL medium	2,000 µL	2,500 µL
	NA/MNF	0.1 µL in 10 µL medium	0.3 µL in 10 µL medium	200 µL	220 µL
	MCS	0.66 µL in 250 µL medium	6 µL in 250 µL medium	2,000 µL	2,500 µL
HCT116	WB	1 µL in 250 µL medium	6 µL in 250 µL medium	2,000 µL	2,500 µL
	NA/MNF	0.1 µL in 10 µL medium	0.3 µL in 10 µL medium	200 µL	220 µL
	MCS	0.5 µL in 250 µL medium	6 µL in 250 µL medium	2,000 µL	2,500 µL

[A]WB, western blot; NA, nuclear area; MNF, micronucleus formation; MCS, mitotic chromosome spread
[B]siRNAs and RNAiMAX were diluted in complete medium.

3.4. WESTERN BLOT ANALYSES

Western blot analyses were utilized to evaluate siRNA-based silencing efficiencies of *FBXO30* expression in 1CT, A1309, and HCT116 cell lines. Semi-quantitative western blots were performed a minimum of three times for each cell line.

3.4.1. Whole Cell Protein Extraction

In general, cells were seeded, transfected with siRNAs, and grown in 6-well tissue culture plates as described in *Section 3.3* and whole cell protein lysates were harvested four days post-transfection. Cell culture medium was aspirated from each well, and cells were washed 3x with 1 mL of cold (4 °C) 1X PBS. Either 80 µL (HCT116) or 60 µL (1CT and A1309) of lysis buffer containing radioimmunoprecipitation assay (RIPA) buffer (Appendix A) and 25X protease inhibitor (Appendix A) were combined and added to each well. Cells were incubated with protease inhibitor on ice for 20 min, tapping every 5 min. Protein lysates were harvested using a cell scrapper and transferred to a labelled 1.5 mL microcentrifuge tube chilled on ice. Protein lysate was sonicated twice for 3 seconds (s) pulses with a Sonifer Cell Disruptor (Branson Sonic Power Co.) with a duty cycle of 50% amplitude and output control set to 6. To isolate proteins and remove and insoluble debris from the samples, lysate was centrifuged at 13,000 x g for 2 minutes in cold room (4 °C) centrifuge (IECMicro-MB centrifuge; GMI). Supernatant was carefully removed to avoid disturbing the pellet and transferred to new, sterile, chilled microcentrifuge tube. Samples are stored at -20 °C for short-term storage or -80 °C for long-term storage (>2 weeks).

3.4.2. Protein Quantification Using Bicinchoninic Acid Assay

To quantify protein concentrations from the harvested protein samples (see *Section 3.4.1.*), a Pierce Bicinchoninic Acid (BCA) Assay kit (Thermo Scientific) was used according to the manufacturer. Briefly, Reagent A (containing BCA) and Reagent B (containing 4% cupric sulfate) were mixed in a 50:1 and 200µL was dispensed per well in a clear 96-well plate (Corning). A set of nine bovine serum albumin (BSA) standards, labelled A-I, were prepared with known concentrations through serial dilution from 0 µg/mL to 2000 µg/mL and 25 µL of each standard was dispensed in duplicate into the 96-well plate. Accordingly, RIPA (20µL/well) and protein

samples (5µL/well) with unknown concentrations were pipetted in triplicate. The plate was agitated for 3-5 s on the Multi-Microplate Genie (Scientific Industries) to homogenize the samples prior to a 30 min incubation at 37 °C in the dark. Following incubation, the SpectraMax iD3 Multi-Mode Microplate Reader (Molecular Devices) was utilized to acquire absorbance measurements at 562 nanometers (nm). The absorbance values from the BCA standards were used to generate a standard curve to quantify the concentration of the protein samples. The three absorbance values calculated for each protein sample were averaged and multiplied by 5 to account for the dilution, to ultimately determine the concentration of the protein samples.

3.4.3. Gel Electrophoresis and Western Blot

Following protein quantification, proteins samples were combined with appropriate volumes of 6X sodium dodecyl sulfate (SDS) Sample Loading Buffer (Appendix A) and RIPA to obtain equimolar concentration of 20 µg/well for each protein sample. To denature proteins, prepared samples were incubated for 5 min at 99 °C in a Thermomixer R heating block (Eppendorf) with orbital mixing at 1 min intervals of 700 revolutions per min (rpm) and immediately place in ice to maintain a denatured state. A Mini-PROTEAN electrophoresis tank (BioRad) with a 4-20% mini-PROTEAN TGX gel (BioRad) was assembled and filled with 1X Running Buffer (Appendix A). A 4 µL volume of BLUelf Prestained Protein Ladder (FroggaBio) molecular weight marker was pipetted into a well, while the remaining wells were filled with 20 µL of the cooled and vortexed denatured protein sample. Samples were electrophoresed at 140 volts (V) at RT for 67 min using a PowerPac HC (BioRad) power supply.

In preparation for the protein transfer, a 0.45 µm nitrocellulose membrane (BioRad) and 3x blotting papers were soaked in 1X Transfer Buffer (Appendix A) for at least 10-15 min prior to transfer. The gel, nitrocellulose membrane, and blotting papers were stacked appropriately in the

Trans-Blot Turbo transfer system (BioRad). Following assembly, a constant 25V was applied for 8 minutes at RT to transfer the protein onto the membrane. Membranes were stained with ~5 mL of total protein stain copper phthalocyanine 3,4', 4'', 4'''-tetrasulfonic acid tetrasodium salt (CPTS; Appendix A) on Belly Dancer (Stovall Life Science Inc.) for 5 min at RT to confirm efficient protein transfer. The membrane was subsequently de-stained by washing with Tris-buffered saline (TBS) containing 0.01% Tween 20 (TBST; Appendix A) for ~10-15 min on Belly Dancer at RT. The membrane was blocked using 5% non-fat milk powder (weight per volume [w/v]) in TBST, with gentle rocking at RT for 1 h. After blocking, primary antibodies targeting FBXO30 or Cyclophilin B (loading control) were diluted in 5% non-fat milk, as specified in Table 3-4. Diluted antibodies were added to the membrane and incubated overnight on a rocker at 4 °C. The next day, primary antibody solution was discarded and the membrane was flash-rinsed and washed 3x with 1X TBST for 10 min on the Belly Dancer set to medium speed. Secondary antibodies conjugated to horseradish peroxidase (HRP) were diluted in 5% non-fat milk as described in Table 3-4 and incubated on membrane for 1 h, gently rocking at RT. Secondary antibodies were removed and the membrane was flash-rinsed and washed 3x for 10 min with 1X TBST.

Table 3-4. List of Antibodies Used for Western Blot Analyses.

Primary Antibodies				
Antibody	**Catalogue Number**	**Source**	**Species**	**Dilution**
FBXO30	ab68224	Abcam	Mouse	1:1,000
Cyclophilin B	ab16045	Abcam	Rabbit	1:150,000
Secondary Antibodies				
Goat α Mouse HRP[A]	115-035-146	Jackson ImmunoResearch	Goat	1:10,000
Goat α Rabbit HRP[A]	111-035-144	Jackson ImmunoResearch	Goat	1:10,000

[A]HRP (Horseradish peroxidase)

3.4.4. Semi-Quantitative Western Blot Analysis

To visualize antibody-labelled proteins, the EZ-ECL kit (FroggaBio) was used as instructed by the manufacturer. Briefly, the stable peroxide solution is combined with luminol/enhancer solution in 1:1 ratio. Simultaneously, the excess TBST was removed from the membrane using a Kimwipe (Kimberly Clark). Approximately 750 µL of ECL visualization solution was applied to the membrane (enough to cover the surface) and allowed to incubate in the dark at RT for 5 min. Following the incubation with the ECL solution, the membrane was placed between two clean and clear page protectors for imaging by ChemiDoc MP Imaging System (BioRad). The ChemiDoc MP Imaging System is set to acquire chemiluminescent images with optimal exposure time determined for each antibody, in which there is a strong signal without pixel saturation. Images were imported into ImageJ software (National Institute of Health) for semi-quantitative analysis of protein abundance. Initially, band intensities are normalized to the loading control (Cyclophilin B) and subsequently presented relative to the non-targeting control

(siControl), which is set to 100% to enable comparison of protein expression levels through band intensities between samples. Western blot figures were assembled in Photoshop (Adobe).

3.5. SINGLE CELL QUANTITATIVE IMAGING MICROSCOPY ASSAYS

Single cell quantitative imaging microscopy (QuantIM) techniques were utilized to evaluate CIN-associated phenotypes, including changes in nuclear areas, micronucleus formation, and alterations in chromosome numbers in 1CT, A1309, and HCT116 following *FBXO30* silencing. Additionally, mitotic chromosome spreads were generated through standardized cytogenetic approaches, to assess the impact of reduced *FBXO30* expression on chromosome numbers relative to the modal karyotype (see Table 3-1). All assays were performed a minimum of three times in each cell line to address experimental reproducibility.

3.5.1. Cell Fixation and DNA Counterstaining for Nuclear Area and Micronucleus Formation Analyses

To identify potential changes in nuclear area and micronucleus formation following *FBXO30* silencing, the McManus laboratory's established QuantIM approaches were utilized[54,62,110]. Following cell seeding (see *Sections 3.3.3*) and siRNA transfection (see *Section 3.3.4*), the medium was aspirated from the 96-well plate, and cells were fixed using fresh 4% paraformaldehyde (PFA) prepared in the fume hood (Appendix A), in which 200 µL PFA/well added for 10 min at RT. PFA was safely disposed, according to the safety data sheet, and cells were washed 3x in 1X PBS (200 µL/well). Nuclei were counterstained with 200 µL/well of 300 nanogram (ng)/mL Hoechst 33342 (Appendix A) in 1X PBS (Appendix A). Plates were stored in the dark at 4 °C for at least 24 h to enable uniform counterstaining across the individual nuclei.

3.5.2. Image Acquisition and Analysis

To acquire optimal images without condensation on the plate lids, cells were allowed to acclimate to RT in the dark prior to imaging. A 3x3 matrix of non-overlapping, two-dimensional (2D) images were acquired from each well with the ImageXpress Confocal HT.ai High-Content Imaging System (Molecular Devices) equipped with a 20x Water Apo LambdaS CFI objective lens (0.95 numerical aperture). The IN-Carta Image Analysis software (Molecular Devices) was subsequently employed to optimize all images acquired from the wells by defining the following parameters: size, signal intensity and filters. For each experiment, the parameters were optimized and maintained constant throughout the analyses. A primary mask filter was employed to define nuclear area sizes through automatic detection of nuclei with clearly defined boundaries for accurate segmentation of primary nuclei across all conditions, while an exclusion filter removed partial nuclei found < 50 µm along the image periphery[62,110]. A maximal mean fluorescent intensity filter was also applied to each image to eliminate brightly illuminated cellular debris or mitotic and apoptotic cells[62,110]. Additionally, IN-Carta Image Analysis software applied a secondary mask with a ring width of 15 µm from the primary nucleus to define the cell body boundary and automatically score micronuclei with high accuracy[62,110]. Micronuclei were defined as extranuclear Hoechst-stained bodies with maximum size of 30 µm with no visible attachment to the primary nucleus[62,110]. Micronuclei were identified as Hoechst-stained bodies located outside the primary mask (*i.e.*, nucleus) yet remained within the secondary mask (*i.e.*, cell body). The total number of micronuclei per well was calculated and normalized to the total number of nuclei detected, in order to determine the frequency of micronucleus formation per siRNA condition. A minimum of 1000 nuclei were imaged per well with six wells for each condition (n= 6). Each experiment was performed a minimum of three times (N= 3).

Nuclear area and micronucleus formation data were imported into Prism v10 (GraphPad), where two-sample Kolmogorov-Smirnov (KS) tests to assess changes in nuclear areas and Mann-Whitney (MW) tests to assess micronucleus formation were performed, as described in *Section 3.6*. Cumulative distribution frequency graphs were generated to visualize nuclear area data, while dot plots were created to analyze rank order of micronucleus formation. All figures were generated in Photoshop (Adobe).

3.5.3. Mitotic Chromosome Spreads and Chromosome Enumeration

To generate mitotic chromosome spreads, cells were seeded (see Table 3-2) on autoclaved coverslips and silenced according to Table 3-3. Four days post-transfection, cells were treated with KaryoMAX Colcemid (Gibco) at a dilution of 100 ng/mL (Appendix A) in complete medium for 1.2 h (HCT116) or 3.5 h (1CT and A1309) at 37 °C. Colcemid will inhibit microtubule polymerization and enrich for mitotic cells. The medium and Colcemid were aspirated and ~2 mL of 75 millimolar (mM) potassium chloride (KCl) hypotonic solution (Appendix A) was added to each well for ~18 min (HCT116) or 20 min (1CT and A1309) to rupture the cells. Subsequently, cells were fixed with 3:1 ratio of methanol-acetic acid mixture (Appendix A) in 3x 10 min intervals. The fixative was aspirated from the wells and coverslips were placed on edge of well to evaporate overnight. Once dry, coverslips were mounted on glass microscope slides with 4',6-diamidino-2-phenylindole (DAPI) Mounting Medium (Vector Laboratories; Appendix A) and stored at 4 °C in the dark. The slides were imaged with a Zeiss AxioImager Z2 microscope equipped with a Plan-APOCHROMAT 63x oil-immersion DIC M27 lens with a 1.40 numerical aperture. A minimum of 100 images were acquired per siRNA condition. Image files were converted to 8-bit TIFFs and imported into ImageJ software for visual assessment and manual enumeration of the chromosomes. Three categories including losses (< the modal number), small-

scale gains (≤ 9 chromosomes between the modal karyotype and large-scale gains) and large-scale gains (≥ 10 chromosomes above modal karyotype) were designated to aberrant chromosome spreads that deviated from the modal karyotype of the cell line (see Table 3-1). A total of three distinct biological replicates were enumerated per cell line. Data were imported into Prism v10 (GraphPad) in which graphs were generated and Student's t-tests were performed. All figures were assembled in Photoshop.

3.6. STATISTICAL ANALYSES

The number of biological replicates (N) and technical replicates (n) are indicated for all experiments presented in this thesis. All statistical analyses were performed using Prism v10.

3.6.1. Mann-Whitney Tests

The Mann-Whitney (MW) test is a non-parametric statistical test that compares the rank orders of two datasets and presents a p-value based on the mean ranks between an experimental condition and the control. In this study, MW tests were employed to assess the statistical significance of mRNA expression, fraction genome altered, aneuploidy score, and tumor break load of *FBXO30* shallow deletions in CRC patient samples relative to diploid patient samples[103]. Additionally, MW tests were used to evaluate the difference in micronucleus formation in siRNA conditions vs. control in non-malignant and malignant cell lines. P-values ≤ 0.05 are considered statistically significant and represented by asterisks in figures as: *p-value < 0.05; **p-value < 0.01; ***p-value < 0.001; ****p-value < 0.0001.

3.6.2. Log-Rank (Mantel-Cox) Tests

The log-rank test is a non-parametric statistical test that compares the survival distribution between two groups and presents a p-value based on the difference of survival times between the

groups. In this thesis, log-rank tests were employed to assess survival outcomes (progression-free survival, disease-free survival, and overall survival) of CRC patient with *FBXO30* shallow deletions relative to those diploids for *FBXO30* copy numbers[103]. A p-value ≤ 0.05 is deemed statistically significant.

3.6.3. Two- Sample Kolmogorov-Smirnov Tests

The two-sample Kolmogorov-Smirnov (KS) test is a non-parametric test that compares the cumulative distribution frequency of two datasets and calculates a p-value based on the maximum difference between two distributions. In this study, a p-value ≤ 0.05 is considered statistically significant and represented by asterisks in figures as: ****p-value < 0.0001.

3.6.4. Student's T-tests

The Student's t-test is a parametric test that compares the mean of two unpaired groups and generates a p-value based on the probability that the difference between the two means occurs by chance. In this thesis, a p-value ≤ 0.05 is considered statistically significant and represented by asterisks in figures as: *p-value < 0.05; **p-value < 0.01.

CHAPTER 4: RESULTS

4.1. BIO-INFORMATIC ANALYSES IMPLICATE *FBXO30* SHALLOW DELETIONS IN CRC PROGRESSION AND SURVIVAL

To evaluate the clinical relevance of *FBXO30* copy number losses in cancer, the open-access TCGA patient sample data were analyzed via cBioPortal[103-105]. All data were imported into Prism v10 for statistical analyses, as indicated in *Section 3.6*. Due to the nature of the publicly available TCGA dataset, no ethics approval was required to conduct these studies.

4.1.1. High Frequency of *FBXO30* Copy Number Losses in Cancer

To assess the prevalence of *FBXO30* copy number losses in cancer, TCGA data for ten common solid cancer types (bladder, breast, colorectal, esophagus, glioblastoma, kidney, liver, prostate, testicular, uterine) were evaluated using cBioPortal to identify *FBXO30* deep and shallow deletions[103-105]. To account for tumor and molecular heterogeneity, the broad terms, deep deletion and shallow deletion, are used in large-scale bulk sequencing datasets, including TCGA data[103]. Deep deletions describe the algorithmically determined loss or near-loss of both copy numbers in patient samples, whereas shallow deletions are defined as a single copy number loss, possibly heterozygous, without analysis at allele-specific sites[104,105]. As shown in Figure 4-1A, *FBXO30* deep deletions are rare in patient samples across all solid tumor types evaluated due to gene dosage effect in which the cells cannot compensate for the near loss or loss of both *FBXO30* copy numbers. However, shallow deletions were more readily observed across all ten cancer types, including a 13% alteration frequency in CRC (Fig. 4-1A), which represents ~3,300 of the ~25,2000 Canadians diagnosed annually, supporting the possibility that *FBXO30* loss may promote oncogenesis[5]. Furthermore, as observed in Figure 4-1B, *FBXO30* shallow deletions correspond with a significant decrease in mRNA expression relative to diploid CRC patient samples (see *Section 3.6.1*.; MW

test; ****p-value < 0.0001). Due to the nature of the TCGA research network, there is no available protein expression data of *FBXO30* shallow deletions and diploid copy numbers in CRC patients.

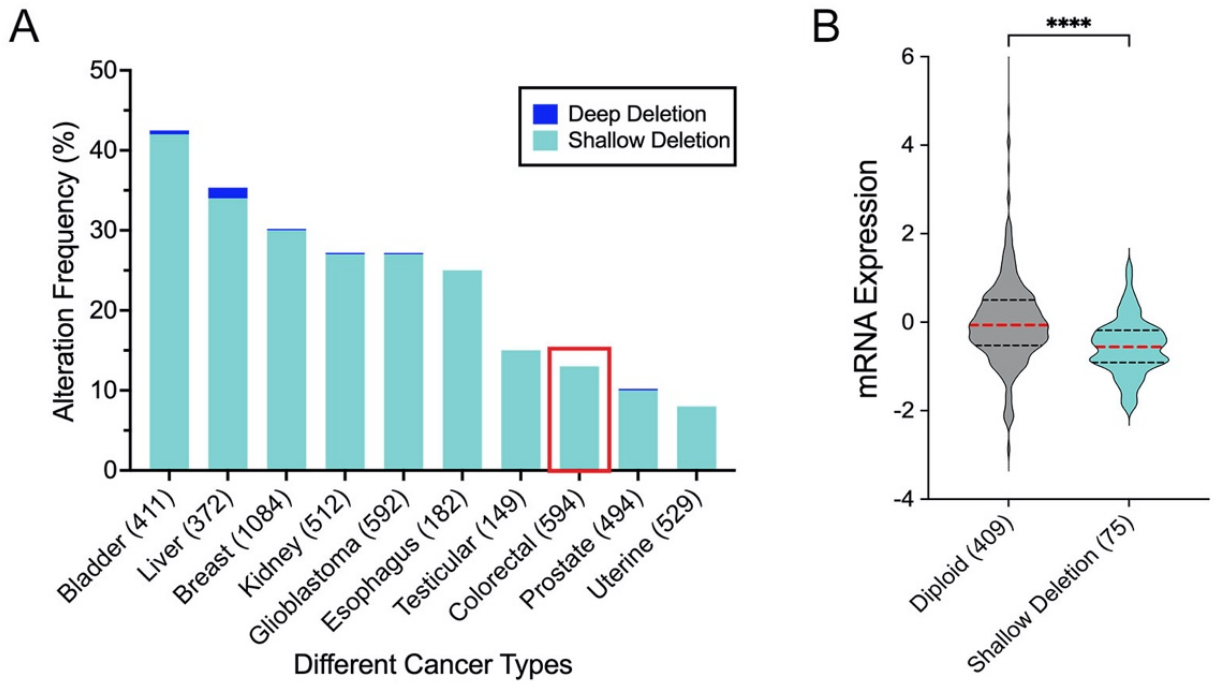

Figure 4-1. *FBXO30* Expression is Significantly Altered in CRC.
(A) Bar graph presents TCGA patient data for *FBXO30* copy number losses in ten different solid tumor types[103]. Total patient cases indicated in brackets. The red box highlights the CRC samples. ***(B)*** Violin plot reveals that *FBXO30* shallow deletions correlate with significant decreases in mRNA expression z-score relative to diploid levels in CRC patient samples. Dashed lines represent the 1st, 2nd (median; red line), and 3rd quartiles. The asterisks (****) represent significance with a p-value <0.0001 using a MW test.

4.1.2. Reduced *FBXO30* Expression Corresponds with Genome Instability

To examine whether *FBXO30* copy number losses are associated with CIN, three genome instability-associated phenotypes, namely the fraction genome altered, aneuploidy score, and tumor break load, were assessed in TCGA CRC patient samples using cBioPortal[103-105]. The fraction genome altered indicates the percentage of the genome exhibiting copy number alterations within the diploid (unaltered) control and *FBXO30* shallow deletion samples. Aneuploidy score reflects the number of altered chromosome arms in the diploid and *FBXO30* shallow deletion CRC

patient samples. Finally, tumor break load quantifies the sum of chromosome breaks per tumor sample in CRC patients with *FBXO30* shallow deletions compared to diploid samples[106]. *FBXO30* shallow deletions correspond with significant increases in fraction genome altered, aneuploidy score, and tumor break load in CRC patient samples relative to diploid CRC samples (see *Section 3.6.1.*, MW test; ***p-value <0.001; ****p-value <0.0001).

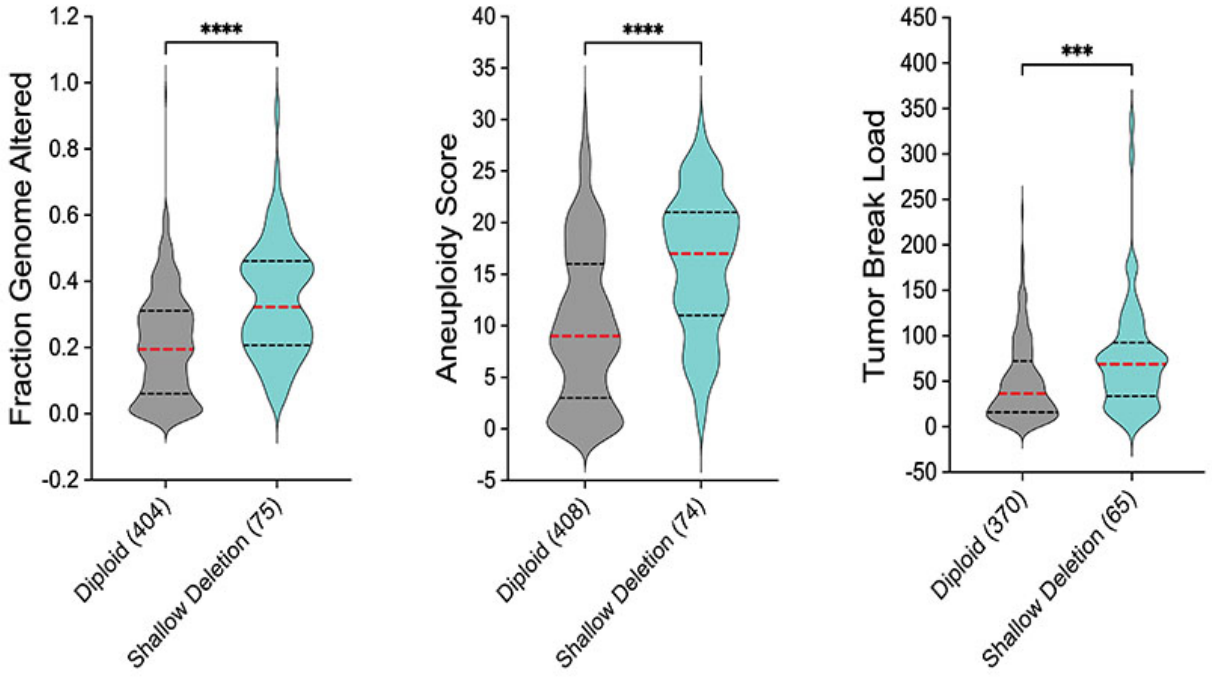

Figure 4-2. *FBXO30* Shallow Deletions Correspond with Increases in Genome Instability Markers in CRC Patient Tumor Samples.
Violin plots reveal that *FBXO30* shallow deletions correspond with significant increases in the fraction genome altered (left), aneuploidy score (middle), and tumor break load (right). All patient data are extracted from TCGA using cBioPortal, with the total number of patient samples indicated in brackets[103-105]. Dashed lines represent the 1st, 2nd (median; red line), and 3rd quartiles. The asterisks (***; ****) represent significance in MW tests, with a p-value <0.001 or p-value <0.0001, respectively.

4.1.3. *FBXO30* Shallow Deletions in CRC are Associated with Poor Patient Outcomes

FBXO30 shallow deletions correspond with worse patient outcomes in TCGA CRC patient data, suggesting that reduced *FBXO30* expression impacts patient survival in a clinically relevant context[103]. KM curves were generated comparing CRC patients with *FBXO30* shallow deletions with patients with diploid *FBXO30* copy numbers. Log-rank (Mantel-Cox) tests exhibit that *FBXO30* shallow deletions result in significantly worse CRC patient outcomes for progression-free survival, disease-specific survival, and overall survival, compared to *FBXO30* diploid patient samples (Fig. 4-3).

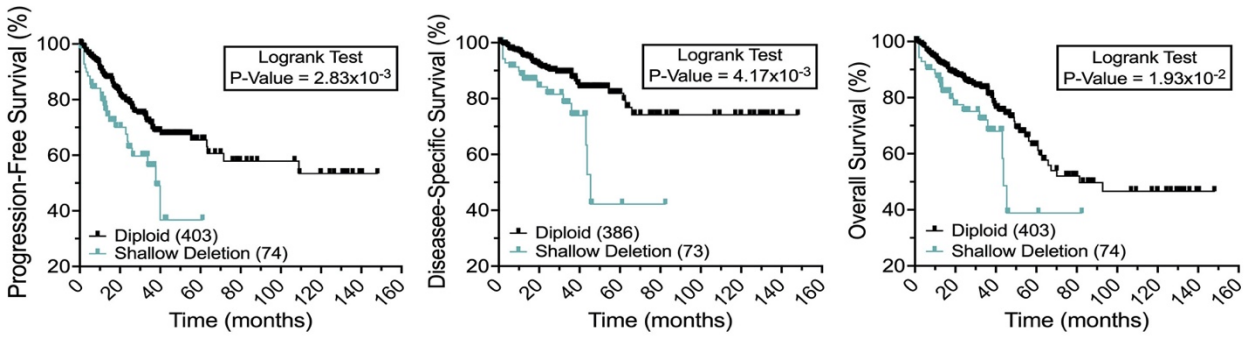

Figure 4-3. *FBXO30* Shallow Deletions are Associated with Worse CRC Patient Survival. KM curves reveal significant decreases in progression-free survival (left), disease-specific survival (middle), and overall survival (right) for CRC patients with *FBXO30* shallow deletions relative to those with diploid *FBXO30* copy numbers. Data were extracted from the TCGA patient sample data via cBioPortal[103-105].

The collective CRC patient data findings presented above support the possibility that reduced *FBXO30* expression may promote early CRC development[103]. Therefore, relevant malignant and non-malignant colonic epithelial cell lines are utilized in this study to evaluate the impact of reduced *FBXO30* on CIN and early CRC development.

4.2. IDENTIFYING THE MOST EFFICIENT *FBXO30* SIRNA SILENCING DUPLEXES IN HCT116 CELLS

Briefly, a set of four individual siRNA duplexes (siBFXO30-1, -2, -3, -4) targeting distinct coding regions within the *FBXO30* transcripts of both isoforms, along with the pool siRNA (siFBXO30-P; equimolar combination of each individual siFBXO30-1 to -4) were tested to identify the two most efficient individual siRNAs in HCT116 cells. These initial experiments were performed in the HCT116 cell line to optimize siRNA concentrations prior to conducting the CIN analyses in three colonic epithelial cell lines (HCT116, 1CT, and A1309). Three distinct semi-quantitative western blots were performed in HCT116 cells. As shown in Figure 4-4, siFBXO30-2 and -4, were identified as the two most effective silencers with the remaining FBXO30 abundance presented < 5% relative to the siControl (Fig S1, Appendix B). Contrarily, siFBXO30-1 proved the least effective with ~40% residual abundance of FBXO30, whereas siFBXO30-3 was highly effective, with a remaining ~5% abundance in FBXO30 levels, but reduced cell viability. Since siFBXO30-2 and siFBXO30-4 were identified as the most efficient *FBXO30* silencers of both FBXO30 isoforms, these two individual siRNAs, along with the pool, were used in all subsequent experiments, including western blots and CIN assays across all three cell lines.

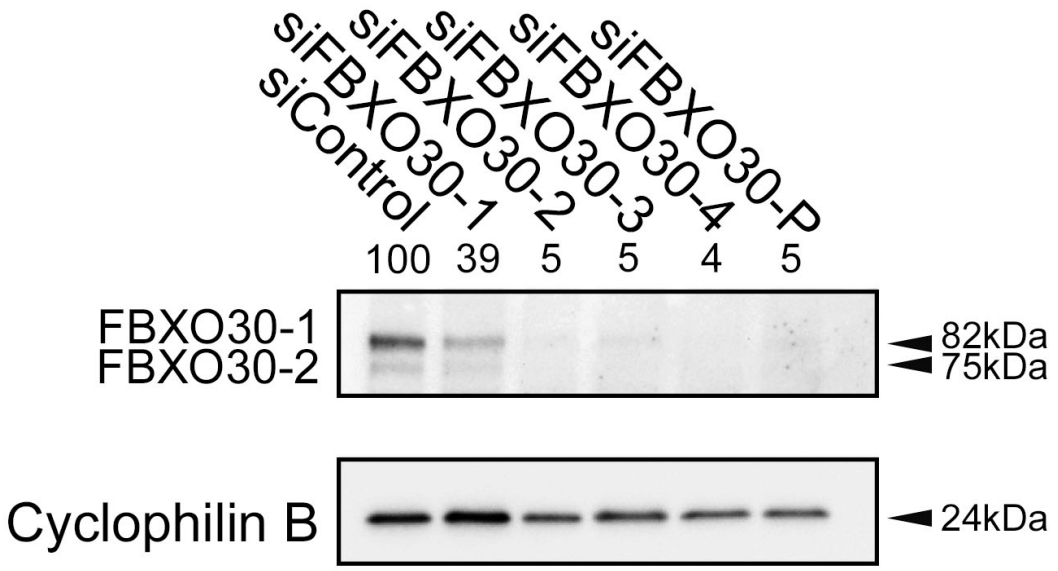

Figure 4-4. Western blot Confirms *FBXO30* Silencing in HCT116 Cells.
Semi-quantitative western blot reveals reduced FBXO30 abundance in HCT116 cells following siRNA-based silencing with individual (siFBXO30-1 to -4) and pool (siFBXO30-P) siRNA duplexes. FBXO30 abundance was first normalized to the corresponding loading control (Cyclophilin B) and is presented relative to siControl, which is set to 100%. FBXO30 has a molecular mass of 82 kilodaltons (kDa), and its alternative splice variant has a molecular mass of 75 kDa. Cyclophilin B has a molecular mass of 20 kDa. N represents biological replicates (N= 3).

4.3. AIM 1: To Determine the Impact of Reduced *FBXO30* Expression on CIN in Non-malignant Colonic Epithelial Cell Contexts.

CRC patient sample data show that *FBXO30* copy number losses correspond with genome instability and poor patient outcomes, yet its impact on CIN remains to be demonstrated in clinically relevant colonic cellular contexts. To address this research aim, the effect of reduced *FBXO30* on CIN was assessed in two male, non-malignant, non-transformed colonic epithelial cell lines, 1CT and A1309, using transient siRNA-based approaches.

4.3.1. *FBXO30* is Efficiently Silenced in 1CT Cells

Prior to assessing the impact of reduced *FBXO30* expression on CIN-associated phenotypes, including changes in nuclear area, micronucleus formation, and changes in chromosome numbers, we first be established that *FBXO30* can be efficiently silenced in 1CT cells. Utilizing the two

individual siRNAs along with the pool (see Section 4.2), *FBXO30* was efficiently silenced in 1CT cells (Fig. 4-5; Fig S2, Appendix B). As shown in Figure 4-5, silencing with siFBXO30-2, siFBXO30-4, and siFBXO30-P reduced FBXO30 abundance to < 5% of the endogenous levels in siControl (see Section 3.4.4.).

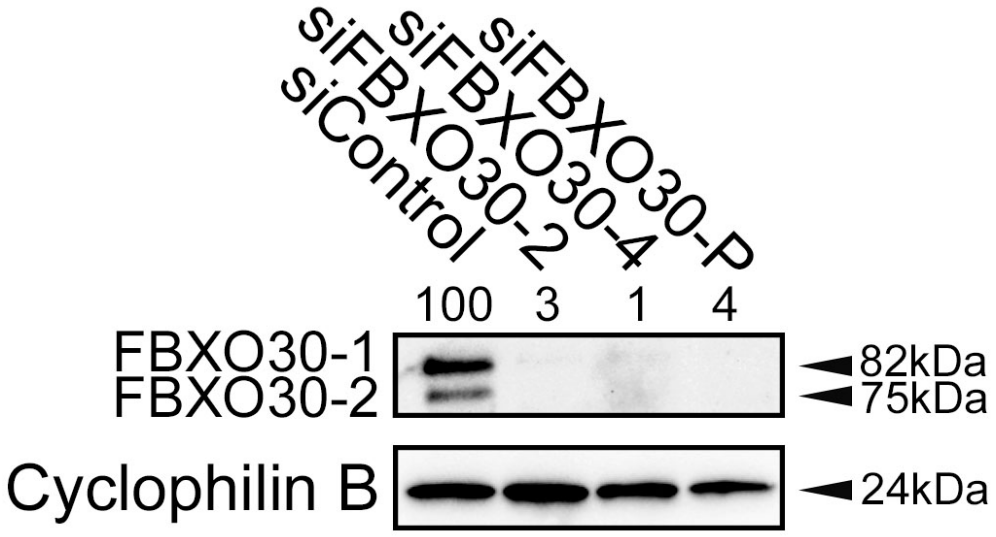

Figure 4-5. *FBXO30* is Efficiently Silenced in 1CT Cells.
Semi-quantitative western blot reveals reduced FBXO30 abundance in 1CT cells following silencing with siFBXO30-2, -4 and -P. FBXO30 abundance was normalized to the corresponding loading control (Cyclophilin B) and is presented relative to siControl (100%). (N=3)

4.3.2. Reduced *FBXO30* Expression Induces CIN-Associated Phenotypes in 1CT Cells.

Following the validation of *FBXO30* silencing in 1CT cells, the impact of reduced *FBXO30* expression on CIN was assessed through single-cell QuantIM assays on changes in nuclear areas and micronucleus formation. Qualitative images show Hoechst-counterstained nuclei with striking apparent changes in nuclear areas following *FBXO30* silencing relative to siControl (Fig. 4-6A). These visual changes are associated with statistically significant increases (rightward shifts) and decreases (leftward shifts) in nuclear area distributions relative to siControl (Fig. 4-6B**)** as determined by two-sample KS tests (p-value <0.05; Table S1, Appendix B). Across all replicates,

both individual siRNAs induced statistically significant increases in nuclear areas, with siFBXO30-2 depicting a notable visual and statistical increases in nuclear areas (Fig. 4-6B). Although siFBXO30-4 exhibits significant increases in nuclear area sizes according to the two-sample KS test, the curve overlaps with the siControl, suggesting a weaker effect on changes in nuclear area sizes (Fig. 4-6B). In regard to siFBXO30-P, it induced significant decreases in nuclear areas in all three replicates (Fig. 4-6B).

Next, the analysis of micronucleus formation was performed and is represented by a high-resolution image depicting a representative nucleus with their corresponding micronucleus (Fig. 4-6C). Quantitative analysis of micronucleus formation following *FBXO30* silencing reveals that siFBXO30-2 and -4 induced significant increases in micronucleus formation relative to siControl, while siFBXO30-P did not alter the frequency of micronuclei in any of the three replicates (MW test, p-value <0.05, Fig. 4-6D; Table S2, Appendix B).

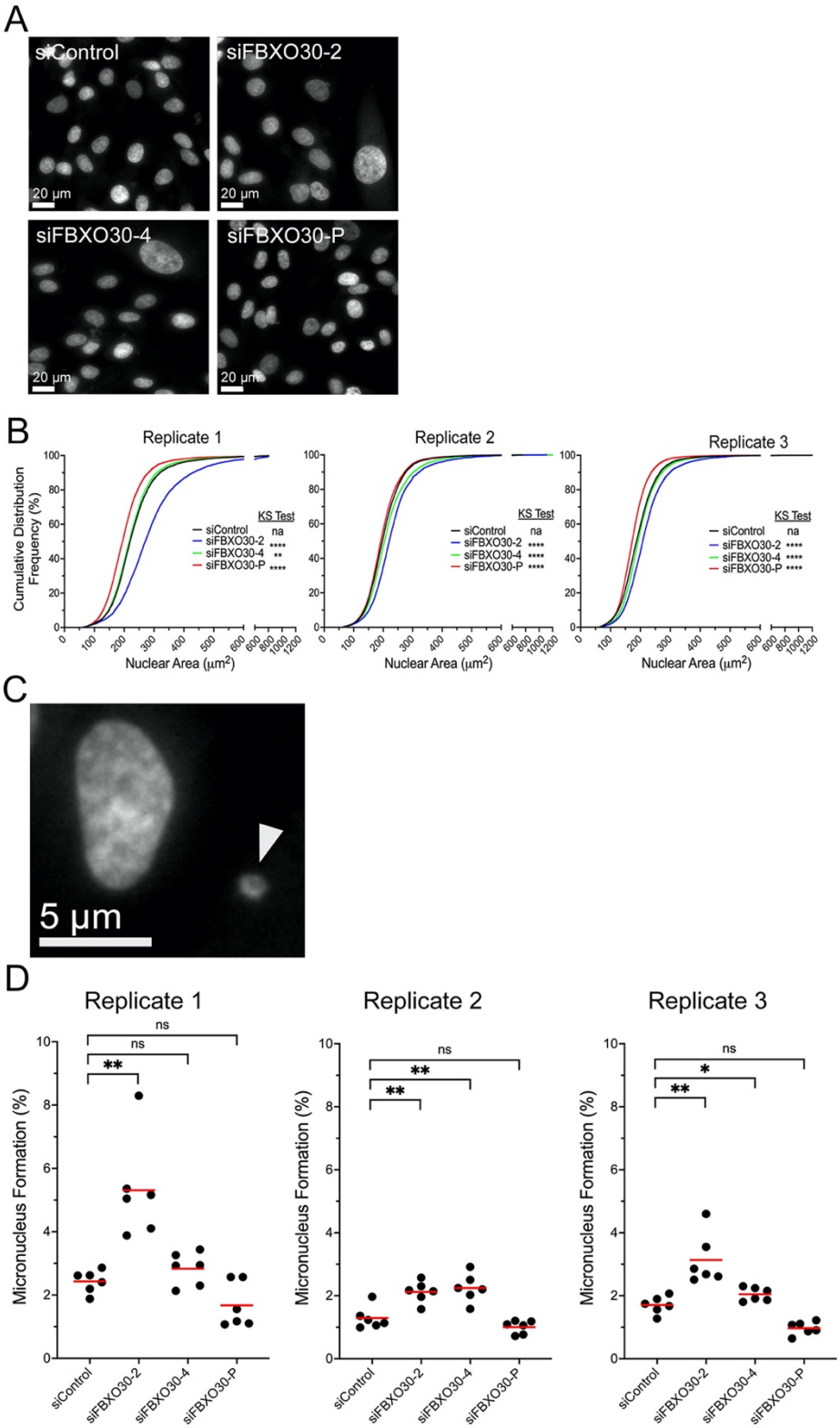

Figure 4-6. *FBXO30* Silencing Induces Significant Changes in Nuclear Areas and Micronucleus Formation in 1CT Cells.

(A) Low-resolution images of Hoechst-counterstained nuclei exhibiting visual changes in nuclear sizes following *FBXO30* silencing compared to siControl. ***(B)*** Cumulative distribution frequency graphs

reveal statistically significant increases (siFBXO30-2, -4; rightward shifts) and decreases (siFBXO30-P; leftward shifts) in nuclear areas following *FBXO30* silencing relative to the siControl (two-sample KS test; na; not applicable; **p-value <0.01; ****p-value <0.0001; N= 3, n= 6). N represents biological replicates, while n represents technical replicates. ***(C)*** High-resolution image of Hoechst-counterstained nucleus with an associated micronucleus (white arrowhead). ***(D)*** Dot plots presenting statistically significant increases in micronucleus formation following silencing with siFBXO30-2, -4 relative to the siControl. (MW test; ns= not significant; *p-value <0.05; **p-value <0.01; red bars= median; N= 3, n= 6).

Although changes in nuclear area and micronucleus formation were evaluated following *FBXO30* silencing, these assays do not directly assess chromosome numbers. Accordingly, to assess the impact of reduced *FBXO30* expression on chromosome numbers, mitotic chromosome spreads were generated and enumerated in triplicate in 1CT cells. Briefly, 1CT cells are a male diploid colonic epithelial cell line with a modal number of 46 chromosomes (46XY). Metaphase spreads were first assessed and classified as either modal (equal to 46 chromosomes) or aberrant (not equal to 46 chromosomes). To further investigate potential mechanism(s) contributing to CIN, aberrant spreads were subsequently sub-categorized into one of three groups based on their chromosome counts (Fig. 4-7A): 1) losses (< 46 chromosomes); 2) small-scale gains (47-55 chromosomes); or 3) large-scale gains (≥ 56 chromosomes). This sub-classification enabled more detailed analyses of the nature of chromosome abnormalities and provided preliminary insight into the types of errors potentially underlying the CIN phenotype. A total of 100 mitotic chromosome spreads were analyzed per condition (siControl; siFBXO30-2; siFBXO30-4; siFBXO30-P). Overall, the frequency of aberrant chromosome spreads was determined for siRNA-2, -4, and -P, with 3.6-fold, 3.6-fold, and 3.4-fold increases respectively, in aberrant chromosome numbers relative to the siControl (Fig. 4-7B). Following sub-categorization of aberrant spreads, it was determined that losses and small-scale gains accounted for most, ~90% of all aberrant chromosome counts (Fig. 4-7C). Similar findings were observed in all three replicates, in which combined siRNA conditions revealed a 2.7-fold increase in aberrant chromosome numbers using siFBXO30-

2 and 2.5-fold increases in aberrant chromosome numbers using siFBXO30-4 and -P relative to siControl (Fig. 4-7D; Table S3**,** Appendix B). Collectively, these data are consistent with reduced *FBXO30* expression inducing CIN in a non-malignant, non-transformed colonic cellular context.

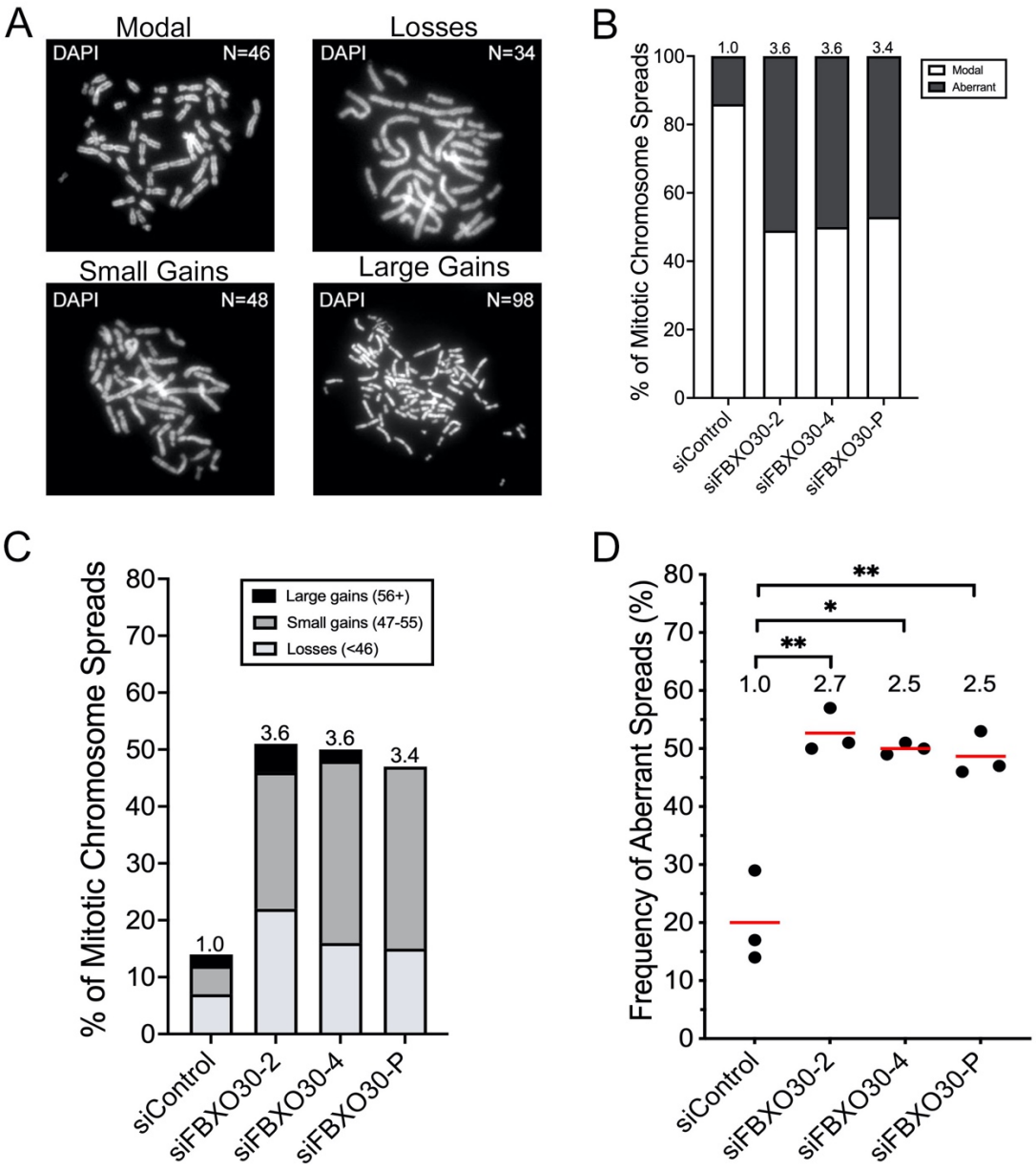

Figure 4-7. Reduced *FBXO30* Corresponds with Significant Increases in Aberrant Chromosome Numbers in 1CT Cells.

(A) High-resolution images of DAPI-counterstained chromosomes presenting the modal number of chromosomes (46), chromosome losses (<46), small-scale chromosome gains (47-55), and large-scale chromosome gains (≥56). Chromosome numbers are indicated in the top right corner of each image. ***(B)*** Bar graph depicting the frequency of aberrant mitotic spreads relative to the modal karyotype following *FBXO30* silencing. ***(C)*** Bar graph presenting fold-increases in aberrant chromosome categories (losses, small-scale changes, and large-scale changes) in the different siRNA conditions relative to the siControl. Numbers above each condition represent the fold-increase in aberrant chromosome numbers. ***(D)*** Dot plot reveals fold-increases in aberrant chromosome numbers in combined siRNA conditions of three replicates relative to the siControl. Numbers above silencing condition represent the fold-increase in aberrant chromosome numbers. (Student's t-test; *p-value <0.05; **p-value <0.01; red bars= mean; N=3, n=6).

4.3.3. *FBXO30* is Efficiently Silenced in A1309 Cells

Similar to the 1CT results, the efficacy of *FBXO30* silencing in the A1309 cell line was determined using an siRNA-based approach with siFBXO30-2, -4, and -P. In agreement with 1CT findings, *FBXO30* was efficiently silenced in A1309 cells, with residual FBXO30 protein levels detected at 1% (siFBXO30-2), 4% (siFBXO30-4), and 2% (siFBXO30-P) compared to siControl (Fig. 4-8; Fig. S3, Appendix B). Although some variation occurred between replicates in A1309 cells, *FBXO30* silencing consistently reduced FBXO30 protein levels to < 5% relative to the siControl (Fig. 4-5 and Fig. 4-8).

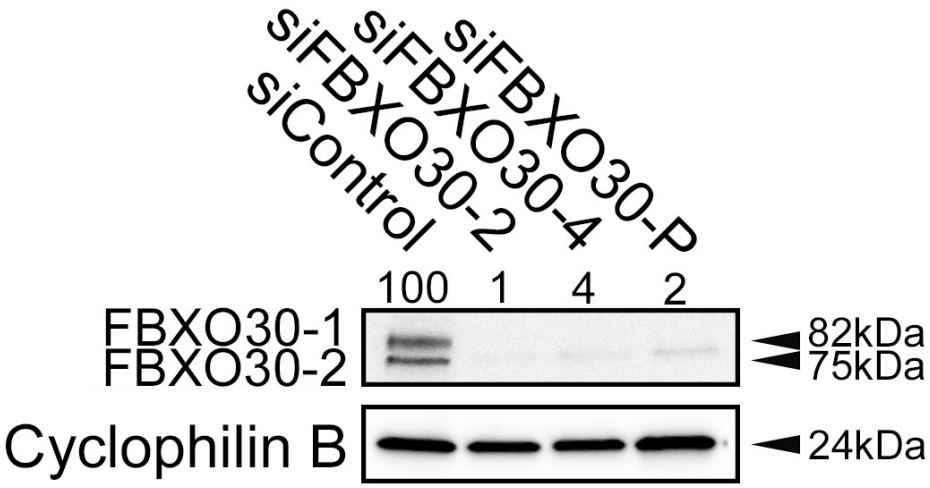

Figure 4-8. *FBXO30* is Silenced Effectively in A1309 Cells.
Western blot reveals reduced FBXO30 abundance in A1309 cells following silencing with siFBXO30-2, -4 and -P. FBXO30 abundance was normalized to the associated loading control, (Cyclophilin B) and is compared to siControl (100%). (N= 3)

4.3.4. Reduced *FBXO30* Expression Induces CIN-Associated Phenotypes in A1309 Cells

Since *FBXO30* was efficiently silenced in A1309 cells, the effects of *FBXO30* silencing on nuclear areas and micronucleus formation were evaluated. Representative images of Hoechst-counterstained nuclei display clear visual differences in nuclear areas following *FBXO30* silencing (Figure 4-9A) that correspond with significant increases (rightward shifts) in nuclear area

distributions in all siRNA conditions relative to siControl in all three replicates (Fig. 4-9B; two-sample KS test; p-value <0.05; Table S4, Appendix B). It is important to note that passage number can strongly affect the efficacy of *FBXO30* silencing as higher passage clones often present with genetic drift, clonal evolution, and altered morphology and growth rates over time[111]. Within each replicate, siFBXO30-2 exhibited the greatest increase in nuclear area distributions; however, siFBXO30-4 and -P superimpose the siControl, indicating a weaker phenotype (Fig. 4-9B). Quantitative analyses showed significant increases in micronucleus formation using siFBXO30-2 in all replicates and siFBXO30-4 in one replicate relative to siControl (4-9D; MW test, p-value <0.05; Table S5, Appendix B). However, siFBXO30-P did not affect micronucleus formation as shown in Figure 4-9D, suggesting the combined siRNA condition does not induce changes in micronucleus formation.

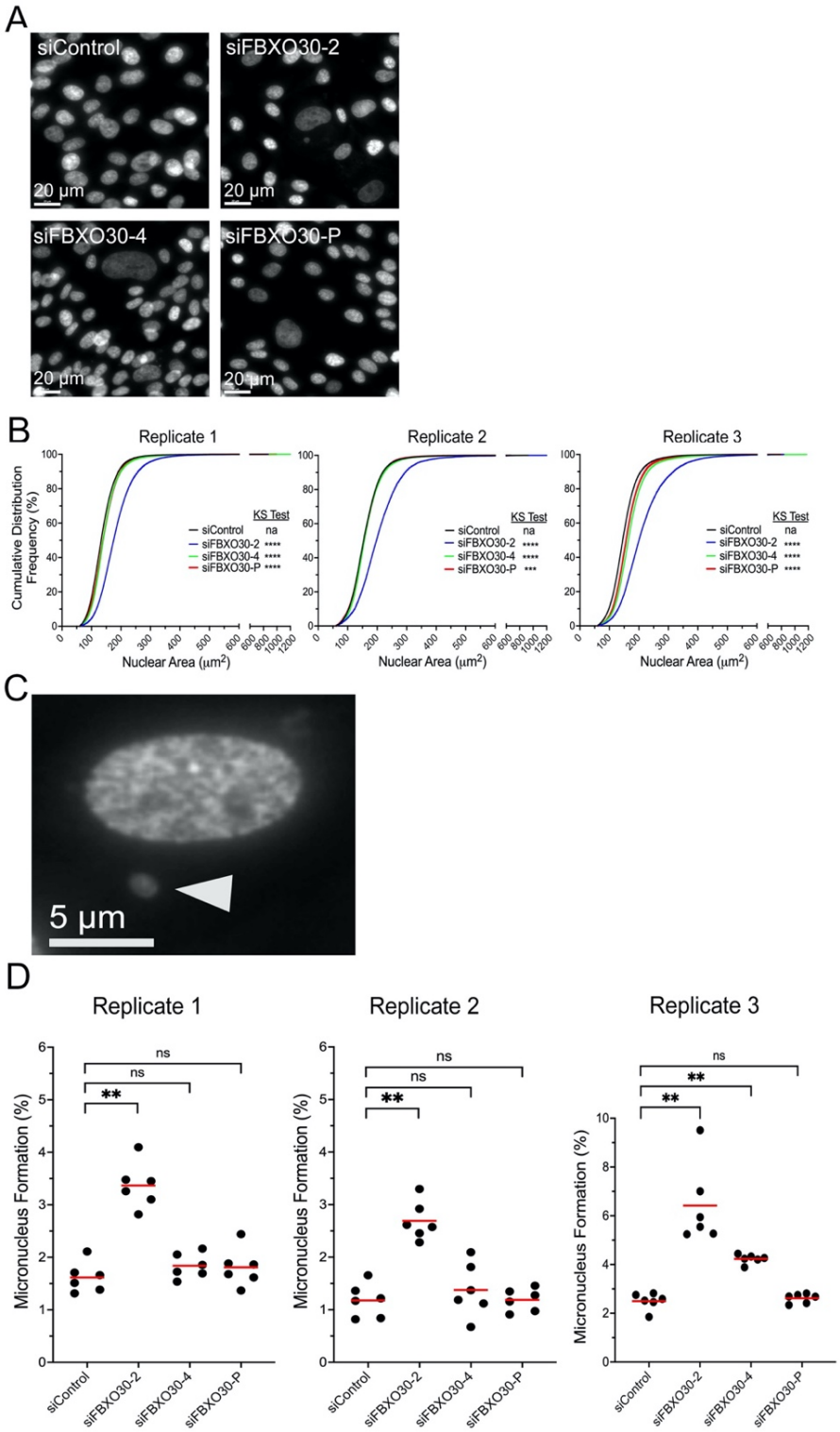

Figure 4-9. *FBXO30* Silencing Induces Significant Increases in CIN Phenotypes in A1309 Cells. ***(A)*** Low-resolution images of Hoechst-counterstained nuclei indicating visual changes in nuclear sizes following *FBXO30* silencing relative to siControl. ***(B)*** Cumulative distribution frequency graphs reveal statistically significant increases (siFBXO30-2, -4, -P; rightward shifts) in nuclear areas following *FBXO30* silencing relative to the siControl (two-sample KS test; na; not applicable; ****p-value

<0.0001; N= 3, n= 6). ***(C)*** High-resolution image of Hoechst-counterstained nucleus with corresponding micronucleus (arrowhead). ***(D)*** Dot plots reveal statistically significant increases in micronucleus formation following silecning with siFBXO30-2 relative to the siControl. (MW test; ns= not significant; **p-value <0.01; red bars= median; N= 3, n= 6). Replicate 1 was on passage 12, replicate 2 was on passage 15, and replicate 3 was on passage 21.

To assess the impact of reduced *FBXO30* expression on chromosome complements, mitotic chromosome spreads were generated and enumerated in A1309 cells. A1309 cells are defined as a diploid and male, karyotypically stable cell line with a modal karyotype of 46XY. As such, deviations from the modal karyotype are characterized as losses (< 46 chromosomes), small-scale gains (47-55 chromosomes), or large-scale gains (≥ 56 chromosomes), as shown in Figure 4-10A. Aberrant chromosome spreads presented with 1.7, 1.5, and 1.7-fold increase in siFBXO30-2, 4, and -P respectively relative to siControl, with the majority of aberrant spreads comprising of chromosome losses (Fig. 4-10B, C**)**. Cumulative data from three replicates show that *FBXO30* silencing using the individual siRNAs, along with the pool, induced significant fold-increases in aberrant chromosome numbers relative to the siControl (Fig. 4-10D; Table S6, Appendix B**)**. In agreement with data from the 1CT cell line, siFBXO30-2 induced the maximum fold-increase (*i.e.*, 1.8-fold increase) in aberrant chromosome numbers across all replicates in A1309 cells (Fig. 4-10D**)**. Collectively, the chromosome enumeration data, along with analyses of nuclear area and micronucleus formation analyses, suggest that *FBXO30* is a novel CIN gene in the A1309 cells. Therefore, *FBXO30* silencing induced CIN-associated phenotypes in two non-malignant colonic epithelial and is consistent with reduced expression inducing CIN that may promote CRC tumorigenesis.

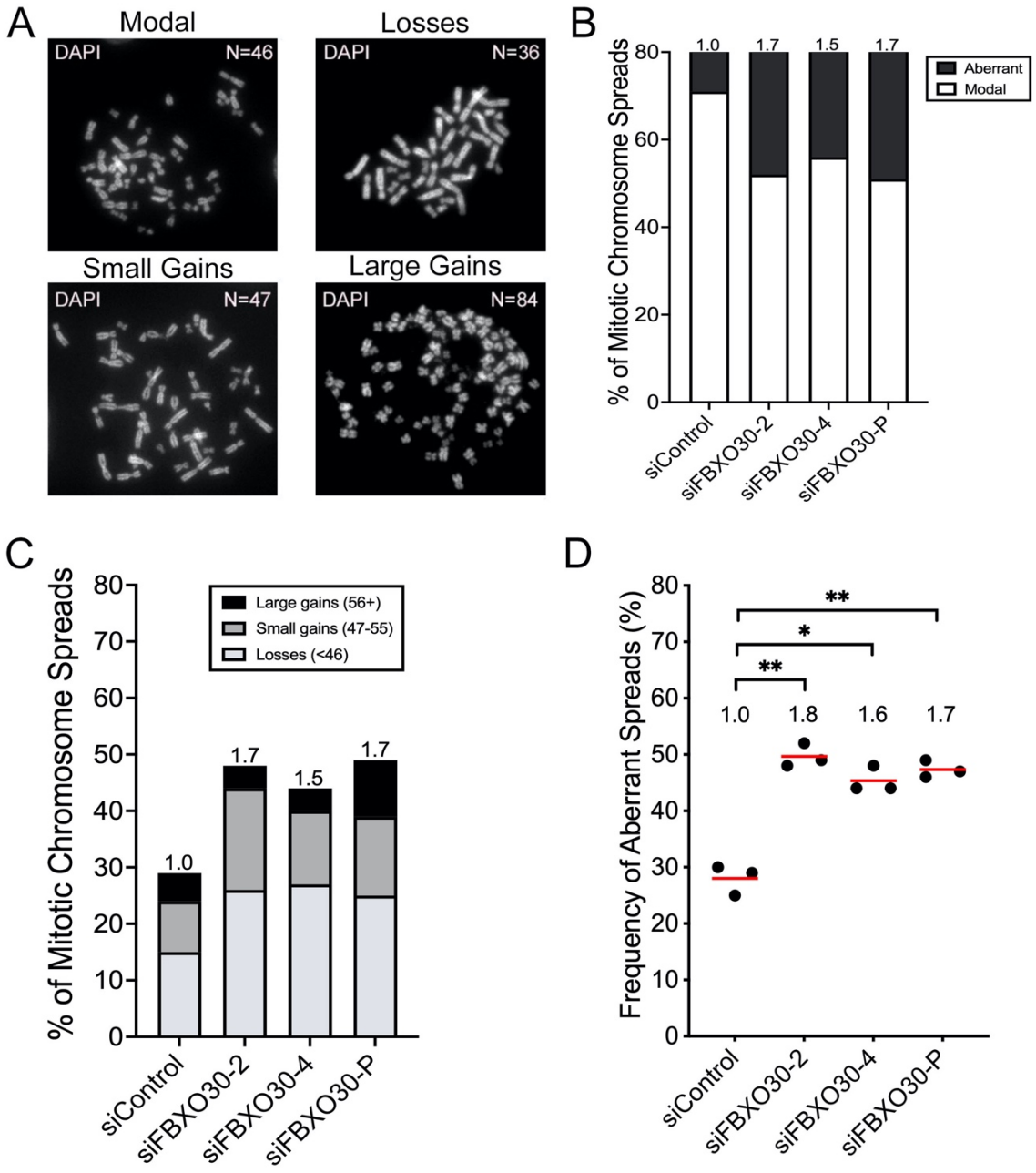

Figure 4-10. Reduced *FBXO30* Expression Induces Significant Increases in Aberrant Chromosome Numbers in A1309 Cells.

(A) High-resolution images of DAPI-counterstained chromosomes exhibiting the modal number of chromosomes (46), chromosome losses (<46), small-scale chromosome gains (47-55), and large-scale chromosome gains (≥56). Chromosome numbers are indicated in the top right corner of each image. ***(B)*** Bar graph depicting the frequency of aberrant mitotic spreads relative to the modal karyotype following *FBXO30* silencing. ***(C)*** Bar graph presents the fold-increases in aberrant chromosome number categories in the different siRNA conditions relative to the control, following *FBXO30* silencing. ***(D)*** Dot plot presents the cumulative replicate data of the different siRNA conditions, inducing fold-increases in aberrant chromosome numbers relative to the siControl (Student's t-test; **p-value <0.01; red bars= mean; N=3, n=6).

4.4. AIM 2: To Determine the Impact Reduced *FBXO30* Expression has on CIN in a Malignant Colorectal Cancer Context.

Preliminary data from *Research Aim 1* indicate that *FBXO30* silencing induces CIN-associated phenotypes in two non-malignant, non-transformed colonic epithelial cell lines. However, the impact of reduced *FBXO30* expression on CIN has yet to be examined in a clinically relevant malignant CRC cellular context. In this study, the HCT116 cell line, a karyotypically stable male CRC cell line, is used to address this research gap and to evaluate the impact of reduced *FBXO30* expression on CIN in a malignant CRC context.

4.4.1. *FBXO30* is Effectively Silenced in HCT116 Cells

Previous semi-quantitative western blots in HCT116 cells included the set of four individual siRNA duplexes and the pool to determine the two most efficient silencers of *FBXO30* expression (Fig. 4-4; Fig. S4, Appendix B). As shown in Figure 4-11, siFBXO30-2, -4, -P exhibit similar *FBXO30* silencing to the other cell lines, with silencing efficacy reducing FBXO30 abundance of both isoforms to < 5% of the siControl. Western blots were performed in triplicate to validate that FBXO30 and the alternative splice variant can be effectively silenced in a CRC malignant context (Fig. 4-11).

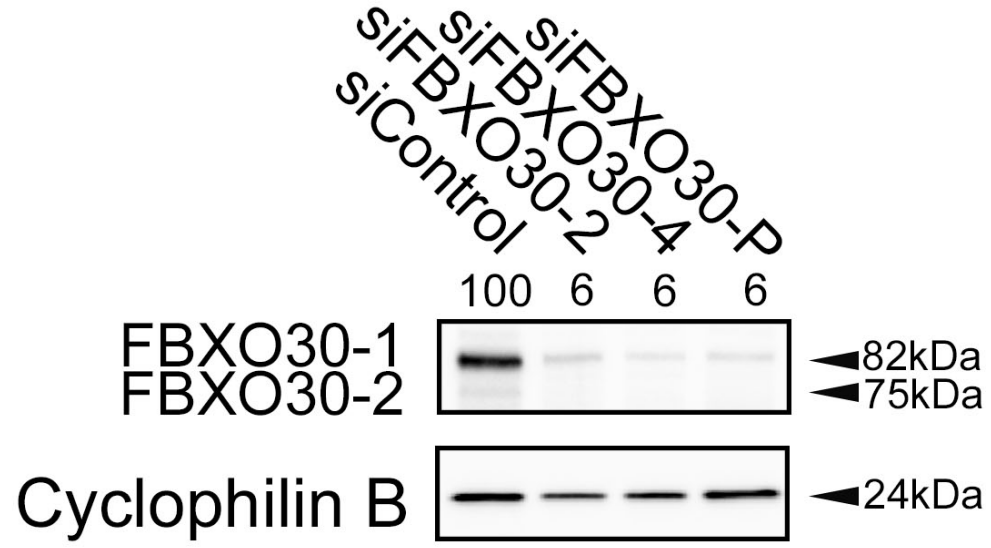

Figure 4-11. *FBXO30* is Efficiently Silenced in HCT116 Cells.
Semi-quantitative western blot presents diminished FBXO30 abundance relative to the siControl after silencing with siFBXO30-2, -4, and -P. FBXO30 was normalized to the loading control (Cyclophilin B) and is presented relative to siControl (100%). (N= 3)

4.4.2. Reduced *FBXO30* Expression Induces CIN-Associated Phenotypes in HCT116 Cells

Following validation of *FBXO30* silencing, images of Hoechst-counterstained nuclei show that silencing induces significant increases (rightward shift) in cumulative nuclear area distributions relative to siControl (Fig. 4-12A, B; two-sample KS test; p-value <0.05; Table S7, Appendix B). Similar to the non-malignant cell lines, siFBXO30-2 presents significant increases in nuclear area sizes, while siFBXO30-4 closely resembles the siControl in all three replicates (Fig. 4-12B). Conversely, siFBXO30-P in the malignant context exhibits a stronger phenotype like siFBXO30-2 (Fig. 4-12B). Representative image of Hoechst-counterstained nucleus and associated micronucleus (Fig. 4-12C) depict significant increases in micronucleus formation in all siRNA conditions (siFBXO30-2, -4, and -P) relative to siControl in replicate 2 (MW test; p-value <0.05; Fig. 4-12 D; Table S8, Appendix B). Whereas replicate 1 reveals no significant increase in micronucleus formation under any of the siRNA conditions (Fig. 4-12 D). Replicate 3 reveals a significant increase in micronucleus formation relative to siControl using siFBXO30-2, whereas

the other siRNA conditions exhibit heterogeneity among technical replicates yet remain non-significant (Fig. 4-12 D). These data suggest that reduced *FBXO30* expression induces significant increases in nuclear areas in HCT116 cells yet presents greater variability in micronucleus formation.

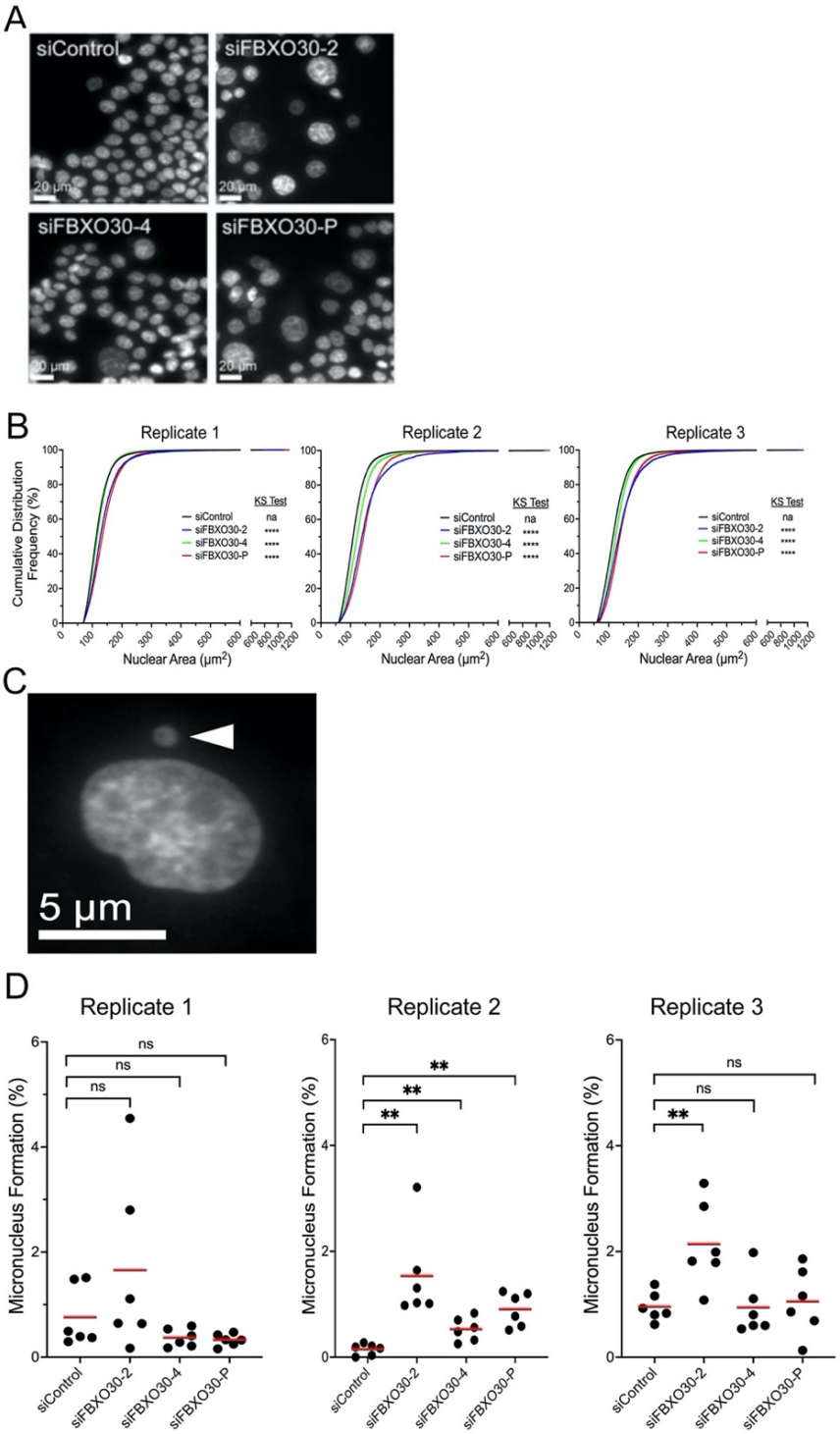

Figure 4-12. Reduced *FBXO30* Expression Corresponds with Significant Increases in CIN Phenotypes in HCT116 Cells.

(A) Low-resolution images of Hoechst-counterstained nuclei exhibiting visual changes in nuclear areas following *FBXO30* silencing relative to siControl. ***(B)*** Cumulative distribution frequency graphs reveal statistically significant increases (siFBXO30-2, -4, -P; rightward shifts) in nuclear areas following *FBXO30* silencing relative to the control. (Two-sample KS test; na; not applicable; ****p-value <0.0001; N=3, n=6). ***(C)*** High-resolution image of Hoechst-counterstained nuclei with associated

micronucleus (white arrowhead). ***(D)*** Dot plot depicting statistically significant increases in micronucleus formation following silencing with siFBXO30-2 relative to the control. (MW test; ns= not significant; **p-value <0.01; red bars= median; N=3, n=6). Replicate 1 was on passage 19, replicate 2 was on passage 25, and replicate 3 was on passage 28.

To compare with our 1CT and A1039 results, mitotic chromosome spreads were generated in HCT116 cells to evaluate changes in chromosome numbers following *FBXO30* silencing in a male, malignant, near-diploid CRC cell line, with a modal karyotype of 45X. Any deviations from the modal karyotype are defined as aberrant spreads consisting of losses (< 45 chromosomes), small-scale gains (46-54 chromosomes), or large-scale gains (≥ 55 chromosomes), as shown in Figure 4-13A, C. Generally, *FBXO30* silencing with siFBXO30-2, -4, and -P resulted in significant 1.6-, 1.4-, and 1.5- fold increases in aberrant mitotic chromosome spreads compared to the siControl, with ~90% of all aberrant spreads comprising of losses and small gains (Fig. 4-13B, C). Combined siRNA conditions from each replicate indicate that the two individual siRNAs, siFBXO30-2 and -4, and -P induced significant increases in aberrant chromosome numbers relative to the siControl, with maximum 1.6, 1.4, and 1.5-fold increases observed, respectively (Student's t-test; p-value <0.05; Fig. 4-7D; Table S9, Appendix B). Collectively, these data suggest *FBXO30* is a novel CIN gene in HCT116 cells.

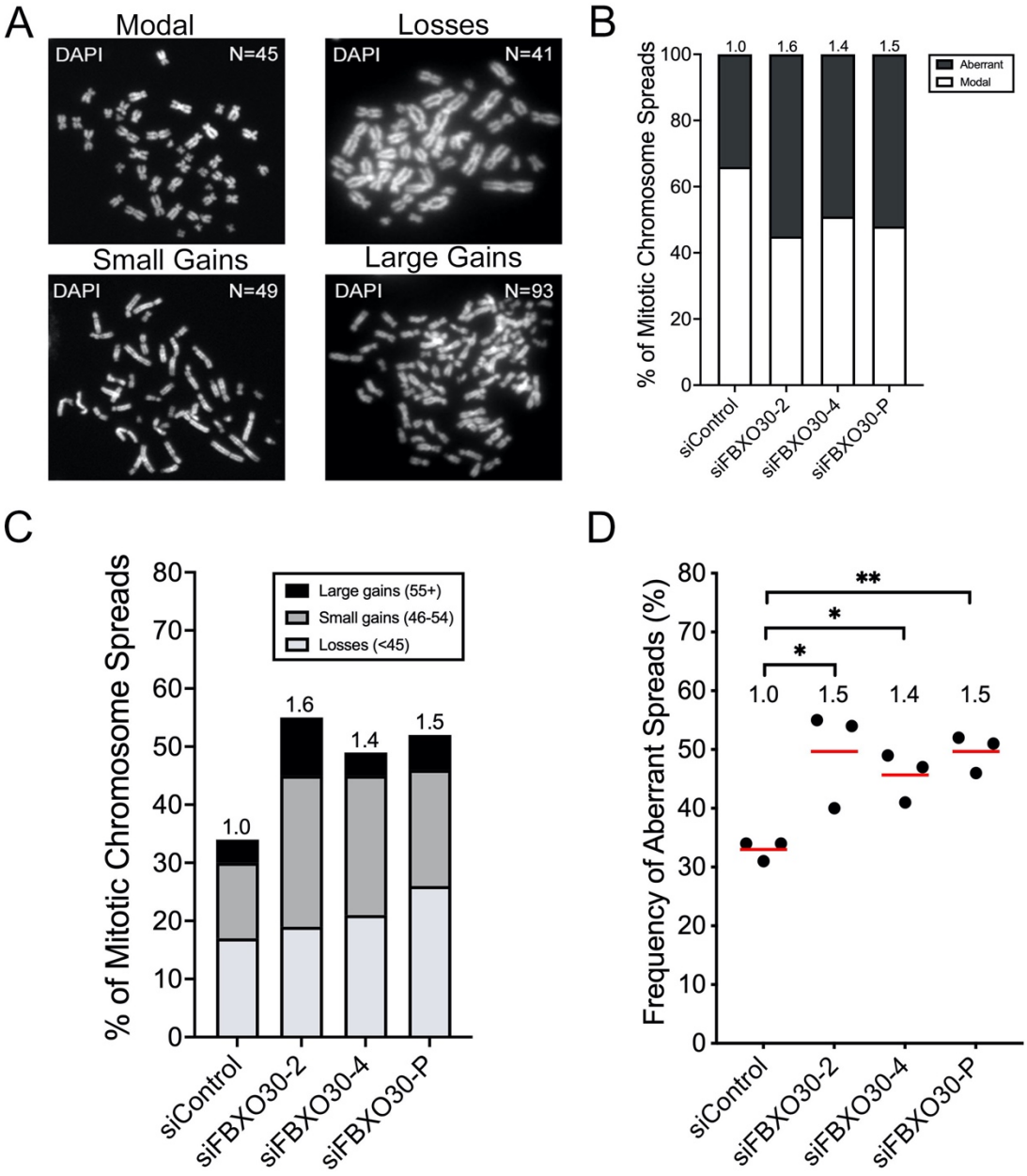

Figure 4-13. *FBXO30* Silencing Causes Significant Changes in Chromosome Numbers in HCT116 Cells.

(A) High-resolution images of DAPI-counterstained chromosomes exhibiting the modal number of chromosomes (45), chromosome losses (<45), small-scale chromosome gains (46-54), and large-scale chromosome gains (55+). Chromosome numbers are indicated in the top right corner of each image. ***(B)*** Bar graph presenting the impact of *FBXO30* silencing on chromosome numbers in mitotic spreads relative to the modal karyotype. ***(C)*** Bar graph depicting fold-changes in aberrant chromosome numbers across the different siRNA conditions following *FBXO30* silencing relative to the control. ***(D)*** Dot plot presents combined siRNA conditions with significant increases in aberrant chromosome numbers following *FBXO30* silencing is achieved (Student's t-test; **p-value <0.01; red bars= mean; N= 3, n= 6).

CHAPTER 5: SUMMARY, DISCUSSION, CONCLUSIONS, AND SIGNIFICANCE

5.1. SUMMARY

In this research project, I employed siRNA-based approaches in non-malignant and malignant colonic epithelial cell lines to evaluate the impact of reduced *FBXO30* on CIN. In *Research Aim 1*, transient siRNA-based gene silencing reduced endogenous FBXO30 levels in two karyotypically stable non-malignant, non-transformed colonic epithelial cell lines, 1CT and A1309. In *Research Aim 2*, analogous siRNA-based techniques decreased *FBXO30* expression in HCT116 cells, a CRC malignant cell line. In the non-malignant cells, transient *FBXO30* silencing resulted in significant increases and decreases in nuclear area, increases in micronucleus formation with siFBXO30-2 and -4, and increases in aberrant chromosome numbers in 1CT cells. Whereas *FBXO30* silencing induced significant increases in nuclear area, increases in micronucleus formation only with siFBXO30-2, and a significant increase in aberrant chromosome numbers in A1309 cells. Furthermore, the results from *Research Aim 2* showed reduced *FBXO30* abundance in HCT116 cells, resulted in significant increases in nuclear area in all siRNA conditions, significant increases in micronucleus formation with siFBXO30-2, and significant increases in mitotic spreads harboring aberrant chromosome numbers. Although *FBXO30* silencing in each cell line consistently exhibited a similar reduction in FBXO30 expression levels with siFBXO30-2, -4, and -P (*i.e.*, FBXO30 abundance remains < 5% relative to siControl), results from the CIN assays revealed dynamic and heterogeneous changes in CIN-associated phenotypes between replicates and in the different cell lines. As such, siFBXO30-2 may be generating potential off-target effects as it results often differ from the other siRNAs by promoting notably stronger CIN phenotypes. Alternatively, CIN drives cellular and genetic heterogeneity and may induce differing outcomes across siRNA conditions in the different cell lines, as transient changes in *FBXO30* copy

numbers may be implicated in the mechanisms underlying CIN[65,112]. Collectively, this study identifies *FBXO30* as a novel CIN gene in both non-malignant and malignant colonic epithelial cells and may be implicated in early events driving CRC development.

5.2. DISCUSSION

5.2.1. *FBXO30* Silencing Induces Greater Increases in Nuclear Area Sizes in the Non-malignant Cell Lines than in the Malignant Cells

As mentioned above, CIN is defined as the increased rate of gains or losses of whole chromosomes and/or chromosome fragments[55,94,113,114]. Therefore, it is expected that reduced *FBXO30* expression would induce increases and decreases of chromosome complements, which would be revealed in nuclear areas and mitotic chromosome spread assays. 1CT and A1309 cells are non-transformed and non-malignant and were expected to respond differently to *FBXO30* silencing than the malignant CRC cell line, HCT116. Previous studies have established that 1CT and A1309 cells are diploid and retain a relatively uniform, larger baseline nuclear area than HCT116 cells, which exhibit greater nuclear pleomorphism[53,55,94,107]. Whereas, HCT116 is a near-diploid CRC cell line with underlying aneuploidy due to loss of the Y chromosome and harbors an *MLH1* mutation that disrupts the high-fidelity mismatch repair pathway, rendering the cells more susceptible to further DNA mutations[115,116]. Due to the loss of DNA mismatch repair gene *MLH1*, it greatly increases incidence of spontaneous mutations in HCT116 cells[117] that may give rise to greater nuclear morphology heterogeneity[118,119]. Additionally, HCT116 cells retains wild-type *TP53*, enabling the cells to mediate apoptosis or quiescence following extreme damage from cellular stress[115,116,119], such as *FBXO30* silencing. Apoptotic cells would be excluded from nuclear area analyses due to intensity filter applications (see Section 3.5.2.) and any quiescent cells

included in the data would represent decreases in nuclear area sizes[120,121]. Collectively, these features of the HCT116 cell line may contribute to the increased heterogeneity in nuclear areas observed in the non-malignant cell lines compared to the malignant HCT116 cells (Figs. 4-6, 4-9, and 4-10).

5.2.2. *FBXO30* Silencing with siFBXO30-P Corresponds with Significant Decreases in Nuclear Areas in 1CT Cells

Previous studies from the McManus laboratory have established that silencing of SCF complex members and F-box proteins (*e.g.*, *SKP1*, *CUL1*, *SKP2*, *FBXO7*, *FBXO5*) resulted in significant increases in nuclear areas across each replicate and in multiple cell lines[53,55,92-94], including 1CT, A1309, and HCT116. However, in this study, silencing *FBXO30* with siFBXO30-P in 1CT cells was associated with significant decreases in nuclear areas. Large-scale increases in DNA content (*e.g.*, ploidy) are better tolerated in cancer contexts as compensation mechanisms more readily buffer excess gene dosage over large-scale losses of genetic content[122-124]. Thus, it is expected that large decreases in chromosome complements are lethal, and the cell population following *FBXO30* silencing would favor increases in nuclear areas. A possible explanation for the significant decreases in nuclear area observed in 1CT cells using siFBXO30-P is confluency. Once homogeneously seeded non-transformed cells reach confluency in a tissue culture dish, they cease proliferation due to a phenomenon known as contact inhibition[125]. The mechanical force (*i.e.*, contact with neighboring cells) arises following successive cell divisions and triggers morphological and physiological changes in the cells, marked by decreases in nuclear area, mobility, and mitosis[125,126]. 1CT cells that reached confluency could lead to the accumulation of cells in the G0 quiescent state of the cell cycle, in which cells are not actively dividing and ultimately result in significant decreases in cumulative nuclear areas as observed with siFBXO30-

P in Figure 4-6. Evidence of confluency in siFBXO30-P condition in 1CT cells is shown in Supplementary Figure 5, in which images of Hoechst-counterstained nuclei in siFBXO30-P conditions of each replicate exhibit increases in nuclear counts relative to the images from the siControl. This suggests the cells in siFBXO30-P conditions have attained confluency, which inhibited their growth and proliferation and led to G0 quiescence. Due to the fact that this phenotype is unique to siFBXO30-P and is present in all three replicates, while the siControl does not exhibit confluency, suggests the confluency in siFBXO30-P could be attributed to an increase in the proliferation rate of the 1CT cells. If siFBXO30-P induces a significant increase in cellular proliferation, it would produce more cells per well than the other siRNA conditions, resulting in contact inhibition induced G0 quiescence, and ultimately leading to significant decreases in nuclear areas in 1CT cells. In order to assess G0 quiescent cells in the siFBXO30-P condition, cells could also be stained with Pyronin Y, a stain with specificity toward RNA[127]. Quiescent cells exhibit global downregulation of transcription and translation[120], which would enable Pyronin Y staining to differentiate between low RNA-containing quiescent cells and actively dividing cells within the population. A limitation to the CIN assays in this study is the lack of temporal experiments to examine CIN progression over successive cell generations, which includes the inability to assess the cellular proliferation rates. Therefore, to validate whether siFBXO30-P induces significant increases in cellular proliferation in 1CT cells, a cell viability assay could be employed to assess the growth of 1CT cells treated with siFBXO30-P relative to siControl over a time course of 7-days post-transfection.

5.2.3. Reduced *FBXO30* Expression Corresponds with Increases in Micronucleus Formation Using the Two Individual siRNAs that may Induce Chromatid Breaks and Chromosome Condensation Errors

As described in Section 1.3.3, micronuclei are small extranuclear bodies that arise from lagging chromosomes or acentric chromosome fragments generated during mis-segregation events[73]. In this study, notable differences in the frequency of micronucleus formation were observed following siFBXO30-2, -4, and -P silencing between replicates and cell lines. It is possible that FBXO30 is not equally silenced within a given population following silencing, leading to variation between replicates. Despite semi-quantitative western blots showing efficient silencing across all cell lines (Fig. 4-5, 4-8, 4-11), western blots present a population average and therefore masks the variation in silencing efficiencies occurring between individual cells within a population. Hence, it is possible that varying levels of *FBXO30* expression may contribute to the heterogeneity in micronucleus formation across replicates for each silencing condition. Another possibility is a synergistic effect from the pre-existing gene mutations contained within in each cell line (see Table 3-1). Recall that 1CT has wild-type *KRAS*, *TP53*, and *APC*, while HC116 and A1309 possess *KRAS* mutations, with A1309 harboring an additional 50 % knockdown of *TP53* and expresses a truncated form of APC. Previous research has determined that the expression of oncogenic *KRAS*, such as $KRAS^{G13D}$ in HCTT16 cells, induces mitotic delays and defects in chromosome segregation, including misaligned or lagging chromosomes in anaphase[128]; whereas, cells with wild-type *KRAS* did not show mitotic delay or defects in chromosome alignment[128]. Additionally, *TP53* exhibits an essential role in maintaining genome stability by regulating cellular response (*e.g.*, proliferation and apoptosis) in the presence of severe DNA damage[47]. Loss of *TP53* leads to increased mis-segregation events, resulting in chromosome gains and losses and driving

the survival of aneuploid cells[47]. Thus, *TP53* knockdown may enable cells with DNA damage to undergo uncontrolled proliferation following *FBXO30* silencing. Finally, APC regulates microtubule dynamics and proper chromosome segregation, so in cases of *APC* loss, a greater increase in micronuclei may be observed[129]. According to the adenocarcinoma pathway, *KRAS*, *TP53*, and *APC* are strongly associated with CRC pathogenesis, yet these mutations alone do not induce CIN. As such, it may be that one or all of the mutations in *KRAS*, *TP53*, and *APC* synergize with *FBXO30* silencing to exacerbate increases in micronucleus formation. Therefore, loss and/or reduced *FBXO30* expression may be a contributing factor in the development of a subset of CRCs.

It is also important to assess the potential downstream consequences of reduced *FBXO30* expression, including its impact on micronucleus formation. It has been established that FBXO30 is a member of the SCF complex, which regulates the timely degradation of target substrates. Previous studies have shown that *FBXO30* silencing is associated with micronucleus formation by destabilizing mitotic spindle dynamics and chromosome condensation through accumulation of target substrates KIF11 and SLBP, ultimately leading to lagging chromosomes or acentric fragments being excluded from the nucleus[96,97]. KIF11 is normally responsible for maintaining centrosome and mitotic spindle dynamics[130,131], and in cases of *KIF11* overexpression, it promotes pericentriolar material (PCM) or centrosome fragmentation, lagging chromosomes, and mitotic catastrophe[130]. As such, KIF11 overexpression is associated with CIN in other human non-transformed cell lines with pronounced increases in micronucleus formation[130]. However, it was observed that the different levels of KIF11 overexpression determined cell fate, as high levels of KIF11 exhibited PCM fragmentation and led to mitotic catastrophe (*i.e.*, a state of irreversible arrest that precedes programmed cell death)[130,132], whereas mild to moderate KIF11 overexpression corresponded with a higher frequency of lagging chromosomes, while the mitotic

spindle remained intact enabling the cells to divide with aneuploidy-type errors[130]. In regards to the accumulation of SLBP in the event of *FBXO30* loss, SLBP accumulation led to histone H3 overloading, resulting in chromosome overcondensation[97]. Over-condensed chromosomes are fragile and more prone to physical breakage in anaphase, leading to chromatid breaks and fragments during segregation[97], and increasing the probability of micronucleus formation. Therefore, the significant increases in micronucleus formation following *FBXO30* silencing may be attributed to KIF11 and SLBP accumulation that induce abnormal chromosome condensation and chromatid breaks.

In this study, siFBXO30-2 consistently induced the strongest CIN phenotypes and was the sole siRNA duplex targeting *FBXO30* to induce significant increases in micronucleus formation in all three cell lines (1CT, A1309, and HCT116). Therefore, two possible explanations are that siFBXO30-2 produces the strongest phenotypes or an off-target effect. The western blots of the four individual siRNAs reflect similar silencing efficacies across each cell line, with < 5% of remaining FBXO30 abundance (Fig. 4-5, 4-8, 4-11**)**, however, western blots are bulk assays limited to averaging protein abundance and does not resolve cell-to-cell silencing efficiencies of the individual siRNAs. To determine off-target effects, additional orthogonal experiments can be performed, such as genetic rescue experiments, to validate whether the phenotype was produced from on-targeting effects of the siRNA duplex. Despite the possibility of off-target effects, the individual siRNA duplexes were designed by Horizon (Dharmacon) to maximize targeting of *FBXO30* transcripts and mitigate the risk of off-target effects. As such, it is most likely that *FBXO30* silencing induced increases in micronuclei by promoting moderate to high accumulation of KIF11 and SLBP in the non-malignant and malignant colonic epithelial cell lines, thereby increasing frequencies in chromatid breaks or lagging chromosomes. As presented within

Supplementary Tables S2, S5, and S8, the mean nuclear count in siFBXO30-2 conditions in 1CT, A1309, and HCT116 cells was the smallest compared to siFBXO30-4, -P and siControl, indicating that siFBXO30-2 induces a form of cell death, most likely apoptosis due to mitotic catastrophe from high levels of KIF11 accumulation[96]. The other individual siRNA, siFBXO30-4, was inconsistent in inducing significant increases in micronuclei, suggesting it may produce a weaker effect due to lower levels of substrate accumulation. However, siFBXO30-P induced a notable increase in micronucleus formation in only one replicate in HCT116 cells, demonstrating an overall inability to increase micronucleus frequency in non-malignant and malignant colonic epithelial cell lines. A possible explanation is that the combined effect of the individual siRNAs in siFBXO30-P dilutes the effects of siFBXO30-2 and -4, resulting in no detectable phenotype being observed. Although it may be suggested that the combined effects of the individual siRNAs in the pool condition could be so effective in inducing CIN that it ultimately results in cell death, assessment of the mean nucleus count (see Appendix B) for siFBXO30-P conditions in all three replicates and across the different cell lines revealed nucleus counts similar to or more than those of siControl. Therefore, *FBXO30* silencing may induce KIF11 and/or SLBP accumulation to promote CIN phenotypes, including micronucleus formation.

5.2.4. Decreased *FBXO30* Expression Results in Larger Increases in Aberrant Chromosome Numbers in 1CT Cells

CRC development arises from the acquisition of a series of mutations in genes that regulate critical cellular processes and signaling pathways, including *APC*, *KRAS*, and *TP53*. Due to the important role of these genes in CRC pathogenesis, there is a need for *in vitro* models (*e.g.*, 1CT and A1309 cells) to represent these genetic alterations in CRCs. In this study, 1CT cells exhibited greater fold-increases in aberrant chromosome spreads compared to A1309 and HCT116 cells

following *FBXO30* silencing due to underlying genetic mutations in the A1309 and HCT116 cell lines. 1CT cells maintain a ~20 % baseline frequency of aberrant chromosome spreads in siControl (see Fig. 4-7), as a result of no underlying mutations to *APC*, *KRAS* or *TP53*. Additionally, 1CT cells retain intact cellular checkpoints that arrest cells with aberrant chromosome numbers in G1[133] and be excluded from the mitotic chromosome spreads, resulting in less aberrant spreads being observed in siControl. Whereas A1309 cells are a model for the adenocarcinoma sequence and maintain a higher ~30% baseline frequency of aberrant spreads in siControl (see Fig. 4-10), with impaired cellular checkpoints from *TP53* knockdown. This suggests that *FBXO30* silencing induces larger fold-increases in aberrant chromosome numbers in 1CT cells, while aberrant spreads will occur at a smaller magnitude in A1309 cells, as seen in Figures 4-7 and 4-10. HCT116 cells are a near diploid cell line that exhibits MSI and an increased susceptibility to CIN[134]. Both A1309 and HCT116 cells harbor oncogenic alterations, that enable them to better tolerate chromosome mis-segregation and aneuploidies[81,135,136], following *FBXO30* silencing. In the event of CIN, HCT116 cells have been shown to enable the proliferation of aneuploidy cells despite retaining normal p53 activity[64], indicating a greater tolerance to CIN perturbations[64,81]. Although A1309 and HCT116 cells are more readily susceptible to CIN, cells with extreme changes (*i.e.*, gains and/or losses) to chromosome content following *FBXO30* silencing may preferentially undergo programmed cell death and fail to be incorporated into the spreads[130]. As such, any extreme changes to chromosome complements will be under-represented in chromosome spreads and reduce the overall amount of large-scale gains enumerated in the aberrant spreads following *FBXO30* silencing. Therefore, reduced *FBXO30* expression induces significant changes in chromosome numbers across all three cell lines, in which the underlying genetic mutations, cell cycle checkpoints, and tolerance to CIN determine that larger fold-increases in aberrant

chromosome numbers will be observed in 1CT cells compared to A1309 and HCT116 cells following *FBXO30* silencing.

5.2.5. Reduced *FBXO30* Expression Corresponds with Significant Chromosome Losses in Non-Malignant and Malignant Cell Lines

Although QuantIM analyses of CIN phenotypes showed that reduced *FBXO30* expression was primarily associated with significant increases in nuclear area across all three cell lines, mitotic chromosome spreads revealed that chromosome losses occurred most frequently. The mechanisms underlying this paradox remain unknown; however, both technical and biological factors may account for this observation. To start, nuclear area analyses are performed exclusively on interphase populations, while mitotic chromosome spreads are limited to mitotic cell populations. Next, cell populations in the mitotic spreads were asynchronous, and only a small sub-population of cells capable of entering and remaining mitosis were analyzed. Third, recall that reduced *FBXO30* expression induced significant increases in nuclear areas, which is indicative of large-scale changes in the DNA content (*i.e.*, polyploidy cells) that were underrepresented in the mitotic spreads. Polyploidy cells may undergo G1 cell cycle arrest through p53-dependepent cell cycle checkpoints[66] or undergo proliferation at slower rates compared to their diploid counterparts[66,67], in which either outcome would lead to their exclusion from the mitotic spreads. Finally, endoreduplication is the aberrant biological process in which cells successively replicate their genomes without entering mitosis[137] and is associated with disease pathogenesis in several cancer types, including CRC[138]. This process was rarely observed in the aberrant mitotic spreads of each cell line following *FBXO30* silencing, suggesting the cells did not achieve polyploidy through endoreduplication or were not captured within the Colcemid treatment window. These observations were evident in the chromosome enumeration data, in which ~10% of all aberrant

spreads in each cell line comprised of large-scale gains, and within those large gains of chromosome complements, they did not reveal a notable increase in endoreduplication events in the treatment conditions relative to siControl. This would suggest that the large-scale gains in the mitotic chromosome spreads were generated from other polyploidy mechanisms, such as mitotic slippage or cytokinesis failure. An additional technical limitation of mitotic chromosome spread assays is the short-time frame for which mitotic cells are captured for analysis. Specifically, the longest time frame of Colcemid exposure to capture mitotic cells was 3.5 hours, indicating cells undergoing aberrant mitosis (*e.g.*, mitotic slippage, endoreduplication) during this short time window would be underrepresented in the final chromosome enumeration analyses. Despite observing significant increases in nuclear areas, chromosome enumeration analyses revealed that over ~50% of mitotic spreads presented with chromosome losses, suggesting a dichotomy in CIN phenotypes. These differences between nuclear area and mitotic chromosome spread analyses in *FBXO30* silencing contexts highlight the importance of employing three complementary assays to assess CIN phenotypes and potentially elucidate the mechanisms underlying the role of reduced *FBXO30* expression on CIN.

5.3. CONCLUSIONS AND SIGNIFICANCE

This thesis provides novel insights into our understanding of reduced *FBXO30* expression on CIN in CRC development. The results of this study have identified *FBXO30* as a novel CIN gene in non-malignant and malignant cells, demonstrating that reduced *FBXO30* expression induces dynamic and heterogeneous changes in CIN phenotypes, including changes in nuclear areas, micronucleus formation, and changes in chromosome numbers. Current literature, along with the data from this thesis, suggest that *FBXO30* normally exhibits a role in maintaining

chromosome and genome stability[96,97], suggesting it may exhibit a tumor-suppressor function in colonic epithelial cells. Interestingly, *FBXO30* has been identified as a tumor suppressor gene in clear cell renal cell carcinoma[98]. Collectively, these findings provide novel insights into the etiological origins of CIN and a solid foundation for future research on CRC development.

In 2024, ~25,200 Canadians were diagnosed, and ~9,400 died from the disease[5], and ~13% of all CRC cases exhibited *FBXO30* copy number losses[103]. Understanding the molecular mechanisms driving CRC development is critical to developing novel therapeutic strategies that exploit CIN genes, such as *FBXO30*, to ultimately improve patient outcomes. Finally, as *FBXO30* copy number losses occur in several cancer types, these findings provide the basis for future work focusing on clinical relevance beyond the CRC contexts examined in this study.

CHAPTER 6: FUTURE DIRECTIONS

This study identified *FBXO30* as a novel CIN gene in which transient siRNA-based silencing of *FBXO30* resulted in CIN phenotypes in both non-malignant and malignant colonic contexts. Despite these results expanding our understanding of the role of reduced *FBXO30* expression in inducing CIN, further studies aimed at determining the long-term impact of reduced *FBXO30* expression on CIN and cellular transformation, early events driving CRC development are essential. Moreover, our knowledge of FBXO30 and its associated target proteins is severely limited, thus, studies aimed at identifying SCF^{FBXO30} target proteins would provide novel insights into the SCF complex and its role in driving pathogenic events of early CRC development. Elucidating the SCF^{FBXO30} target substrates will enable future studies to investigate the molecular mechanisms underlying CIN when *FBXO30* is aberrantly expressed and may provide novel targets for precision medicine strategies that ultimately improve CRC patient outcomes.

6.1. EVALUATING THE LONG-TERM EFFECTS OF REDUCED *FBXO30* EXPRESSION ON CIN AND CELLULAR TRANSFORMATION *IN VITRO* AND *IN VIVO*

Although we established, using siRNA-based silencing, that reduced *FBXO30* is a novel CIN gene in 1CT, A1309, and HCT116 cell lines, the long-term impact of reduced *FBXO30* expression on CIN and cellular transformation remains to be examined. Using CRISPR/Cas9 technologies, *FBXO30* heterozygous ($FBXO30^{+/-}$) and homozygous ($FBXO30^{-/-}$) clones could be generated in 1CT and A1309 cells, to assess the ongoing and dynamic changes in CIN phenotypes across successive cell generations. The heterozygous ($FBXO30^{+/-}$) clones are clinically relevant models that would replicate the clinical state and provide insight into CRC etiology. Furthermore, since *FBXO30* is a non-essential gene, homozygous ($FBXO30^{-/-}$) clones would provide valuable

insights into the loss of function phenotypes. Following the generation of the *FBXO30* clones, they could undergo analysis of CIN and cellular transformation assays at different passages to observe potential temporal shifts in clonal evolution. The CIN assays would be the same as those employed in Chapter 3 (see *Section 3.5*), whereas cellular transformation could be assessed by evaluating such phenotypes as cellular proliferation rates, clonogenic growth capacity and the anchorage-independent growth assay to assess the capacity of clones to grow in 3D without attachment to a cell culture plate[55,94]. Previous studies of the McManus laboratory have established *in vitro* models of other F-box protein knockout clones in the A1309 cell line to assess the long-term impact of aberrantly expressed SCF complex members on CIN and cellular transformation in CRC pathogenesis[55,94]. For example, reduced *FBXO7* expression in i*n vitro* models using A1309 cells exhibited phenotypes associated with cellular transformation, including clonogenic and anchorage-independent growth, representing the transition of normal cells into malignant cells[94]. Additionally, the A1309 *SKP2*$^{+/-}$ clones also promoted cellular transformation events, as evidenced by enhanced anchorage-independent growth[55]. Despite these studies providing novel insights into early events (*i.e.*, CIN and cellular transformation) that may contribute to CRC development, our understanding of the mechanisms driving CIN in sporadic CRC patients remains incomplete. However, newly emerging techniques to evaluate clonal evolution have transitioned from bulk-assays, towards single-cell sequencing and multi-omic approaches. Single cell sequencing on *FBXO30* knockout clones will assess cellular heterogeneity and complexity that arises in the cell population over successive generations[139-141]. Utilizing the Chromium X series instrument from the QuIPS platform, clones can be barcoded to generate an RNA library that can be subsequently sent for next generation sequencing to determine the transcriptome of the individual clones. Therefore, developing *FBXO30* knockout clones will contribute to our fundamental understanding

of CRC pathogenesis and aid in developing novel therapeutics for CRC patients with *FBXO30* deficiencies.

In vitro models are indispensable and may reveal that the long-term impact of reduced *FBXO30* expression imparts karyotypic changes that enable cellular transformation in non-malignant colonic epithelial cells. Thus, the next logical step is to evaluate the role of *FBXO30* and its tumorigenic potential in an *in vivo* context. Yuan *et al.* evaluated the role of *FBXO30* in ccRCC, in which *FBXO30* inhibition promoted proliferation, migration, invasion, and epithelial-mesenchymal transition and *FBXO30* acted as a tumor suppressor in mouse models to inhibit tumor growth[98]. However, this study examined *FBXO30* overexpression in nude mice that were subcutaneously injected in the flank with ccRCC cells transfected with control (*i.e.*, empty vector) or *FBXO30* overexpressing vectors[98]. *FBXO30* overexpression notably inhibited tumor growth and metastasis, evidenced by lower tumor weight and size and fewer metastatic nodules in the lung[98]. To date, no mouse or 3D organoid models evaluating reduced *FBXO30* expression in colonic epithelial cells have been published, indicating a gap in research regarding a lack of clinically relevant models to examine the impact of reduced *FBXO30* expression on tumorigenesis and early events promoting CRC development. In this regard, *FBXO30*$^{+/-}$ clones could be orthotopically injected into the colon of immunodeficient mice, such as NOD scid gamma (NSG) mice. Selecting NSG mice over other immunodeficient mice strains, such as BALB/c nude mice can be attributed to a few factors. NSG mice are deficient in T-cells, B-cells, and natural killer (NK) cells enabling a shorter latency period and greater tumorigenesis with uptake of patient-derived xenografts, while BALB/c nude mice retain B-cells and NK cells that lead to higher resistance toward implantation of external cells[142]. Thus, NSG mice will be better suited for the implantation of *FBXO30*$^{+/-}$ clones to evaluate tumorigenesis in *vivo*. The most common orthotopic colon model in mice requires

surgical techniques to open the abdomen, and the cells are injected into the cecum wall[143,144]. Orthotopic injection is the preferred method as it recapitulates the hypoxic environment of the colon, the clones are exposed to the native microenvironment, and tumorigenesis mirrors the clinical setting; however, orthotopic injection is limited by technician experience, as it is time-consuming, can induce trauma to the mice, and tumor formation must be monitored by expensive imaging modalities, such as *in vivo* imaging system (IVIS) to avoid sacrificing the animal[143,144]. To circumvent the consequences of open surgery on mice, a minimally invasive endoscopic cell implantation technique has been developed[143-145] that enables the injection of cells into the mucosa of any section of the colon to closely replicate human CRC growth and metastasis. Hence, *FBXO30* knockout clones could be endoscopically injected into NSG mice at late-stage passages to assess whether clonal evolution impacts CRC development. Regardless, the development of *in vivo* mouse models will be critical to determine the effect of *FBXO30* heterozygous loss on tumorigenesis at early and late stages of CRC development.

6.2. IDENTIFYING NOVEL SCF^{FBXO30} TARGET PROTEINS

There is limited information regarding FBXO30 and its protein substrates, suggesting a need to identify misregulated protein targets following reduced *FBXO30* expression. The identification of FBXO30 protein targets will provide novel insights into the underlying cellular mechanisms promoting CIN and could be exploited as therapeutic targets. Normally, co-immunoprecipitation assays coupled with mass spectrometry is the most common approach to identify novel protein targets and/or interactions[146]. However, a fundamental limitation of this approach is the inability to detect transient or weak interactions, and the SCF complex rapidly degrades target proteins in a span of minutes[85,146,147], which suggests these interactions may go

undetected in traditional immunoprecipitation/mass spectrometry analyses. Therefore, novel approaches, including biotin identification (BioID) assays, are emerging to address the limitations of these standardized protein target identification assays. BioID is a proximity-dependent labeling system that employs a mutated biotin protein ligase (BirA) from *E. coli* to promiscuously biotinylate proteins in close spatial proximity[148,149]. An expression vector that fuses BirA to the protein of interest and covalently tags all biotin within a 10 nm radius to biotinylate proteins based on close spatial proximity[148-150]. Major advantages of BioID assays include its ability to be performed in live cells, to be applied to insoluble proteins, and to identify transient and/or weak interactions that would normally be undetected in traditional immunoprecipitation assays[148]. Since biotinylation rarely occurs under normal cellular conditions, biotinylated proteins can be selectively isolated using standard biotin-affinity capture using streptavidin beads, and employed in subsequent analyses, such as mass spectrometry or western blots[148]. However, BirA possesses limitations, including slow catalytic activity requiring long time periods for biotin labelling (*e.g.*, ~18-hours)[148,149]. To resolve the requirement for longer labelling periods, TurboID was developed as a modified biotin ligase system with a faster biotin labelling cycle of ~15 min[149,150]. To assess SCF^{FBXO30} target substrates, a transgenic cell line (*e.g.*, 1CT cell line) expressing the TurboID ligase fused to the bait protein (*i.e.*, FBXO30) must be generated and subsequently treated with biotin[151]. Following biotin labelling, cells are lysed for protein extraction and biotinylated proteins are selectively captured through affinity purification with streptavidin-coated beads[151]. The captured proteins are subsequently digested with trypsin and analyzed using chromatography-tandem mass spectrometry to identify the FBXO30 interactome[151]. In all cases, proteins identified by mass spectrometry must undergo validation, by such approaches as western blots or proximity ligation assays, a microscopy-based approach that detects protein-protein interactions *in situ*.

Western blots can be used to assess levels of protein abundance following *FBXO30* depletion of the identified substrates from mass spectrometry; while proximity ligation assays use antibodies with oligonucleotide probes to target proteins of interest that will hybridize in close proximity to one another creating a fluorescent signal under microscopy to indicate interactions[152,153]. Novel FBXO30 target substrates are dysregulated following *FBXO30* silencing, and their endogenous accumulation may severely impact genome stability and provide novel mechanistic insights into the underlying mechanisms giving rise to CIN.

6.3. DETERMINING THE UNDERLYING MECHANISMS BY WHICH REDUCED *FBXO30* EXPRESSION INDUCES CIN

Normal *FBXO30* expression and function are essential to maintain genome stability by marking specific proteins for proteolytic degradation to regulate key cellular processes, including cell cycle progression, DNA repair and replication, mitotic spindle formation, centrosome duplication, and chromosome dynamics[56,85,92,97]. Previous studies have established that diminished expression of core SCF complex members (*e.g.*, *SKP1, CUL1,* and *RBX1*) and other additional F-box proteins induces Cyclin E1 accumulation, which may contribute to CIN in cancer development[51,55,92-94]. However, the role of FBXO30 in the SCF complex is poorly understood. Current literature has linked FBXO30 as a regulator of two substrates: KIF11 and SLBP, in which reduced *FBXO30* expression resulted in the accumulation of these two substrates[96,97]. KIF11 is a spindle motor protein critical to the formation and maintenance of mitotic spindle architecture to ensure proper chromosome segregation[100,154,155]. Numerous studies have identified KIF11 upregulation in various cancers (*e.g.*, gliomas, adrenocortical carcinomas, non-small cell lung cancer, hepatocellular carcinomas) including CRCs and is associated with poor patient prognosis

by promoting cancer proliferation and metastasis[154]. Additionally, SLBP is required for efficient histone H3 pre-mRNA processing at the 3' end by regulating nuclear export, translation, and degradation of histones[101,156,157]. Histones are abundant during S-phase replication to package newly synthesized DNA into nucleosomes and organize the chromatin[97]. As such, *FBXO30* depletion led to infective degradation of SLBP and accumulation of histones causing abnormal chromatin condensation and cell cycle arrest[97]. Understanding the target substrates of FBXO30 can provide mechanistic insight into how reduced F*BXO30* expression induces CIN in early CRC development.

A study of oocyte meiosis investigated the impact of *FBXO30* depletion on chromosome segregation that also revealed an increase in SLBP accumulation, led to histone H3 overload (*i.e.*, excess of soluble histone available in the cellular environment), chromosome overcondensation as determined by cytological features in chromosome spreads, and inhibition of chromosome segregation[97]. This suggests that *FBXO30* exhibits a role in chromosome dynamics and should be investigated beyond the context of this preliminary research study. Fluorescent *in situ* hybridization (FISH) approaches can be used on *FBXO30*$^{+/-}$ clones to monitor changes to chromosome dynamics. FISH applies customizable oligo-based probes targeting distinct chromatin regions, such as histones or centromeres to track DNA copy number alterations *(e.g.*, deletions, amplifications), aneuploidies, chromosomal breaks and rearrangements in interphase nuclei of fixed cells[158]. Utilizing FISH probes in *FBXO30*$^{+/-}$ clones may reveal the underlying mechanisms promoting chromosome defects that ultimately lead to CIN. Additionally, Lui et *al*.[96] examined the role of *FBXO30* in mammopoiesis, the development and cell differentiation of the mammary glands[96]. They determined that FBXO30 interacts with KIF11, in which *FBXO30*$^{-/-}$ mice showed KIF11 accumulation and led to defects in centrosome dynamics, mitotic spindle formation,

and cell proliferation[96]. Although these research studies present notable findings regarding the mechanisms by which reduced *FBXO30* expression may induce CIN through substrate accumulation, this remains to be examined in cancer, specifically in a CRC context.

Despite the scarcity of established FBXO30 substrates, Cyclin E1 is an established SCF complex substrate of many other F-box proteins (*e.g.*, FBXW7 and SKP2)[55,159,160] and core complex members[92,93], suggesting the evolutionary conservation of cell checkpoint regulators and that FBXO30 may also regulate Cyclin E1 protein levels.[55,92,160]. Future studies should seek to identify target substrate by combining TurboID with mass spectrometry (see *Section 6.2*) to provide novel insights into the impact of reduced *FBXO30* expression on Cyclin E1 turnover and establish whether Cyclin E1 is a target of SCF^{FBXO30}. Additional studies examining the impact of reduced *FBXO30* expression and subsequent SLBP and KIF11 accumulation on CIN in CRC development are needed as SLBP and KIF11 are the only current known targets of SCF^{FBXO30} and remain to be defined in a cancer context. Western blots, indirect immunofluorescence, or mass spectrometry can all be used to directly evaluate the impact of reduced *FBXO30* expression on target substrates. Finally, phenotypic rescue experiments co-silencing *FBXO30* and a substrate (*e.g.*, SLBP, KIF11, or Cyclin E1) could provide mechanistic insight into FBXO30's regulation of protein targets. Collectively, these future studies will be essential to gain novel insights into the potential mechanisms by which reduced *FBXO30* expression may promote CIN and cellular transformation, and its contributions to the early events driving CRC development.

REFERENCES

1 Darmadi, D., Mohammadian-Hafshejani, A. & Kheiri, S. Global Disparities in Colorectal Cancer: Unveiling the Present Landscape of Incidence and Mortality Rates, Analyzing Geographical Variances, and Assessing the Human Development Index. *J Prev Med Hyg* **65**, E499-E514 (2024). https://doi.org/10.15167/2421-4248/jpmh2024.65.4.3071

2 Li, Q. *et al.* Signaling pathways involved in colorectal cancer: pathogenesis and targeted therapy. *Signal Transduct Target Ther* **9**, 266 (2024). https://doi.org/10.1038/s41392-024-01953-7

3 Ionescu, V. A., Gheorghe, G., Bacalbasa, N., Chiotoroiu, A. L. & Diaconu, C. Colorectal Cancer: From Risk Factors to Oncogenesis. *Medicina (Kaunas)* **59** (2023). https://doi.org/10.3390/medicina59091646

4 Gandini, A. *et al.* Early-Onset colorectal Cancer: From the laboratory to the clinic. *Cancer Treat Rev* **130**, 102821 (2024). https://doi.org/10.1016/j.ctrv.2024.102821

5 Brenner, D. R. *et al.* Projected estimates of cancer in Canada in 2024. *CMAJ* **196**, E615-E623 (2024). https://doi.org/10.1503/cmaj.240095

6 Elias, B. *et al.* The burden of cancer risk in Canada's indigenous population: a comparative study of known risks in a Canadian region. *Int J Gen Med* **4**, 699-709 (2011). https://doi.org/10.2147/IJGM.S24292

7 Rouhafzay, A. & Yousefi, J. Geographical Disparities in Colorectal Cancer in Canada: A Review. *Curr Oncol Rep* **26**, 1249-1257 (2024). https://doi.org/10.1007/s11912-024-01574-x

8 Hossain, M. S. *et al.* Colorectal Cancer: A Review of Carcinogenesis, Global Epidemiology, Current Challenges, Risk Factors, Preventive and Treatment Strategies. *Cancers (Basel)* **14** (2022). https://doi.org/10.3390/cancers14071732

9 Alzahrani, S. M., Al Doghaither, H. A. & Al-Ghafari, A. B. General insight into cancer: An overview of colorectal cancer (Review). *Mol Clin Oncol* **15**, 271 (2021). https://doi.org/10.3892/mco.2021.2433

10 Barzi, A., Lenz, A. M., Labonte, M. J. & Lenz, H. J. Molecular pathways: Estrogen pathway in colorectal cancer. *Clin Cancer Res* **19**, 5842-5848 (2013). https://doi.org/10.1158/1078-0432.CCR-13-0325

11 Rennert, G., Rennert, H. S., Pinchev, M., Lavie, O. & Gruber, S. B. Use of hormone replacement therapy and the risk of colorectal cancer. *J Clin Oncol* **27**, 4542-4547 (2009). https://doi.org/10.1200/JCO.2009.22.0764

12 Tsukanov, V. V., Vasyutin, A. V. & Tonkikh, J. L. Risk factors, prevention and screening of colorectal cancer: A rising problem. *World J Gastroenterol* **31**, 98629 (2025). https://doi.org/10.3748/wjg.v31.i5.98629

13 Roshandel, G., Ghasemi-Kebria, F. & Malekzadeh, R. Colorectal Cancer: Epidemiology, Risk Factors, and Prevention. *Cancers (Basel)* **16** (2024). https://doi.org/10.3390/cancers16081530

14 Liao, Z., Guo, J. T., Yang, F., Wang, S. P. & Sun, S. Y. Screening of colorectal cancer: Methods and strategies. *World J Clin Oncol* **15**, 799-805 (2024). https://doi.org/10.5306/wjco.v15.i7.799

15 Adefemi, K., Knight, J. C., Zhu, Y. & Wang, P. P. Racial and sociodemographic distribution of colorectal cancer screening in Canada: A cross-sectional study. *Can J Public Health* **115**, 371-383 (2024). https://doi.org/10.17269/s41997-024-00859-9

16 Lopes, S. R. *et al.* Colorectal cancer screening: A review of current knowledge and progress in research. *World J Gastrointest Oncol* **16**, 1119-1133 (2024). https://doi.org/10.4251/wjgo.v16.i4.1119
17 De Vera, M. A. *et al.* Early-Age-Onset Colorectal Cancer in Canada: Evidence, Issues and Calls to Action. *Curr Oncol* **29**, 3149-3159 (2022). https://doi.org/10.3390/curroncol29050256
18 Chlorogiannis, D. D. *et al.* Tissue classification and diagnosis of colorectal cancer histopathology images using deep learning algorithms. Is the time ripe for clinical practice implementation? *Prz Gastroenterol* **18**, 353-367 (2023). https://doi.org/10.5114/pg.2023.130337
19 Nakayama, G., Tanaka, C. & Kodera, Y. Current Options for the Diagnosis, Staging and Therapeutic Management of Colorectal Cancer. *Gastrointest Tumors* **1**, 25-32 (2013). https://doi.org/10.1159/000354995
20 Yang, Y., Wang, Y. & Wang, Z. Construction of a new clinical staging system for colorectal cancer based on the lymph node ratio: A validation study. *Front Surg* **9**, 929576 (2022). https://doi.org/10.3389/fsurg.2022.929576
21 Faris, C. *et al.* Incidence and Dynamics of CRC Stage Migration: A Regional vs. a National Analysis. *Cancers (Basel)* **16** (2024). https://doi.org/10.3390/cancers16193245
22 Riihimaki, M., Hemminki, A., Sundquist, J. & Hemminki, K. Patterns of metastasis in colon and rectal cancer. *Sci Rep* **6**, 29765 (2016). https://doi.org/10.1038/srep29765
23 Shin, A. E., Giancotti, F. G. & Rustgi, A. K. Metastatic colorectal cancer: mechanisms and emerging therapeutics. *Trends Pharmacol Sci* **44**, 222-236 (2023). https://doi.org/10.1016/j.tips.2023.01.003
24 Kumar, A. *et al.* Current and emerging therapeutic approaches for colorectal cancer: A comprehensive review. *World J Gastrointest Surg* **15**, 495-519 (2023). https://doi.org/10.4240/wjgs.v15.i4.495
25 Mao, J. X., Gao, R., Wang, Y., Yan, X. B. & Wang, H. H. Surgical treatment of colorectal cancer: A multidimensional review. *World J Gastrointest Surg* **17**, 107785 (2025). https://doi.org/10.4240/wjgs.v17.i8.107785
26 Fadlallah, H. *et al.* Colorectal cancer: Recent advances in management and treatment. *World J Clin Oncol* **15**, 1136-1156 (2024). https://doi.org/10.5306/wjco.v15.i9.1136
27 Haynes, J. & Manogaran, P. Mechanisms and Strategies to Overcome Drug Resistance in Colorectal Cancer. *Int J Mol Sci* **26** (2025). https://doi.org/10.3390/ijms26051988
28 Salva de Torres, C. *et al.* Current and Emerging Treatment Paradigms in Colorectal Cancer: Integrating Hallmarks of Cancer. *Int J Mol Sci* **25** (2024). https://doi.org/10.3390/ijms25136967
29 Xie, Y. H., Chen, Y. X. & Fang, J. Y. Comprehensive review of targeted therapy for colorectal cancer. *Signal Transduct Target Ther* **5**, 22 (2020). https://doi.org/10.1038/s41392-020-0116-z
30 Johdi, N. A. & Sukor, N. F. Colorectal Cancer Immunotherapy: Options and Strategies. *Front Immunol* **11**, 1624 (2020). https://doi.org/10.3389/fimmu.2020.01624
31 Kaviyarasan, V. *et al.* Advancements in immunotherapy for colorectal cancer treatment: a comprehensive review of strategies, challenges, and future prospective. *Int J Colorectal Dis* **40**, 1 (2024). https://doi.org/10.1007/s00384-024-04790-w
32 Kastrinos, F. & Syngal, S. Inherited colorectal cancer syndromes. *Cancer J* **17**, 405-415 (2011). https://doi.org/10.1097/PPO.0b013e318237e408

33 Aelvoet, A. S., Buttitta, F., Ricciardiello, L. & Dekker, E. Management of familial adenomatous polyposis and MUTYH-associated polyposis; new insights. *Best Pract Res Clin Gastroenterol* **58-59**, 101793 (2022). https://doi.org/10.1016/j.bpg.2022.101793
34 Pino, M. S. & Chung, D. C. The chromosomal instability pathway in colon cancer. *Gastroenterology* **138**, 2059-2072 (2010). https://doi.org/10.1053/j.gastro.2009.12.065
35 Nguyen, L. H., Goel, A. & Chung, D. C. Pathways of Colorectal Carcinogenesis. *Gastroenterology* **158**, 291-302 (2020). https://doi.org/10.1053/j.gastro.2019.08.059
36 Fearon, E. R. & Vogelstein, B. A genetic model for colorectal tumorigenesis. *Cell* **61**, 759-767 (1990). https://doi.org/10.1016/0092-8674(90)90186-i
37 Dow, L. E. *et al.* Apc Restoration Promotes Cellular Differentiation and Reestablishes Crypt Homeostasis in Colorectal Cancer. *Cell* **161**, 1539-1552 (2015). https://doi.org/10.1016/j.cell.2015.05.033
38 Wang, T., Fu, J., Huang, Y. & Fu, C. Mechanism of APC truncation involved in colorectal cancer tumorigenesis (Review). *Oncol Lett* **29**, 2 (2025). https://doi.org/10.3892/ol.2024.14748
39 Fredericks, E., Dealtry, G. & Roux, S. beta-Catenin Regulation in Sporadic Colorectal Carcinogenesis: Not as Simple as APC. *Can J Gastroenterol Hepatol* **2018**, 4379673 (2018). https://doi.org/10.1155/2018/4379673
40 Najdi, R., Holcombe, R. F. & Waterman, M. L. Wnt signaling and colon carcinogenesis: beyond APC. *J Carcinog* **10**, 5 (2011). https://doi.org/10.4103/1477-3163.78111
41 Bahmanyar, S., Nelson, W. J. & Barth, A. I. Role of APC and its binding partners in regulating microtubules in mitosis. *Adv Exp Med Biol* **656**, 65-74 (2009). https://doi.org/10.1007/978-1-4419-1145-2_6
42 Takeda, M. *et al.* The Role of KRAS Mutations in Colorectal Cancer: Biological Insights, Clinical Implications, and Future Therapeutic Perspectives. *Cancers (Basel)* **17** (2025). https://doi.org/10.3390/cancers17030428
43 Meng, M. *et al.* The current understanding on the impact of KRAS on colorectal cancer. *Biomed Pharmacother* **140**, 111717 (2021). https://doi.org/10.1016/j.biopha.2021.111717
44 Yang, L. *et al.* Oncogenic KRAS drives radioresistance through upregulation of NRF2-53BP1-mediated non-homologous end-joining repair. *Nucleic Acids Res* **49**, 11067-11082 (2021). https://doi.org/10.1093/nar/gkab871
45 Kalimutho, M. *et al.* Enhanced dependency of KRAS-mutant colorectal cancer cells on RAD51-dependent homologous recombination repair identified from genetic interactions in Saccharomyces cerevisiae. *Mol Oncol* **11**, 470-490 (2017). https://doi.org/10.1002/1878-0261.12040
46 Liebl, M. C. & Hofmann, T. G. The Role of p53 Signaling in Colorectal Cancer. *Cancers (Basel)* **13** (2021). https://doi.org/10.3390/cancers13092125
47 Hertel, A. & Storchova, Z. The Role of p53 Mutations in Early and Late Response to Mitotic Aberrations. *Biomolecules* **15** (2025). https://doi.org/10.3390/biom15020244
48 Marmol, I., Sanchez-de-Diego, C., Pradilla Dieste, A., Cerrada, E. & Rodriguez Yoldi, M. J. Colorectal Carcinoma: A General Overview and Future Perspectives in Colorectal Cancer. *Int J Mol Sci* **18** (2017). https://doi.org/10.3390/ijms18010197
49 Chan, D. K. H. & Buczacki, S. J. A. Tumour heterogeneity and evolutionary dynamics in colorectal cancer. *Oncogenesis* **10**, 53 (2021). https://doi.org/10.1038/s41389-021-00342-x

50 Papaccio, F. *et al.* Decoding chromosomal instability insights in CRC by integrating omics and patient-derived organoids. *J Exp Clin Cancer Res* **44**, 77 (2025). https://doi.org/10.1186/s13046-025-03308-8
51 Vishwakarma, R. & McManus, K. J. Chromosome Instability; Implications in Cancer Development, Progression, and Clinical Outcomes. *Cancers (Basel)* **12** (2020). https://doi.org/10.3390/cancers12040824
52 Baergen, A. K., Jeusset, L. M., Lichtensztejn, Z. & McManus, K. J. Diminished Condensin Gene Expression Drives Chromosome Instability That May Contribute to Colorectal Cancer Pathogenesis. *Cancers (Basel)* **11** (2019). https://doi.org/10.3390/cancers11081066
53 Campos Gudino, R., Neudorf, N. M., Andromidas, D., Lichtensztejn, Z. & McManus, K. J. Loss of EMI1 compromises chromosome stability and is associated with cellular transformation in colonic epithelial cell contexts. *Br J Cancer* **131**, 1516-1528 (2024). https://doi.org/10.1038/s41416-024-02855-9
54 Lepage, C. C., Morden, C. R., Palmer, M. C. L., Nachtigal, M. W. & McManus, K. J. Detecting Chromosome Instability in Cancer: Approaches to Resolve Cell-to-Cell Heterogeneity. *Cancers (Basel)* **11** (2019). https://doi.org/10.3390/cancers11020226
55 Neudorf, N. M., Thompson, L. L., Lichtensztejn, Z., Razi, T. & McManus, K. J. Reduced SKP2 Expression Adversely Impacts Genome Stability and Promotes Cellular Transformation in Colonic Epithelial Cells. *Cells* **11** (2022). https://doi.org/10.3390/cells11233731
56 Thompson, L. L., Jeusset, L. M., Lepage, C. C. & McManus, K. J. Evolving Therapeutic Strategies to Exploit Chromosome Instability in Cancer. *Cancers (Basel)* **9** (2017). https://doi.org/10.3390/cancers9110151
57 Baran, B. *et al.* Difference Between Left-Sided and Right-Sided Colorectal Cancer: A Focused Review of Literature. *Gastroenterology Res* **11**, 264-273 (2018). https://doi.org/10.14740/gr1062w
58 Thompson, S. L., Bakhoum, S. F. & Compton, D. A. Mechanisms of chromosomal instability. *Curr Biol* **20**, R285-295 (2010). https://doi.org/10.1016/j.cub.2010.01.034
59 Melendez-Florez, M. P., Ortega-Recalde, O., Rangel, N. & Rondon-Lagos, M. Chromosomal Instability and Clonal Heterogeneity in Breast Cancer: From Mechanisms to Clinical Applications. *Cancers (Basel)* **17** (2025). https://doi.org/10.3390/cancers17071222
60 Zhang, X. & Kschischo, M. Distinct and Common Features of Numerical and Structural Chromosomal Instability across Different Cancer Types. *Cancers (Basel)* **14** (2022). https://doi.org/10.3390/cancers14061424
61 Siri, S. O., Martino, J. & Gottifredi, V. Structural Chromosome Instability: Types, Origins, Consequences, and Therapeutic Opportunities. *Cancers (Basel)* **13** (2021). https://doi.org/10.3390/cancers13123056
62 Lepage, C. C., Thompson, L. L., Larson, B. & McManus, K. J. An Automated, Single Cell Quantitative Imaging Microscopy Approach to Assess Micronucleus Formation, Genotoxicity and Chromosome Instability. *Cells* **9** (2020). https://doi.org/10.3390/cells9020344
63 Batistao, H. K. A., Oliveira-Silva, J. M., Oliveira, V. B., de Araujo, B., II & Castro-Gamero, A. M. Quantitative and qualitative methods for measuring chromosomal

instability in tumor cells. *Cancer Genet* **300-301**, 36-46 (2026). https://doi.org/10.1016/j.cancergen.2025.11.008

64 Funk, L. C., Zasadil, L. M. & Weaver, B. A. Living in CIN: Mitotic Infidelity and Its Consequences for Tumor Promotion and Suppression. *Dev Cell* **39**, 638-652 (2016). https://doi.org/10.1016/j.devcel.2016.10.023

65 Potapova, T. & Gorbsky, G. J. The Consequences of Chromosome Segregation Errors in Mitosis and Meiosis. *Biology (Basel)* **6** (2017). https://doi.org/10.3390/biology6010012

66 Conway, P. J., Dao, J., Kovalskyy, D., Mahadevan, D. & Dray, E. Polyploidy in Cancer: Causal Mechanisms, Cancer-Specific Consequences, and Emerging Treatments. *Mol Cancer Ther* **23**, 638-647 (2024). https://doi.org/10.1158/1535-7163.MCT-23-0578

67 Matsumoto, T. *et al.* Proliferative polyploid cells give rise to tumors via ploidy reduction. *Nat Commun* **12**, 646 (2021). https://doi.org/10.1038/s41467-021-20916-y

68 Liu, P., Wang, L. & Yu, H. Polyploid giant cancer cells: origin, possible pathways of formation, characteristics, and mechanisms of regulation. *Front Cell Dev Biol* **12**, 1410637 (2024). https://doi.org/10.3389/fcell.2024.1410637

69 Schmidt, M. J. *et al.* Polyploid cancer cells reveal signatures of chemotherapy resistance. *Oncogene* **44**, 439-449 (2025). https://doi.org/10.1038/s41388-024-03212-z

70 Huang, P. *et al.* Polyploid giant cancer cells and tumor budding: translation from basic research to clinical application. *Front Oncol* **15**, 1611920 (2025). https://doi.org/10.3389/fonc.2025.1611920

71 Ottaiano, A. *et al.* Polyploid and Chromosomal Copy Number Gain Cells in Metastatic Colon Cancer: Exploratory Genotype-Phenotype Correlations. *Cancers (Basel)* **18** (2026). https://doi.org/10.3390/cancers18060994

72 Druzhkova, I. *et al.* Cell hiding in colorectal cancer: correlation with response to chemotherapy in vitro and in vivo. *Sci Rep* **14**, 28762 (2024). https://doi.org/10.1038/s41598-024-79948-1

73 Krupina, K., Goginashvili, A. & Cleveland, D. W. Causes and consequences of micronuclei. *Curr Opin Cell Biol* **70**, 91-99 (2021). https://doi.org/10.1016/j.ceb.2021.01.004

74 Di Bona, M. & Bakhoum, S. F. Micronuclei and Cancer. *Cancer Discov* **14**, 214-226 (2024). https://doi.org/10.1158/2159-8290.CD-23-1073

75 Kalsbeek, D. & Golsteyn, R. M. G2/M-Phase Checkpoint Adaptation and Micronuclei Formation as Mechanisms That Contribute to Genomic Instability in Human Cells. *Int J Mol Sci* **18** (2017). https://doi.org/10.3390/ijms18112344

76 Utani, K., Kohno, Y., Okamoto, A. & Shimizu, N. Emergence of micronuclei and their effects on the fate of cells under replication stress. *PLoS One* **5**, e10089 (2010). https://doi.org/10.1371/journal.pone.0010089

77 Duan, H. *et al.* Micronuclei: origins, assays, mechanisms, diseases and treatments. *Signal Transduct Target Ther* **11** (2026). https://doi.org/10.1038/s41392-025-02538-8

78 Karaman, A., Binici, D. N., Kabalar, M. E. & Calikusu, Z. Micronucleus analysis in patients with colorectal adenocarcinoma and colorectal polyps. *World J Gastroenterol* **14**, 6835-6839 (2008). https://doi.org/10.3748/wjg.14.6835

79 Zhang, C. Z. *et al.* Chromothripsis from DNA damage in micronuclei. *Nature* **522**, 179-184 (2015). https://doi.org/10.1038/nature14493

80 Thompson, J. S. *et al.* Predicting resistance to chemotherapy using chromosomal instability signatures. *Nat Genet* **57**, 1708-1717 (2025). https://doi.org/10.1038/s41588-025-02233-y

81 Kuznetsova, A. Y. *et al.* Chromosomal instability, tolerance of mitotic errors and multidrug resistance are promoted by tetraploidization in human cells. *Cell Cycle* **14**, 2810-2820 (2015). https://doi.org/10.1080/15384101.2015.1068482
82 Orr, B., Godek, K. M. & Compton, D. Aneuploidy. *Curr Biol* **25**, R538-542 (2015). https://doi.org/10.1016/j.cub.2015.05.010
83 Zaalberg, I. C. *et al.* Aneuploidy patterns in colorectal cancer. *Cell Rep* **45**, 116721 (2026). https://doi.org/10.1016/j.celrep.2025.116721
84 Hosea, R., Hillary, S., Naqvi, S., Wu, S. & Kasim, V. The two sides of chromosomal instability: drivers and brakes in cancer. *Signal Transduct Target Ther* **9**, 75 (2024). https://doi.org/10.1038/s41392-024-01767-7
85 Thompson, L. L., Rutherford, K. A., Lepage, C. C. & McManus, K. J. The SCF Complex Is Essential to Maintain Genome and Chromosome Stability. *Int J Mol Sci* **22** (2021). https://doi.org/10.3390/ijms22168544
86 Zheng, N., Zhou, Q., Wang, Z. & Wei, W. Recent advances in SCF ubiquitin ligase complex: Clinical implications. *Biochim Biophys Acta* **1866**, 12-22 (2016). https://doi.org/10.1016/j.bbcan.2016.05.001
87 Xie, J., Jin, Y. & Wang, G. The role of SCF ubiquitin-ligase complex at the beginning of life. *Reprod Biol Endocrinol* **17**, 101 (2019). https://doi.org/10.1186/s12958-019-0547-y
88 Tekcham, D. S. *et al.* F-box proteins and cancer: an update from functional and regulatory mechanism to therapeutic clinical prospects. *Theranostics* **10**, 4150-4167 (2020). https://doi.org/10.7150/thno.42735
89 Zeng, X. *et al.* SKP1-CUL1-F-box: Key molecular targets affecting disease progression. *FASEB J* **39**, e70326 (2025). https://doi.org/10.1096/fj.202402816RR
90 Thompson, L. L., Rutherford, K. A., Lepage, C. C. & McManus, K. J. Aberrant SKP1 Expression: Diverse Mechanisms Impacting Genome and Chromosome Stability. *Front Cell Dev Biol* **10**, 859582 (2022). https://doi.org/10.3389/fcell.2022.859582
91 Wang, Z., Liu, P., Inuzuka, H. & Wei, W. Roles of F-box proteins in cancer. *Nat Rev Cancer* **14**, 233-247 (2014). https://doi.org/10.1038/nrc3700
92 Thompson, L. L., Baergen, A. K., Lichtensztejn, Z. & McManus, K. J. Reduced SKP1 Expression Induces Chromosome Instability through Aberrant Cyclin E1 Protein Turnover. *Cancers (Basel)* **12** (2020). https://doi.org/10.3390/cancers12030531
93 Lepage, C. C. *et al.* Reduced SKP1 and CUL1 expression underlies increases in Cyclin E1 and chromosome instability in cellular precursors of high-grade serous ovarian cancer. *Br J Cancer* **124**, 1699-1710 (2021). https://doi.org/10.1038/s41416-021-01317-w
94 Palmer, M. C. L. *et al.* The F-box protein, FBXO7, is required to maintain chromosome stability in humans. *Hum Mol Genet* **31**, 1471-1486 (2022). https://doi.org/10.1093/hmg/ddab330
95 Jin, J. *et al.* Systematic analysis and nomenclature of mammalian F-box proteins. *Genes Dev* **18**, 2573-2580 (2004). https://doi.org/10.1101/gad.1255304
96 Liu, Y. *et al.* Fbxo30 Regulates Mammopoiesis by Targeting the Bipolar Mitotic Kinesin Eg5. *Cell Rep* **15**, 1111-1122 (2016). https://doi.org/10.1016/j.celrep.2016.03.083
97 Jin, Y. *et al.* Fbxo30 regulates chromosome segregation of oocyte meiosis. *Cell Mol Life Sci* **76**, 2217-2229 (2019). https://doi.org/10.1007/s00018-019-03038-z
98 Yuan, Y. *et al.* FBXO30 functions as a tumor suppressor and an E3 ubiquitin ligase for hZIP1-mediated HIF-1alpha degradation in renal cell carcinoma. *Int J Oncol* **62** (2023). https://doi.org/10.3892/ijo.2023.5488

99 Silva, J. P. N., Silva, P. M. A. & Bousbaa, H. Kinesin Spindle Protein (KIF11) in Mitosis and Cancer. *Int J Mol Sci* **26** (2025). https://doi.org/10.3390/ijms26188975
100 Gao, W. *et al.* Mitotic Functions and Characters of KIF11 in Cancers. *Biomolecules* **14** (2024). https://doi.org/10.3390/biom14040386
101 Bradford, B. R. & Jin, C. Stem-loop binding protein and metal carcinogenesis. *Semin Cancer Biol* **76**, 38-44 (2021). https://doi.org/10.1016/j.semcancer.2021.08.006
102 Brenner, D. R. *et al.* Projected estimates of cancer in Canada in 2024. *Can Med Assoc J* **196**, E615-E623 (2024). https://doi.org/10.1503/cmaj.240095
103 Hoadley, K. A. *et al.* Cell-of-Origin Patterns Dominate the Molecular Classification of 10,000 Tumors from 33 Types of Cancer. *Cell* **173**, 291-304 e296 (2018). https://doi.org/10.1016/j.cell.2018.03.022
104 Cerami, E. *et al.* The cBio cancer genomics portal: an open platform for exploring multidimensional cancer genomics data. *Cancer Discov* **2**, 401-404 (2012). https://doi.org/10.1158/2159-8290.CD-12-0095
105 Gao, J. *et al.* Integrative analysis of complex cancer genomics and clinical profiles using the cBioPortal. *Sci Signal* **6**, pl1 (2013). https://doi.org/10.1126/scisignal.2004088
106 Lakbir, S. *et al.* Tumour break load is a biologically relevant feature of genomic instability with prognostic value in colorectal cancer. *Eur J Cancer* **177**, 94-102 (2022). https://doi.org/10.1016/j.ejca.2022.09.034
107 Zhang, L. *et al.* Exome Sequencing of Normal and Isogenic Transformed Human Colonic Epithelial Cells (HCECs) Reveals Novel Genes Potentially Involved in the Early Stages of Colorectal Tumorigenesis. *BMC Genomics* **16 Suppl 1**, S8 (2015). https://doi.org/10.1186/1471-2164-16-S1-S8
108 Waghela, B. N., Vaidya, F. U. & Pathak, C. Upregulation of NOX-2 and Nrf-2 Promotes 5-Fluorouracil Resistance of Human Colon Carcinoma (HCT-116) Cells. *Biochemistry (Mosc)* **86**, 262-274 (2021). https://doi.org/10.1134/S0006297921030044
109 Yang, M. *et al.* Astragalin Inhibits the Proliferation and Migration of Human Colon Cancer HCT116 Cells by Regulating the NF-kappaB Signaling Pathway. *Front Pharmacol* **12**, 639256 (2021). https://doi.org/10.3389/fphar.2021.639256
110 Campos Gudino, R., Rutherford, K. A. & McManus, K. J. Evaluating Chromosome Instability and Genotoxicity Through Single Cell Quantitative Imaging Microscopy. *Methods Mol Biol* **2825**, 309-331 (2024). https://doi.org/10.1007/978-1-0716-3946-7_18
111 Prasad, C. P., Tripathi, S. C., Kumar, M. & Mohapatra, P. Passage number of cancer cell lines: Importance, intricacies, and way-forward. *Biotechnol Bioeng* **120**, 2049-2055 (2023). https://doi.org/10.1002/bit.28496
112 Klaasen, S. J. & Kops, G. Chromosome Inequality: Causes and Consequences of Non-Random Segregation Errors in Mitosis and Meiosis. *Cells* **11** (2022). https://doi.org/10.3390/cells11223564
113 Geigl, J. B., Obenauf, A. C., Schwarzbraun, T. & Speicher, M. R. Defining 'chromosomal instability'. *Trends Genet* **24**, 64-69 (2008). https://doi.org/10.1016/j.tig.2007.11.006
114 Leylek, T. R., Jeusset, L. M., Lichtensztejn, Z. & McManus, K. J. Reduced Expression of Genes Regulating Cohesion Induces Chromosome Instability that May Promote Cancer and Impact Patient Outcomes. *Sci Rep* **10**, 592 (2020). https://doi.org/10.1038/s41598-020-57530-9

115 Vilar, E. *et al.* Microsatellite instability due to hMLH1 deficiency is associated with increased cytotoxicity to irinotecan in human colorectal cancer cell lines. *Br J Cancer* **99**, 1607-1612 (2008). https://doi.org/10.1038/sj.bjc.6604691
116 Huang, Y. *et al.* Expressing MLH1 in HCT116 cells increases cellular resistance to radiation by activating the PRKAC. *Exp Biol Med (Maywood)* **247**, 426-432 (2022). https://doi.org/10.1177/15353702211059829
117 Hsieh, P. & Yamane, K. DNA mismatch repair: molecular mechanism, cancer, and ageing. *Mech Ageing Dev* **129**, 391-407 (2008). https://doi.org/10.1016/j.mad.2008.02.012
118 Yamamoto, T. & Uehara, R. Cell shape instability during cytokinesis in tetraploid HCT116 cells. *Biochem Biophys Res Commun* **678**, 39-44 (2023). https://doi.org/10.1016/j.bbrc.2023.08.038
119 Yoon, M. H. *et al.* p53 induces senescence through Lamin A/C stabilization-mediated nuclear deformation. *Cell Death Dis* **10**, 107 (2019). https://doi.org/10.1038/s41419-019-1378-7
120 Braun, S. *et al.* Nuclear Dynamics in Quiescent Cells: Conserved Mechanisms from Yeasts to Mammals. *Biomolecules* **16** (2026). https://doi.org/10.3390/biom16020203
121 Marescal, O. & Cheeseman, I. M. Cellular Mechanisms and Regulation of Quiescence. *Dev Cell* **55**, 259-271 (2020). https://doi.org/10.1016/j.devcel.2020.09.029
122 Di, Y. *et al.* Divergent proteome tolerance against gain and loss of chromosome arms. *Mol Cell* **85**, 4268-4278 e4266 (2025). https://doi.org/10.1016/j.molcel.2025.10.023
123 Nair, N. U. *et al.* Chromosome 7 Gain Compensates for Chromosome 10 Loss in Glioma. *Cancer Res* **84**, 3464-3477 (2024). https://doi.org/10.1158/0008-5472.CAN-24-1366
124 Forche, A. Large-Scale Chromosomal Changes and Associated Fitness Consequences in Pathogenic Fungi. *Curr Fungal Infect Rep* **8**, 163-170 (2014). https://doi.org/10.1007/s12281-014-0181-2
125 Puliafito, A. *et al.* Collective and single cell behavior in epithelial contact inhibition. *Proc Natl Acad Sci U S A* **109**, 739-744 (2012). https://doi.org/10.1073/pnas.1007809109
126 Nakamura, F. The Role of Mechanotransduction in Contact Inhibition of Locomotion and Proliferation. *Int J Mol Sci* **25** (2024). https://doi.org/10.3390/ijms25042135
127 Qiu, L., Liu, M. & Pan, K. A triple staining method for accurate cell cycle analysis using multiparameter flow cytometry. *Molecules* **18**, 15412-15421 (2013). https://doi.org/10.3390/molecules181215412
128 Perera, D. & Venkitaraman, A. R. Oncogenic KRAS triggers MAPK-dependent errors in mitosis and MYC-dependent sensitivity to anti-mitotic agents. *Sci Rep* **6**, 29741 (2016). https://doi.org/10.1038/srep29741
129 Zhang, L. & Shay, J. W. Multiple Roles of APC and its Therapeutic Implications in Colorectal Cancer. *J Natl Cancer Inst* **109** (2017). https://doi.org/10.1093/jnci/djw332
130 Dale, K. L., Armond, J. W., Hynds, R. E. & Vladimirou, E. Modest increase of KIF11 expression exposes fragilities in the mitotic spindle, causing chromosomal instability. *J Cell Sci* **135** (2022). https://doi.org/10.1242/jcs.260031
131 Zhou, Y. *et al.* KIF11 is upregulated in colorectal cancer and silencing of it impairs tumor growth and sensitizes colorectal cancer cells to oxaliplatin via p53/GSK3beta signaling. *J Cancer* **12**, 3741-3753 (2021). https://doi.org/10.7150/jca.52103
132 Sazonova, E. V., Petrichuk, S. V., Kopeina, G. S. & Zhivotovsky, B. A link between mitotic defects and mitotic catastrophe: detection and cell fate. *Biol Direct* **16**, 25 (2021). https://doi.org/10.1186/s13062-021-00313-7

133 Margolis, R. L., Lohez, O. D. & Andreassen, P. R. G1 tetraploidy checkpoint and the suppression of tumorigenesis. *J Cell Biochem* **88**, 673-683 (2003). https://doi.org/10.1002/jcb.10411
134 Roschke, A. V., Stover, K., Tonon, G., Schaffer, A. A. & Kirsch, I. R. Stable karyotypes in epithelial cancer cell lines despite high rates of ongoing structural and numerical chromosomal instability. *Neoplasia* **4**, 19-31 (2002). https://doi.org/10.1038/sj.neo.7900197
135 Thompson, S. L. & Compton, D. A. Proliferation of aneuploid human cells is limited by a p53-dependent mechanism. *J Cell Biol* **188**, 369-381 (2010). https://doi.org/10.1083/jcb.200905057
136 Vasudevan, A. *et al.* Single-Chromosomal Gains Can Function as Metastasis Suppressors and Promoters in Colon Cancer. *Dev Cell* **52**, 413-428 e416 (2020). https://doi.org/10.1016/j.devcel.2020.01.034
137 Fang, J. *et al.* Cellular polyploidy in organ homeostasis and regeneration. *Protein Cell* **14**, 560-578 (2023). https://doi.org/10.1093/procel/pwac064
138 Shu, Z., Row, S. & Deng, W. M. Endoreplication: The Good, the Bad, and the Ugly. *Trends Cell Biol* **28**, 465-474 (2018). https://doi.org/10.1016/j.tcb.2018.02.006
139 Wu, X. *et al.* Single-cell sequencing to multi-omics: technologies and applications. *Biomark Res* **12**, 110 (2024). https://doi.org/10.1186/s40364-024-00643-4
140 Vandereyken, K., Sifrim, A., Thienpont, B. & Voet, T. Methods and applications for single-cell and spatial multi-omics. *Nat Rev Genet* **24**, 494-515 (2023). https://doi.org/10.1038/s41576-023-00580-2
141 Lim, J. *et al.* Advances in single-cell omics and multiomics for high-resolution molecular profiling. *Exp Mol Med* **56**, 515-526 (2024). https://doi.org/10.1038/s12276-024-01186-2
142 Wu, J. *et al.* Comparison between NOD/SCID mice and BALB/c mice for patient-derived tumor xenografts model of non-small-cell lung cancer. *Cancer Manag Res* **10**, 6695-6703 (2018). https://doi.org/10.2147/CMAR.S181272
143 Oliveira, R. C., Abrantes, A. M., Tralhao, J. G. & Botelho, M. F. The role of mouse models in colorectal cancer research-The need and the importance of the orthotopic models. *Animal Model Exp Med* **3**, 1-8 (2020). https://doi.org/10.1002/ame2.12102
144 Zhang, L. & Bu, P. Generation of an orthotopic mouse model to study colorectal cancer metastasis. *STAR Protoc* **2**, 100792 (2021). https://doi.org/10.1016/j.xpro.2021.100792
145 Bettenworth, D. *et al.* Endoscopy-guided orthotopic implantation of colorectal cancer cells results in metastatic colorectal cancer in mice. *Clin Exp Metastasis* **33**, 551-562 (2016). https://doi.org/10.1007/s10585-016-9797-7
146 Free, R. B., Hazelwood, L. A. & Sibley, D. R. Identifying novel protein-protein interactions using co-immunoprecipitation and mass spectroscopy. *Curr Protoc Neurosci* **Chapter 5**, Unit 5 28 (2009). https://doi.org/10.1002/0471142301.ns0528s46
147 Galan, J. M. & Peter, M. Ubiquitin-dependent degradation of multiple F-box proteins by an autocatalytic mechanism. *Proc Natl Acad Sci U S A* **96**, 9124-9129 (1999). https://doi.org/10.1073/pnas.96.16.9124
148 Roux, K. J., Kim, D. I., Burke, B. & May, D. G. BioID: A Screen for Protein-Protein Interactions. *Curr Protoc Protein Sci* **91**, 19 23 11-19 23 15 (2018). https://doi.org/10.1002/cpps.51

149 Hollstein, L. S., Schmitt, K., Valerius, O., Stahlhut, G. & Poggeler, S. Establishment of in vivo proximity labeling with biotin using TurboID in the filamentous fungus Sordaria macrospora. *Sci Rep* **12**, 17727 (2022). https://doi.org/10.1038/s41598-022-22545-x
150 May, D. G., Scott, K. L., Campos, A. R. & Roux, K. J. Comparative Application of BioID and TurboID for Protein-Proximity Biotinylation. *Cells* **9** (2020). https://doi.org/10.3390/cells9051070
151 Park, T. K. & Kim, T. W. A brief guide to analyzing TurboID-based proximity labeling-mass spectrometry in plants. *Mol Cells* **48**, 100236 (2025). https://doi.org/10.1016/j.mocell.2025.100236
152 Greenwood, C. *et al.* Proximity assays for sensitive quantification of proteins. *Biomol Detect Quantif* **4**, 10-16 (2015). https://doi.org/10.1016/j.bdq.2015.04.002
153 Hegazy, M. *et al.* Proximity Ligation Assay for Detecting Protein-Protein Interactions and Protein Modifications in Cells and Tissues in Situ. *Curr Protoc Cell Biol* **89**, e115 (2020). https://doi.org/10.1002/cpcb.115
154 Asbaghi, Y., Thompson, L. L., Lichtensztejn, Z. & McManus, K. J. KIF11 silencing and inhibition induces chromosome instability that may contribute to cancer. *Genes Chromosomes Cancer* **56**, 668-680 (2017). https://doi.org/10.1002/gcc.22471
155 Zhou, Y. *et al.* Loss-of-function of kinesin-5 KIF11 causes microcephaly, chorioretinopathy, and developmental disorders through chromosome instability and cell cycle arrest. *Exp Cell Res* **436**, 113975 (2024). https://doi.org/10.1016/j.yexcr.2024.113975
156 Whitfield, M. L. *et al.* SLBP is associated with histone mRNA on polyribosomes as a component of the histone mRNP. *Nucleic Acids Res* **32**, 4833-4842 (2004). https://doi.org/10.1093/nar/gkh798
157 Mendiratta, S., Gatto, A. & Almouzni, G. Histone supply: Multitiered regulation ensures chromatin dynamics throughout the cell cycle. *J Cell Biol* **218**, 39-54 (2019). https://doi.org/10.1083/jcb.201807179
158 Hu, Q., Maurais, E. G. & Ly, P. Cellular and genomic approaches for exploring structural chromosomal rearrangements. *Chromosome Res* **28**, 19-30 (2020). https://doi.org/10.1007/s10577-020-09626-1
159 Bhaskaran, N. *et al.* Fbw7alpha and Fbw7gamma collaborate to shuttle cyclin E1 into the nucleolus for multiubiquitylation. *Mol Cell Biol* **33**, 85-97 (2013). https://doi.org/10.1128/MCB.00288-12
160 Nakayama, K. *et al.* Targeted disruption of Skp2 results in accumulation of cyclin E and p27(Kip1), polyploidy and centrosome overduplication. *EMBO J* **19**, 2069-2081 (2000). https://doi.org/10.1093/emboj/19.9.2069

APPENDIX A: SOLUTIONS

CELL CULTURE

1X McCoy's 5A Complete Medium + 10% Fetal Bovine Serum (FBS)

Name	Amount
McCoy's 5A Medium (Hyclone)	450.0 mL
FBS (Sigma-Aldrich)	50.0 mL
Total Volume	500.0 mL

1X Complete X-Medium + 2% Cosmic Calf Serum (CCS)

Name	Amount
Dulbecco's Modified Eagle Medium (DMEM) with High Glucose (Hyclone)	780.0 mL
Medium 199 (Hyclone)	195.0 mL
CCS (Hyclone)	20.0 mL
Insulin (Sigma; 10 µg/mL)	5.0 mL
Hydrocortisone (Sigma; 1 µg/mL)	50.0 µL
Apotransferrin (Sigma; 2 µg/mL)	40.0 µL
Epidermal Growth Factor (EGF; PeproTech; 20 ng/mL)	20.0 µL
Sodium Selenite (Sigma; 5 nM)	1.0 µL
Total Volume	~1.0 L

Cupric Sulfate Pentahydrate

Name	Amount
Cupric Sulfate Pentahydrate	26.0 g
Milli-Q Water	Up to 1.0 L
Total Volume	1.0 L

10X Phosphate Buffered Saline (PBS; Stock Solution)

Name	Amount
NaCl	80.0 g
KCl	2.0 g
Na2HPO4	14.4 g
KH_2PO_4	2.4 g
Milli-Q Water	Up to 1.0 L
Total Volume	1.0 L

- Titrate to pH 7.4

1X Phosphate Buffered Saline (PBS; Working Solution)

Name	Amount
10X PBS (Stock Solution)	100.0 mL
Milli-Q Water	900.0 mL
Total Volume	1.0 L

GENE SILENCING

1X siRNA Buffer

Name	Amount
5X siRNA Buffer (Dharmacon)	100.0 µL
Diethyl pyrocarbonate (DEPC)-treated Water	400.0 µL
Total Volume	500.0 µL

WESTERN BLOTS

Radioimmunoprecipitation Assay (RIPA) Buffer

Name	Amount
50 mM Tris – pH 8.0	5.0 mL
150 mM NaCl	7.5 mL
Sodium Dodecyl Sulfate (SDS; 0.1% [w/v])	500.0 µL
Sodium Deoxycholate (0.5% [w/v])	0.5 g
NP40 (1% [w/v])	1.0 mL
Milli-Q Water	Up to 100.0 mL
Total Volume	100.0mL

- Wrap in aluminum foil to protect from light
- Store at 4 °C

25X Protease Inhibitor

Name	Amount
Protease Inhibitor Complete EDTA-free (Roche)	1 tablet
Milli-Q Water	2.0 mL
Total Volume	2.0 mL

- Vortex to fully dissolve table
- Store at -20 °C in 50 µL aliquots

Protein Extraction Buffer

Name	Amount
RIPA Buffer	955.0 µL
25X Protease Inhibitor	45.0 µL
Total Volume	1.0 mL

4X Tris-HCl/SDS, pH 6.8 (0.5M Tris-HCl Containing 0.4 % SDS)

Name	Amount
Tris	6.05 g
Sodium Dodecyl Sulfate (SDS)	2.0 g
Milli-Q Water	Up to 100.0 mL
Total Volume	100.0mL

- Titrate to pH 6.8 with 1N HCl
- Store at 4 °C

6X SDS Sample Loading Buffer

Name	Amount
4X Tris-HCl/SDS	6.5 mL
Glycerol	3.0 mL
SDS	1.0 mL
β-mercaptoethanol	600.0 µL
Bromophenol Blue	1.2 mg
Total Volume	~10.0 mL

- Store in 0.5 mL aliquots at -20 °C
- Warm to RT before use

10X Running Buffer (Stock Solution)

Name	Amount
Tris Base	30.0 g
Glycine	144.0 g
SDS	10.0 g
Milli-Q Water	Up to 1.0 L
Total Volume	1.0 L

1X Running Buffer (Working Solution)

Name	Amount
10X Running Buffer (Stock Solution)	100.0 mL
Milli-Q Water	900.0 mL
Total Volume	1.0 L

1X Transfer Buffer

Name	Amount
Trans-blot Turbo 5X Transfer Buffer (BioRad)	40 mL
Anhydrous Ethyl Alcohol	40 mL
Milli-Q Water	120.0 mL
Total Volume	200.0 mL

Copper Phthalocyanine 3,4',4'',4'''-tetrasulfonic Acid Tetrasodium Salt (CPTS)

Name	Amount
CPTS	50.0 mg
HCl	1.0 mL
Milli-Q Water	Up to 1.0 L
Total Volume	1.0 L

10X Tris Buffered Saline (TBS; Stock Solution)

Name	Amount
NaCl	80.0 g
KCl	2.0 g
1 M Tris – pH 7.5	250.0 mL
Milli-Q Water	Up to 1.0 L
Total Volume	1.0 L

1X TBS-Tween20 (TBST)

Name	Amount
10X TBS (Stock Solution)	100.0 mL
Tween20	1.0 mL
Milli-Q Water	Up to 1.0 L
Total Volume	1.0 L

- Wrap in aluminum foil to protect from light
- Store at RT

Non-fat Milk Blocking Solution (5% [w/v])

Name	Amount
Non-fat Milk Powder (Carnation)	5.0 g
1X TBST	Up to 100.0 mL
Total Volume	100.0 mL

CHROMOSOME INSTABILITY ASSAYS

Paraformaldehyde Fixative (4% [w/v])

Name	Amount
Paraformaldehyde	0.88 g
1X PBS	22.0 mL
Total Volume	22.0 mL

- Bring to a slight boil to dissolve paraformaldehyde
- Cool to RT prior to use

Hoechst 33342 (1 mg/mL, Stock Solution)

Name	Amount
Hoechst 33342 (Thermo Scientific)	10.0 mg
1X PBS	Up to 10.0 mL
Total Volume	10.0mL

- Protect from light
- Store at -20 °C

Hoechst 33342 (300 ng/mL, Working Solution)

Name	Amount
Hoechst 33342 (Stock Solution)	6.0 µL
1X PBS	22.0 mL
Total Volume	22.0 mL

Colcemid (100 ng/mL, Working Solution)

Name	Amount
KaryoMAX Colcemid (Gibco; 10 µg/mL)	20.0 µL
Complete Cell Culture Medium	1.0 mL
Total Volume	~1.0 mL

KCl (1 M, Stock Solution)

Name	Amount
KCl	7.5 g
Milli-Q Water	Up to 100.0 mL
Total Volume	100.0 mL

KCl (75 mM, Working Solution)

Name	Amount
KCl (1 M, Stock Solution)	1.5 mL
Milli-Q Water	20.0 mL
Total Volume	21.5 mL

3:1 Methanol Acetic Acid Fixative

Name	Amount
Methanol	45.0 mL
Acetic Acid	15.0 mL
Total Volume	60.0 mL

4',6-Diamidino-2-phenylindole (DAPI; 50 µg/mL, Stock Solution)

Name	Amount
DAPI (Sigma-Aldrich; 5 mg/mL)	10.0 µL
1X PBS	990.0 µL
Total Volume	1.0 mL

- Protect from light
- Store at 4 °C

DAPI Mounting Media

Name	Amount
DAPI (50 µg/mL, Stock Solution)	10.0 µL
Vectashield Mounting Medium (Vector Laboratories)	990.0 µL
Total Volume	1.0 mL

APPENDIX B: SUPPLEMENTARY TABLES

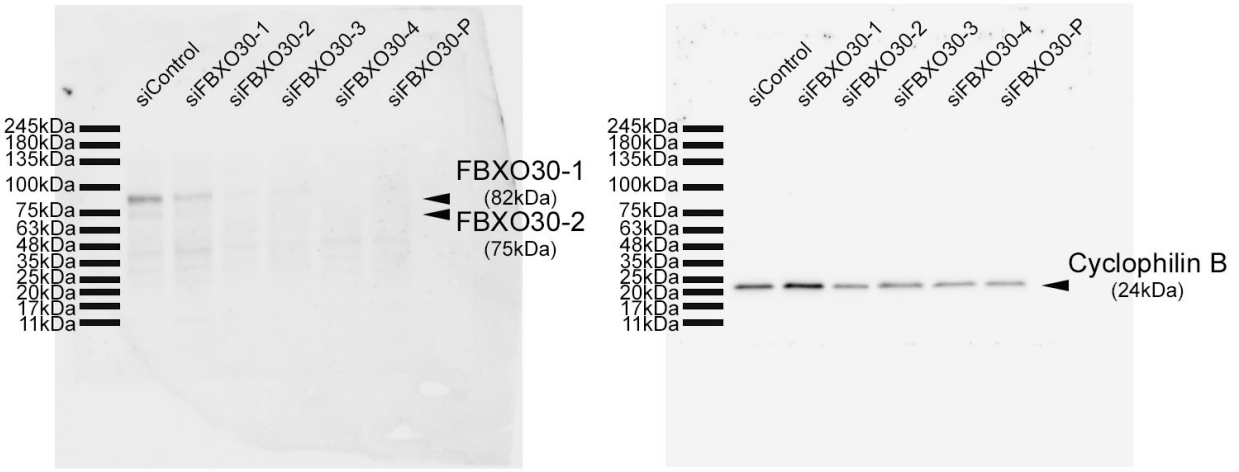

Figure S1- Supporting Original Unprocessed Western blot of *FBXO30* silencing Confirmation in HCT116 Cells.
Raw images corresponding to the optimized and cropped western blot images presented in Figure 4-4. Conditions for each lane are labelled above, whereas the specific antibody targets are presented to the right of each blot. The position and sizes of molecular weight markers (BLUelf Prestained Protein Ladder; FroggaBio) are indicated by black lines to the left of each blot.

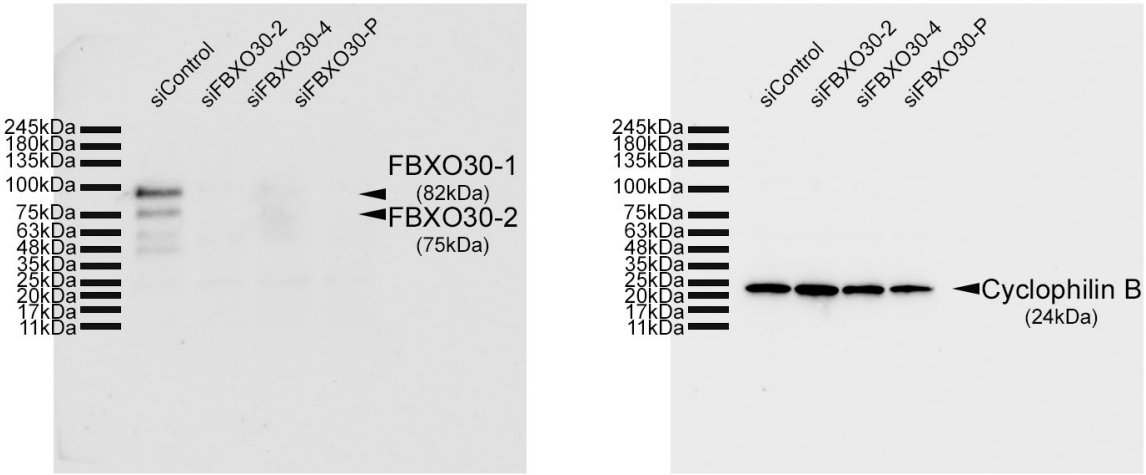

Figure S2- Supporting Original Unprocessed Western blot of *FBXO30* silencing Validation in 1CT Cells.
Raw images corresponding to the optimized and cropped western blot images presented in Figure 4-5. Conditions for each lane are labelled above, whereas the specific antibody targets are presented to the right of each blot. The position and sizes of molecular weight markers (BLUelf Prestained Protein Ladder; FroggaBio) are indicated by black lines to the left of each blot.

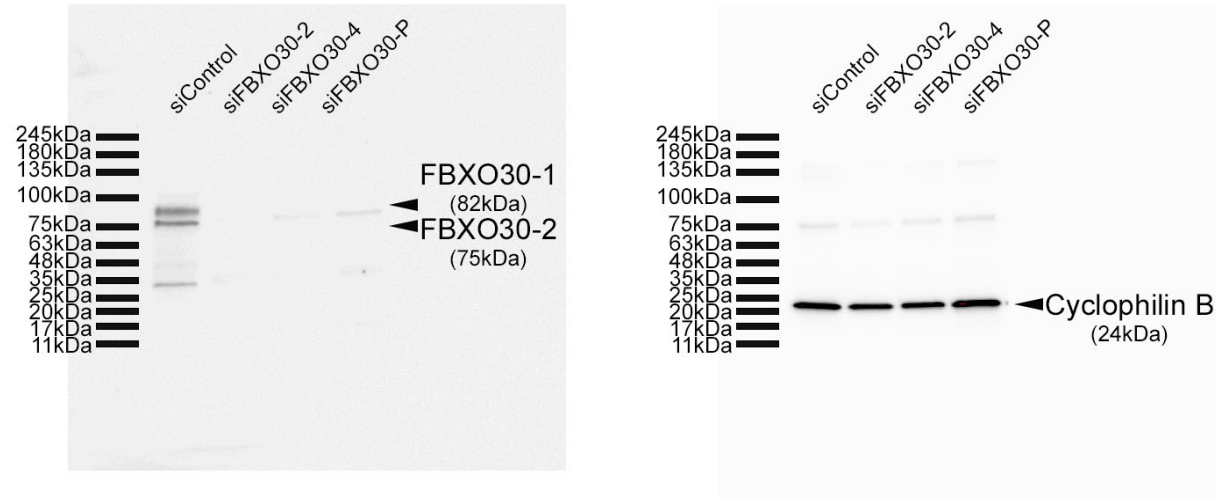

Figure S3- Supporting Original Unprocessed Western blot of *FBXO30* silencing Validation in A1309 Cells.

Raw images corresponding to the optimized and cropped western blot images presented in Figure 4-8. Conditions for each lane are labelled above, whereas the specific antibody targets are presented to the right of each blot. The position and sizes of molecular weight markers (BLUelf Prestained Protein Ladder; FroggaBio) are indicated by black lines to the left of each blot.

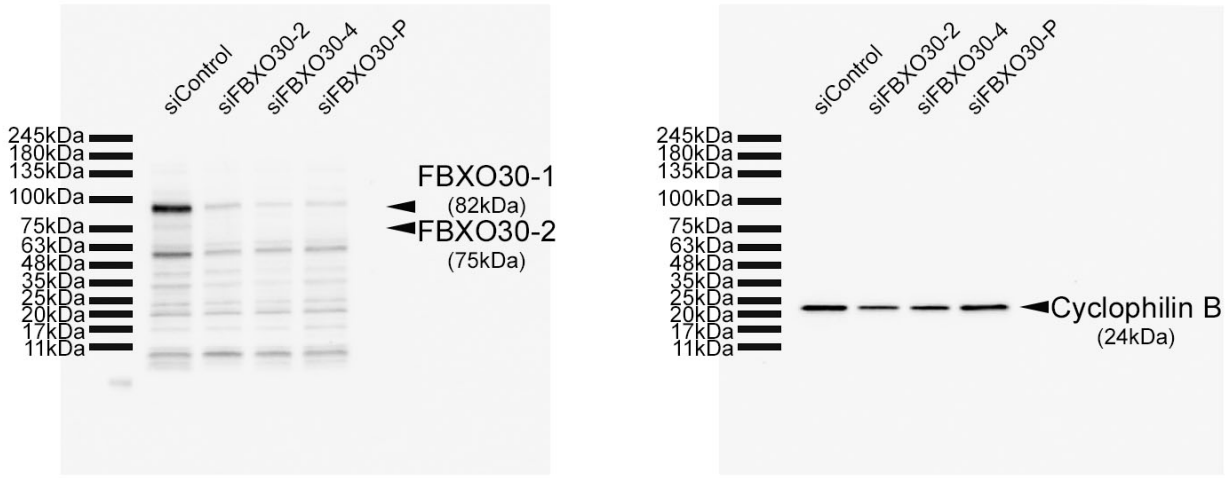

Figure S4- Supporting Original Unprocessed Western blot of *FBXO30* silencing in HCT116 Cells.

Raw images corresponding to the optimized and cropped western blot images presented in Figure 4-11. Conditions for each lane are labelled above, whereas the specific antibody targets are presented to the right of each blot. The position and sizes of molecular weight markers (BLUelf Prestained Protein Ladder; FroggaBio) are indicated by black lines to the left of each blot.

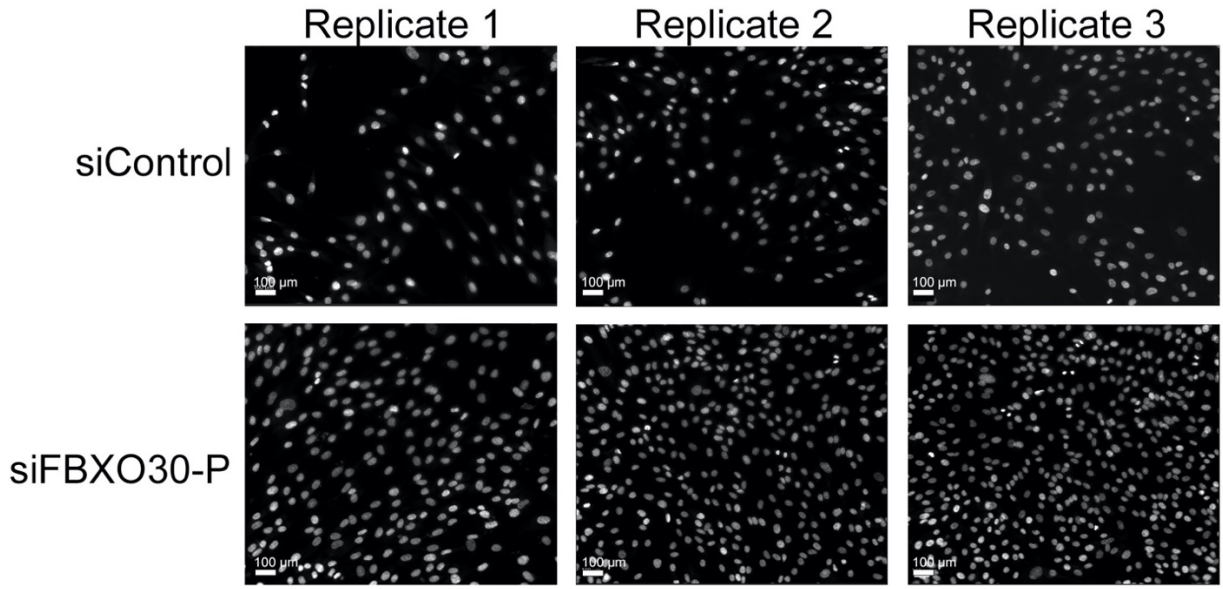

Figure S5- Hoechst-stained Images of Nuclei in *FBXO30* Silencing Conditions in 1CT Cells. Images of Hoechst-stained nuclei depict cell confluency in siFBXO30-P relative to siControl in all three replicates of 1CT cells.

Table S1- Two-sample KS Test Reveals Significant Increases in Cumulative Nuclear Area Distributions Following *FBXO30* Silencing in 1CT Cells.

Condition	n[A]	p-value[B]	Significance[C]
Replicate 1			
siControl	> 1,000	-	-
siFBXO30-2	> 500	< 0.0001	****
siFBXO30-4	> 1,000	< 0.01	**
siFBXO30-P	> 1,000	< 0.0001	****
Replicate 2			-
siControl	> 1,000	-	-
siFBXO30-2	> 500	< 0.0001	****
siFBXO30-4	> 800	< 0.0001	****
siFBXO30-P	> 2,000	< 0.0001	****
Replicate 3			
siControl	> 2,000	-	-
siFBXO30-2	> 900	< 0.0001	****
siFBXO30-4	> 1,500	< 0.0001	****
siFBXO30-P	> 3,000	< 0.0001	****

[A]Number of nuclei analyzed
[B]p-values calculated from two-sample KS tests for the listed conditions relative to siControl
[C]Significance level (represented by asterisks)

Table S2- MW Tests Identify Significant Increases in Micronucleus Formation Frequencies Following siFBXO30-2 Silencing in 1CT Cells.

Condition	n[A]	Mean Nucleus Count[B]	Mean MN Count[C]	Mean % MNF[D]	Median Fold Change in MNF[E]	p-value[F]	Significance[G]
Replicate 1							
siControl	6	1,174	28.3	2.4	-	-	-
siFBXO30-2	6	579	29.8	3.9	1.6	< 0.01	**
siFBXO30-4	6	1,432	40.5	2.8	1.2	> 0.05	ns
siFBXO30-P	6	1,930	31.7	1.7	0.7	> 0.05	ns
Replicate 2							
siControl	6	1,434	18.5	1.3	-	-	-
siFBXO30-2	6	724	15	2.1	1.6	< 0.01	**
siFBXO30-4	6	1,022	22.7	2.2	1.7	< 0.01	**
siFBXO30-P	6	2,324	23.7	1.0	0.8	> 0.05	ns
Replicate 3							
siControl	6	2,367	39.7	1.7	-	-	-
siFBXO30-2	6	1,054	33	3.1	1.8	< 0.01	**
siFBXO30-4	6	2,036	41.3	2.1	1.2	< 0.05	*
siFBXO30-P	6	3,065	29.5	1.0	0.6	> 0.05	ns

[A]Number of wells analyzed
[B]Mean number of nuclei analyzed per well
[C]Mean number of micronuclei counted per well
[D]Mean percent MNF (calculated for each well as the MN count / nucleus count x 100)
[E]Median fold change in MNF relative to siControl
[F]p-values calculated from two-sample MW tests for the listed conditions relative to siControl
[G]Significance level (represented by asterisks)

Table S3- Student's T-tests Identify Significant Changes in Chromosome Numbers in 1CT Cells Following *FBXO30* Silencing.

Condition	n[A]	p-value[B]	Significance[C]
siControl	300	-	-
siFBXO30-2	300	< 0.01	**
siFBXO30-4	300	< 0.05	*
siFBXO30-P	300	< 0.01	**

[A]Number of mitotic spreads analyzed (100/condition x 3 replicates)
[B]p-values calculated from Student's T-tests for the listed condition relative to siControl
[C]Significance level (represented by asterisks)

Table S4- Two-sample KS Test Reveals Significant Increases in Cumulative Nuclear Area Distributions Following *FBXO30* Silencing in A1309 Cells.

Condition	n[A]	p-value[B]	Significance[C]
Replicate 1			
siControl	> 4,000	-	-
siFBXO30-2	> 2,000	< 0.0001	****
siFBXO30-4	> 5,000	< 0.0001	****
siFBXO30-P	> 5,000	< 0.0001	****
Replicate 2			-
siControl	> 4,000	-	-
siFBXO30-2	> 1,000	< 0.0001	****
siFBXO30-4	> 4,000	< 0.0001	****
siFBXO30-P	> 4,000	< 0.001	***
Replicate 3			
siControl	> 4,000	-	-
siFBXO30-2	> 2,000	< 0.0001	****
siFBXO30-4	> 4,000	< 0.0001	****
siFBXO30-P	> 4,000	< 0.0001	****

[A]Number of nuclei analyzed
[B]p-values calculated from two-sample KS tests for the listed conditions relative to siControl
[C]Significance level (represented by asterisks)

Table S5- MW Tests Identify Significant Increases in Micronucleus Formation Frequencies Following Silencing with siFBXO30-2 in A1309 Cells.

Condition	n[A]	Mean Nucleus Count[B]	Mean MN Count[C]	Mean % MNF[D]	Median Fold Change in MNF[E]	p-value[F]	Significance[G]
Replicate 1							
siControl	6	5,757	93	1.6	-	-	-
siFBXO30-2	6	3,209	106	3.4	2.1	< 0.01	**
siFBXO30-4	6	5,941	108.8	1.9	1.2	> 0.05	ns
siFBXO30-P	6	5,806	103.6	1.8	1.1	> 0.05	ns
Replicate 2							
siControl	6	4,458	52.5	1.2	-	-	-
siFBXO30-2	6	1,458	39.2	2.7	2.3	< 0.01	**
siFBXO30-4	6	4,820	65.8	1.4	1.2	> 0.05	ns
siFBXO30-P	6	4,058	47.5	1.2	1.0	> 0.05	ns
Replicate 3							
siControl	6	4,878	123.2	2.5	-	-	-
siFBXO30-2	6	2,420	153.8	6.4	2.6	< 0.01	**
siFBXO30-4	6	4,668	197.3	4.2	1.7	< 0.05	*
siFBXO30-P	6	4,864	127.2	2.6	1.0	> 0.05	ns

[A]Number of wells analyzed
[B]Mean number of nuclei analyzed per well
[C]Mean number of micronuclei counted per well
[D]Mean percent MNF (calculated for each well as the MN count / nucleus count x 100)
[E]Median fold change in MNF relative to siControl
[F]p-values calculated from two-sample MW tests for the listed conditions relative to siControl
[G]Significance level (represented by asterisks)

Table S6- Student's T-tests Identify Significant Changes in Chromosome Numbers Following *FBXO30* Silencing in A1309 Cells.

Condition	n[A]	p-value[B]	Significance[C]
siControl	300	-	-
siFBXO30-2	300	< 0.01	**
siFBXO30-4	300	< 0.05	*
siFBXO30-P	300	< 0.01	**

[A]Number of mitotic spreads analyzed (100/condition x 3 replicates)
[B]p-values calculated from Student's T-tests for the listed condition relative to siControl
[C]Significance level (represented by asterisks)

Table S7- Two-sample KS Test Reveals Significant Increases in Cumulative Nuclear Area Distributions Following *FBXO30* Silencing in HCT116 Cells.

Condition	n[A]	p-value[B]	Significance[C]
Replicate 1			
siControl	> 1,000	-	-
siFBXO30-2	> 500	< 0.0001	****
siFBXO30-4	> 1,000	< 0.0001	****
siFBXO30-P	> 2,000	< 0.0001	****
Replicate 2			-
siControl	> 1,000	-	-
siFBXO30-2	> 500	< 0.0001	****
siFBXO30-4	> 1,000	< 0.0001	****
siFBXO30-P	> 900	< 0.0001	****
Replicate 3			
siControl	> 1,000	-	-
siFBXO30-2	> 500	< 0.0001	****
siFBXO30-4	> 1,000	< 0.0001	****
siFBXO30-P	> 1,000	< 0.0001	****

[A]Number of nuclei analyzed
[B]p-values calculated from two-sample KS tests for the listed conditions relative to siControl
[C]Significance level (represented by asterisks)

Table S8- MW Tests Identify Significant Increases in Micronucleus Formation Frequencies Following siFBXO30-2 Silencing in HCT116 Cells.

Condition	n[A]	Mean Nucleus Count[B]	Mean MN Count[C]	Mean % MNF[D]	Median Fold Change in MNF[E]	p-value[F]	Significance[G]
Replicate 1							
siControl	6	1,956	12	0.8	-	-	-
siFBXO30-2	6	1,629	14	1.7	2.1	> 0.05	ns
siFBXO30-4	6	2,607	9.3	0.4	0.5	> 0.05	ns
siFBXO30-P	6	3,532	11.8	0.3	0.4	> 0.05	ns
Replicate 2							
siControl	6	3,038	4.3	0.1	-	-	-
siFBXO30-2	6	770	10.3	1.5	15	< 0.01	**
siFBXO30-4	6	1,858	10	0.5	5	< 0.01	**
siFBXO30-P	6	1,253	10.7	0.9	9	< 0.01	**
Replicate 3							
siControl	6	2,187	19.5	1.0	-	-	-
siFBXO30-2	6	1,019	21.2	2.1	2.1	< 0.01	**
siFBXO30-4	6	1,611	13.3	0.9	0.9	> 0.05	ns
siFBXO30-P	6	1,228	13.8	1.1	1.1	> 0.05	ns

[A]Number of wells analyzed
[B]Mean number of nuclei analyzed per well
[C]Mean number of micronuclei counted per well
[D]Mean percent MNF (calculated for each well as the MN count / nucleus count x 100)
[E]Median fold change in MNF relative to siControl
[F]p-values calculated from two-sample MW tests for the listed conditions relative to siControl
[G]Significance level (represented by asterisks)

Table S9- Student's T-tests Identify Significant Changes in Chromosome Numbers Following *FBXO30* Silencing in HCT116 Cells.

Condition	n[A]	p-value[B]	Significance[C]
siControl	300	-	-
siFBXO30-2	300	< 0.05	*
siFBXO30-4	300	< 0.05	*
siFBXO30-P	300	< 0.01	**

[A]Number of mitotic spreads analyzed (100/condition x 3 replicates)
[B]p-values calculated from Student's T-tests for the listed condition relative to siControl
[C]Significance level (represented by asterisks)